EUROPEAN SCHOOL OF MOLECULAR MEDICINE

NAPLES SITE

UNIVERSITA' DEGLI STUDI DI NAPOLI

"FEDERICO II"

Ph.D. in Molecular Medicine – Ciclo V/XXIII

"Human Genetics"

"Toward the understanding and treatment of human neurodegenerative disorders: a mouse model approach"

Tutor: Prof. Diego Di Bernardo

Internal Supervisor: Prof. Giancarlo Parenti

External Supervisor: Prof. Frank LaFerla

Coordinator: Prof. Francesco Salvatore

Ph.D. student: Serena Abbondante

Academic Year: 2010-2011

TABLES OF CONTENTS:

Part 1: ERT as an efficient approach to treat Mucopolysaccharidosis type II: studies in a mouse model of the disease

INTRODUCTION

1. Biosynthesis and sorting of lysosomal enzyme: the mannose-6-phosphate receptor system
2. Diseases of Lysosomal Storage
    - Therapeutic treatments for LSDs
3. MUCOPOLYSACCHARIDOSES (MPSs)
4. Sulfatases and MSD (MULTIPLE SULFATASE DEFICIT)
5. Mucopolysaccharidosis type II (Hunter syndrome)
    - General phenotype of MPS II patients
    - Mucopolysaccharidosis type II A (MPS II A)
    - Mucopolysaccharidosis type II B
6. The Enzyme Replacement Therapy
    - ERT for MPS diseases
    - ERT for MPS II
    - The Immuno Response To ERT
7. MPS II mouse model

MATERIALS AND METHODS

1. . Animals
2. Blood and tissue collection
3. Ids activity assay
4. . Alcian blue staining
5. Immunohistochemistry and immunofluorescence
6. Staining quantification
7. Electron microscopy and MRI
8. Quantitative analysis of GAG accumulation in the urine
9. Open-field and rotarod tests
10. Electroretinograms recordings
11. Statistical analyses

RESULTS

1. Longitudinal characterization of neuropathological features in MPS II mice
2. MPS II mice are characterized by motor impairments
3. MPS II mice present a progressive reduction of retinal functions
4. MPS II mice present ventricular atrophy
5. From characterization to therapy: Ids activity can be partially rescued in the brain of MPSII mice using the enzyme replacement therapy (ERT).
6. Ids supplied by ERT crosses the blood brain barrier
7. Ids activity is present in all visceral tissues after ERT
8. The Ids enzyme co-localizes with lysosome markers in the brain

9. ERT allows clearance of lysosomal GAGs accumulation in the brains and tissues of MPS II treated mice
10. Ultrastructural analyses of the brain of MSPII mice following ERT
11. Ids activity and GAGs clearance in the brains and tissues of treated and control mice, sacrificed 4 days after the final Ids infusion
12. Partial correction of the brain defects in the treated MPS II mice
13. Treated MPSII mice show improved sensorimotor coordination in the open-field and rotarod tests

DISCUSSION

REFERENCES

FIGURES INDEX

Figure 1. Biosynthesis and trafficking of lysosomal enzymes through mannose-6-phosphate receptor pathways

Figure 2. Example of Lysosomal storage diseases

Figure 3. Catabolism of Dermatan sulfate and Heparan sulfate

Figure 4. Patients affected by MPS II A

Figure 5. Patient affect by MPS II B

Figure 6. Enzyme-replacement therapy (ERT) and enzyme uptake

Figure 7. Phenotype of MPS II mouse model

Figure 8. Histopathological characterization of brain of MPS II mice

Figure 9. MPS II show a progressive loss of Purkinje cells

Figure 10. Behavioral characterization of MPS II mice

Figure 11. Representative ERGs recorded from MPS II (Ids$^{y/-}$) mice and WT mice at 3, 6 and 12 month-old

Figure 12. MPS II mice present ventricular atrophy

Figure 13. Determination of the half-life of the Ids enzyme after ERT

Figure 14. Ids activity measured in the brain homogenates of *Ids*$^{y/-}$ mice following ERT

Figure 15. Ids activity measured in the visceral tissues of *Ids*$^{y/-}$ treated mice following ERT

Figure 16. The Ids enzyme co-localizes with lysosome markers in the brain

Figure 17. Rescue of GAGs accumulation in the brain of Ids$^{y/-}$ treated mice

Figure 18. Total rescue of GAGs accumulation in the visceral tissues of *Ids*$^{y/-}$ mice treated.

Figure 19. Clearance of urine GAGs accumulation after ERT

Figure 20. Clearance of lysosome storage after ERT as evaluated by ultrastructural analysis

Figure 21. Residual levels of Ids activity are sufficient to maintain clearance of GAGs accumulation in brain and visceral tissues

Figure 22. Rescue of the CNS markers after ERT in MPS II mice

Figure 23. Rescue of behavioral phenotype in groups C and D of *Ids*$^{y/-}$ treated mice after ERT

Table 1. Plasma Ids activities according to mouse treatment groups, 4 h after last treatment

Table 2. Plasma Ids activities according to mouse treatment groups, 48 h after last treatment

PART 2: Diabetes Mellitus type 1 induces cognitive dysfunction through tau-dependent mechanism

INTRODUCTION

1. Plasma Ids activities according to mouse treatment groups, 48 h after last treatment
2. Insulin signaling and its neural function
3. Alzheimer Disease and tau proteins
4. Insulin signaling and Alzheimer Disease

MATERIALS AND METHODS

1. Transgenic mice
2. Behavioral Tests
3. Induction of DMT 1, glucose measure and LiCl treatment
4. Tissue preparation
5. Immunoblotting
6. Quantitative and statistical analyses

RESULTS

1. STZ induces diabetes in WT and mtauKO mice

2. The hippocampal cognitive deficit induced by the STZ treatment is tau dependent

3. Cognitive deficits induced by the STZ treatment are correlated to a significant decrease of synaptic markers expression and of molecules involved in memory-related intracellular signaling
4. STZ treatment induces significant tau hyperphosphorylation in WT mice
5. STZ treatment impairs IR/PI3K/AKT pathway with a consequent decrease of GSK3β [Ser9] phosphorylation level
6. Cognitive deficits induced by STZ treatment in WT mice are reversed by Lithium treatment

DISCUSSION

REFERENCES

FIGURES INDEX

Figure 1. Insulin signaling pathway

Figure 2. Metabolism of Amyloid Precursor Protein

Figure 3. Tau structure and function

Figure 4. Streptozotocin treatment induces hippocampal cognitive impairment in WT mice through a tau dependent mechanism

Figure 5. Streptozotocin treatment decreases the content memory-related intracellular signaling molecules and of synaptic-related proteins in WT mice

Figure 6. STZ treatment does not alter cellular composition in different brain structures

Figure 7. Streptozotocin treatment leads to tau hyperphosphorylation in WT mice

Figure 8. Streptozotocin treatment alters the IR/PI3K/AKT pathway in WT and mtauKO mice

Figure 9. Streptozotocin treatment did not affect Cdk5, ERK and p38MAPK total content or phosphorylated levels

Figure 10. Lithium treatment restores the cognitive impairments of WT-STZ mice

TABLE 1. Significant hyperglucemia in WT and mtauKO mice after 3 days and 7 weeks from streptozotocin injection

PART 1

ERT as an efficient approach to treat Mucopolysaccharidosis type II: studies in a mouse model of the disease

ABSTRACT

Mucopolysaccharidosis type II (MPS II) is a lysosomal storage disorder caused by the deficiency of the lysosomal enzyme iduronate 2 sulphates (Ids). The inactivity of this enzyme results in the progressive accumulation of heparan and dermatan sulfates within the lysosomes of various tissues and organs, with consequent cellular degeneration. Patients affected by the severe form of MPS II are characterized, in addition, by a devastating involvement of the central nervous system. The MPSII mouse model reproduces the features of MPSII patients. The characterization of brain phenotype of mouse MPS II showed a progressive GAGs accumulation in almost all the regions of the brain, an increase in inflammation and severe neurodegeneration. Moreover, behavioral tests, showed a deficit in learning and motor coordination. Up to now, the only treatment for MPS II patients is the enzyme replacement therapy (ERT) with the systemic infusion of Ids enzyme; however, this treatment only obtains amelioration of visceral defects, but not of neurological ones. To this aim, we developed a new protocol of ERT to treat both, visceral and neurological defects. Importantly, we were successful in having the infused Ids enzyme reaching the brain with a good rescue of the CNS phenotype and behavioral performances. Among the ERT protocols tested, the one using low Ids concentration, was effective on young and adult MPS II mice.

INTRODUCTION

1. Biosynthesis and sorting of lysosomal enzyme: the mannose-6-phosphate receptor system.

Lysosomal enzymes are hydrolases synthesized as soluble or membrane integrated glycoproteins in the rough endoplasmic reticulum (ER) where they also glycosylated by addiction of N-linked oligosaccharides [1-2]. These enzyme are then trafficked to the cis-Golgi network, where they acquire mannose-6-phosphate (M6P) residues on their high-mannose oligosaccharide chains, by the sequential action of N-acetylglucosaminyl-phosphotransferase and N-acetylglucosamine-1-phophodiester**α**-N acetylglucosaminidase. The phosphorylated enzymes bind to M6P receptors that are located on the membranes of the clathrin-coated vesicles that bud from the trans-Golgi network; these transport vesicles fuse with early and late endosomes, releasing the newly lysosomal enzyme. This process leads to the dissociation of these enzymes from the M6P receptors that are then recycled back to the Golgi. The increase in acidification allows the early and late endosomes to become lysosomes (Fig 1). In addition, in the trans-Golgi network, the oligosaccharides, that are present on lysosomal enzymes, could undergo mannose trimming and the addition of sugars to form complex oligosaccharides that contain galactose and sialic acid, leading to their inclusion in secretory vesicles. A small amount of lysosomal enzymes is secreted from the cells through M6P receptors presented on the plasma membrane where they bind to cell-surface MPRs to be endocytosed [1-4]. Once in the endocytic pathway, internalized lysosomal enzymes can intermingle with those following the biosynthetic route.

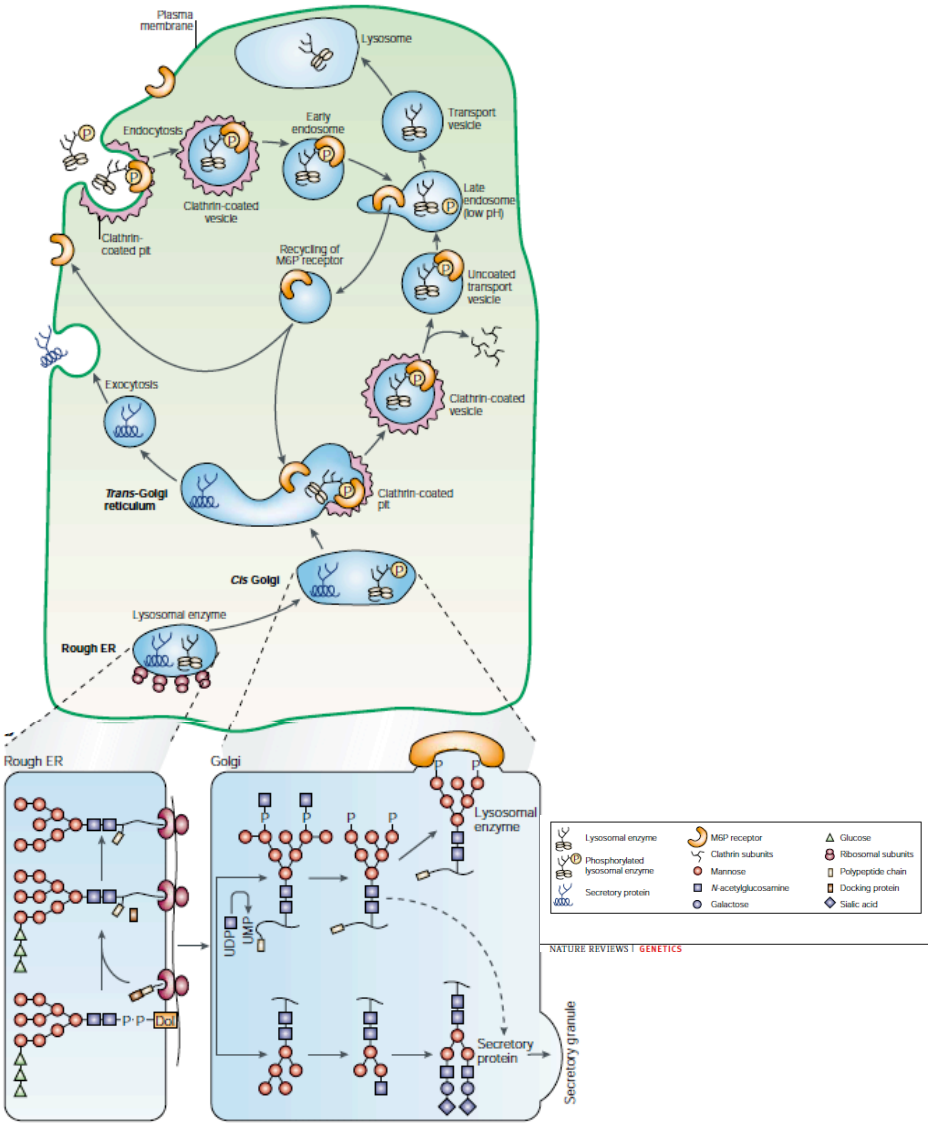

Figure 1. Biosynthesis and trafficking of lysosomal enzymes through mannose-6-phosphate receptor pathways. Lysosomal enzymes are glycoproteins synthetized in the rough endoplasmic reticulum (ER). In the ER membrane they undergo N-glycosylation and they then move to the Golgi compartment where they acquire a mannose 6-phosphate (M6-P) ligand. In the Golgi apparatus, the newly lysosomal enzymes bind the mannose 6-phosphate receptor present on clathrin-coated vesicles and the receptor–protein complex then moves to the late endosome, where the low pH causes it to dissociate. The hydrolase moves on into the lysosome and the receptor then is recycled either to the Golgi.

2. Diseases of Lysosomal Storage.

The lysosome is a cytoplasmic organelle, main site of intracellular digestion of macromolecules which are present in all cell types. To date more than 50 known acid hydrolases have been described; these enzymes degrade most of the intracellular and extracellular macromolecules delivered to them by endocytosis or phagocytosis [5].

Lysosomal storage diseases (LSDs) are a devastating group of more than 40 rare inherited metabolic disorders. LSDs are due to the deficient activity of lysosomal hydrolases involved in degradation of various macromolecules (lipids, glycoproteins, glycogen and mucopolysaccharides). In few cases, also proteins involved in lysosomal transportation, delivery and activators of lysosomal enzymes [6-8] can be affected (Figure 2).

Disease	Defective protein	Storage materials
Mucopolysaccharidoses (MPS)		
MPS I (Hurler, Scheie, Hurler/Scheie)	α-Iduronidase	Dermatan sulphate and heparan sulphate, GM2, GM3, SCMAS
MPS II (Hunter)	Iduronate-2-sulphatase	Dermatan sulphate and heparan sulphate, GM2, GM3, SCMAS
MPS IIIA (Sanfilippo)	Heparan *N*-sulphatase (sulphamidase)	Heparan sulphate, GM2, GM3, GD2, SCMAS, ubiquitin
MPS IIIB (Sanfilippo)	*N*-Acetyl-α-glucosaminidase	Heparan sulphate, GM2,GM3, GD2, unesterified cholesterol, SCMAS
MPS IIIC (Sanfilippo)	Acetyl-CoA: α-glucosamide *N*-acetyltransferase	Heparan sulphate, GM2, GM3, GD2
MPS IIID (Sanfilippo)	*N*-Acetylglucosamine-6-sulphatase	Heparan sulphate, GM2,GM3, GD2
MPS IV A (Morquio-A)	*N*-Acetylgalactosamine-6-sulphate-sulphatase	Keratan sulphate, chondroitin-6-sulphate
MPS IV B (Morquio-B)	β-Galactosidase	Keratan sulphate, oligosaccharides
MPS VI (Maroteaux-Lamy)	*N*-Acetylgalactosamine-4-sulphatase (arylsulphatase B)	Dermatan sulphate, GM2, GM3, unesterified cholesterol
MPS VII (Sly)	β-Glucuronidase	Heparan sulphate, dermatan sulphate, chondroitin-4- and -6-sulphates, GM2, GM3, ubiquitin
Multiple sulphatase deficiency (Austin)	Formylglycine-generating enzyme	Heparan sulphate, dermatan sulphate, chondroitin-4- and -6-sulphates, sulpholipids
Spingolipidoses		
Fabry	α-Galactosidase A	Globotriaosylceramide, galabiosylceramide, globotriaosylsphingosine, blood-group-B glycolipids
Farber lipogranulomatosis	Ceramidase	Ceramide
Gaucher	β-Glucosidase	Glucosylceramide, GM1, GM2, GM3, GD3, glucosylsphingosine
Globoid cell leukodystrophy (Krabbe)	Galactocerebroside β-galactosidase	Galactosylceramide, psychosine lactosylceramide, globotriaosylceramide, globotetraosylceramide, fucosylneolactotetraosylceramide
Metachromatic leukodystrophy	Arylsulphatase A	Sulphatide, 3-O-sulpholactosylceramide, lysosulphatide, seminolipid, gangliotetraosylceramide-bis-sulphate, GM2
Niemann–Pick A and B	Sphingomyelinase	Sphingomyelin, cholesterol, bismonoacylglycerophosphate, GM2, GM3, glucosylceramide, lactosylceramide, globotriaosylceramide, globotetraosylceramide
GM1 gangliosidosis	β-Galactosidase	GM1, GA1, GM2, GM3, GD1A, lyso-GM1, glucosylceramide, lactosylceramide, oligosaccharides, keratan sulphate
GM2 gangliosidosis (Tay–Sachs)	β-Hexosaminidase A	GM2, GD1aGalNac, GA2, lyso-GM2
GM2 gangliosidosis (Sandhoff)	β-Hexosaminidase A and B	GM2, GD1aGalNac, globoside, oligosaccharides, lyso-GM2
Oligosaccharidoses and glycoproteinoses		
Aspartylglucosaminuria	Aspartylglucosaminidase	Aspartylglucosamine
Fucosidosis	α-Fucosidase	Fucose containing oligosaccharides and H-antigen–glycolipid
α-Mannosidosis	α-Mannosidase	Mannose-containing oligosaccharides, GM2, GM3
β-Mannosidosis	β-Mannosidase	Man(β1→4)GlcNAc disaccaride
Sialidosis	Sialidase	Sialyloligosaccharides and sialylglycopeptides
Schindler disease	α-*N*-Acetylgalactosaminidase	Glycopeptides with N- or O-linked oligosaccharides, oligosaccharides
Glycogenosis		
Pompe (glycogen-storage-disease type II)	α-Glucosidase	Glycogen

Figure 2: Example of Lysosomal storage diseases

The specific enzyme deficiency that can result from absence or low levels of the enzyme but also from normal-to-high levels of mutant enzyme (for example to mutations in structurally conservative active site), leads to an accumulation of un-degraded products in lysosomes that causes an enlargement of the cells. This lysosomal storage leads to a reduced ability of lysosomes to fuse with autophagosomes that results in a block (at least partial) of autophagy maturation and defective degradation. Consequently, autophagy substrates such as poly-ubiquitinated protein aggregates and dysfunctional mitochondria accumulate and promote cell death. The accumulation of un-degraded metabolites within the lysosomes is the primary cause of the disease. Moreover, the inflammatory response to cell damage further contributes to cell death. However, it has been suggested that the various range of clinical symptoms in LSDs is also mediated by dysfunction of several pathways due to altered activation of biochemical pathways and altered gene expression. Overall, these altered primary and secondary dysfunctions cause tissue pathology and general organ damage [9-11]. Most of these disorders are autosomal recessively inherited, however a few are X-linked recessively inherited such as Fabry's disease, Hunter syndrome (MPS II) and Danon disease. These disorders occur with incidences of less than 1:100.000, even if a group of them, the Mucopolysaccharidosis (MPS) affect one in every 100,000 to 200,000 live born [12-13]. Although each disorder results from different gene mutations that translate into a deficiency in enzyme activity, they all share a common biochemical characteristic – all lysosomal disorders originate from an abnormal accumulation of substances inside the lysosome. Storage may begin during early embryonic development, and the clinical presentation for LSDs can vary from an early and severe phenotype to late-onset mild disease. Classically, LSDs have not been considered disorders of the newborn. Generally, clinicians are taught that newborns with LSDs appear normal at

birth and that the symptoms develop progressively over the first few months of life or even after many years [14].

The symptoms of lysosomal storage disease vary, depending on the particular disorder and other variables like the age of onset, and can be mild to severe. They can include developmental delay, movement disorders, seizures, dementia deafness and/or blindness and dimorphic features. Patients affected by some lysosomal storage disease can have enlarged liver (hepatomegaly) and enlarged spleens (splenomegaly), pulmonary and cardiac problems, bones that grow abnormally, hematological manifestations and in some of LSDs the neurological involvement.

Lysosomal diseases are most frequently classified according to the major storage compound:

- lipid storage disorders: sphingolipidoses including Gaucher's and Niemann-Pick disease, gangliosidosis (including Tay-Sachs disease) and metachromatic leukodystrophies.
- glycosaminoglycan storage disorders such as mucopolysaccharidoses (including Hunter syndrome and Hurler disease)
- glycoprotein storage disorders
- mucolipidoses

2.1. Therapeutic treatments for LSDs.

In the past, the only therapy for LSDs patients was the supportive care and treatment for symptoms and complications of the disease. In the last few years, important progresses have been made in the development of therapies for some LSDs, as type 1 Gaucher, Fabry's disease , MPS types I, II, and VI, and Pompe diseases [15-18] .

The enzyme replacement therapy (ERT) is a therapeutic treatment that replaces the functional enzyme in patients in whom that particular enzyme is deficient or absent,

since just 1% to 5% of enzyme activity is required to rescue many of these metabolic defects. ERT is widely available for Gaucher disease type 1, Fabry disease, MPS types I, II, and VI, Pompe disease and clinical trials of ERT in Niemann-Pick disease types A and B are in progress. However, there are limitations to this form of treatment: it does not affect all aspects of the disorder to the same degree, and clinical studies have shown that even after prolonged treatment, many symptoms of LSDs are not reversible. Moreover, the replacement enzymes do not cross the blood-brain barrier, and therefore are ineffective in correcting central nervous system (CNS) manifestations. LSD patients can also be treated with hematopoietic stem cell transplantation (HCT) or bone marrow transplantation, which provides a population of cells able to produce the missing enzyme. Although some improvements have been observed in MPS types VI and VII, HCT has had no effect on the other forms of MPS.

Another available treatment is substrate-reduction therapy, in which lysosomal accumulation is counteracted, by reducing the substrate level to better balance residual activity of the deficient enzyme. However, this treatment modality is still experimental. Another potential therapy under development for patients affected by LSD is gene therapy. One of the major advantages of gene therapy is the potential for long-term expression of the therapeutic protein. Studies on direct injection into target tissues, including liver, muscle, and CNS, are also being conducted in animal models. Even in this case, therapies are not yet ready for clinical trials in patients.

3. MUCOPOLYSACCHARIDOSES (MPSs)

The mucopolysaccharidoses (MPSs) are a group of metabolic storage disorders caused by deficiency the of lysosomal enzymes catalyzing the stepwise degradation of glycosaminoglycans (GAGs) and characterized by intra-lysosomal accumulation and increased excretion in urine of partially degraded GAGs, which at last results in cell, tissue, and organ dysfunctions [19-21].

Glycosaminoglycans or mucopolysaccharides (for their viscous, lubricating properties) are large complex carbohydrate molecules that interact with a wide range of proteins involved in physiological and pathological processes. These molecules are present on all animal cell surface in the extracellular matrix, and some are known to bind and regulate a number of distinct proteins, including chemokines, cytokines, growth factors, enzymes and adhesion molecules. Glycosaminoglycans (GAGs) or mucopolysaccharides are composed by linear polysaccharides, whose disaccharide consists of repeating units of amino sugar (*N*-acetylglucosamine, glucosamine that is variously N-substituted, or *N*-acetylgalactosamine) and of uronic acid (D-glucoronic acid or L-iduronic acid) and differ according to the type of hexosamine, hexose or hexuronic acid unit that they contain. There two main types of GAGs. Non-sulphated GAGs include hyaluronic acid, whereas sulphated GAGs include chondroitin sulphate, dermatan sulphate, keratan sulphate, heparin and heparan sulphate. Heparan sulfate is an essential component of nerve cell membranes, and, therefore, accumulation results in progressive mental deterioration. Keratan sulphates accumulation leads to skeletal deformities. Dermatan sulfate is found mostly in skin, but is also found in blood vessels, heart's valves, lungs, and tendons. Chondroitin sulphate is instead found in cartilage, bone and heart valves. GAGs exist as proteoglycans; in fact, GAG chains may be covalently linked to a protein to form proteoglycans. Thus, protein cores made in the rough endoplasmic reticulum are post-translationally modified

with the adding of GAG disaccharides by glycosyltransferase in the Golgi apparatus. The exact mechanism by which GAG accumulation leads to disease features is unknown, but it may involve interference in cellular trafficking of molecules, alteration of the extracellular matrix, and interference with cell signaling and cell receptor functions[22]. GAGs are degraded in the lysosome by exohydrolase activities following partial catabolism by endoenzymes (endoglycosidases, hyaluronidases, heparanases, and endosulfatases). Thus, in the first step, the polysaccharide GAG chains are reduced to oligosaccharides by endohydrolysis, then the action of up to 13 lysosomal exo-enzymes reduces these oligosaccharides to monosaccharides and inorganic sulfate to enable exit from the lysosome [23]. A deficiency of any one of these exo-enzyme activities may cause a lysosomal storage of the GAG substrates for these lysosomal enzyme activities and clinical symptoms of the mucopolysaccharidosis (MPSs). The result is the progressive and permanent accumulation of GAGs in the lysosomes of the cells with consequent cellular damage which affects appearance, physical abilities, organ and system functioning, and, in most cases, mental development. Actually, seven distinct clinical types have been identified and numerous subtypes of MPS. Although each mucopolysaccharidosis (MPS) differs clinically, most patients generally experience a period of normal development followed by a decline in physical and/or mental function.

The MPSs show many common clinical features even if they can have different degrees of severity. These features may not be apparent at birth but progress as storage of GAGs affects bone, skeletal structure, connective tissues and organs, and then there is excretion of urinary GAG fragments and leukocyte inclusion bodies [21,24]. Physical symptoms generally include coarse or rough facial features (including a flat nasal bridge, thick lips, and enlarged mouth and tongue), short stature with disproportionately short trunk (dwarfism), dysplasia (abnormal bone size and/or

shape) and other skeletal irregularities, thickened skin, enlarged organs such as liver (hepatomegaly) or spleen (splenomegaly), hernias, and excessive body hair growth. Short and often claw-like hands, progressive joint stiffness, and carpal tunnel syndrome can restrict hand mobility and function. Recurring respiratory infections are common, as are obstructive airway disease and obstructive sleep apnea. Many affected individuals also have heart disease, often involving enlarged or diseased heart valves. Involvement of the neurological system may include progressive neurodegeneration such as mental delay and impaired motor function. Depending on the mucopolysaccharidosis subtype, affected individuals may have normal intellect or may be profoundly retarded, may experience developmental delay, or may have severe behavioral problems. The vision system of the MPSs patients can be affected where the cornea often becomes cloudy from intracellular storage and there is degeneration of the retina. Some MPSs can lead to hydrocephalus, in which the normal circulation of cerebrospinal fluid becomes blocked over time and causes increased pressure inside the skull. In general, the time of diagnosis usually occurs from about 2 to 4 years of age when the signs and symptoms became very visible. The most commonly used laboratory screening test for an MPS disorder is a urine test for GAGs [21]. It is important to note that the urine test for GAG can occasionally be normal and yet the child may still have an MPS disorder.

4. Sulfatases and MSD (MULTIPLE SULFATASE DEFICIT)

Each Mucopolysaccharidosis is caused by the deficiency of a specific sulfatase. Sulfatases are hydrolases that catalyze the cleavage of sulfate esters from a several substrates, including glycosaminoglycans, sulfolipids, and steroid sulfates [25-26]. This protein family is represented in most eukaryotes and prokaryotes. In prokaryotes sulfatases are involved in sulfur scavenging; however, in vertebrates they are

implicated in the turnover and in the catabolism of sulfated compounds. These sulfated substrates are hydrolyzed by the sulfatases in lysosomes in concert with acidic glycosidases. The high degree of amino acid sequence similarity along the entire length of the proteins and the functional correlation among sulfatases in different species suggest that sulfatases are members of an evolutionary conserved gene family sharing a common ancestor [25,27]. The sulfatase active site contains a highly conserved cysteine residue as part of a metal binding site that presents a posttranslational modification to Formyl-glycine (FGly). This modification is essential for catalytic activity and occurs within the endoplasmic reticulum before the sorting of sulfatases to different cellular compartments and it is highly conserved during evolution . The factor involved in the post-translational modification of the sulfatases is SUMF1 which is a formyl-glycine-generating enzyme (FGE) [28-29]. The gene of SUMF1 (SUlfatase Modifying Factor 1) belongs to a highly conserved gene family, from prokaryotes to eukaryotes and its activity is responsible for the activation of all human sulfatases [30]. Bacterial sulfatases may contain at their active site a cysteine or a serine, and both of these are modified to formyl-glycine, albeit by a different protein machinery.

At the present time, 17 genes encoding for sulfatases have been identified in humans [26,31-33]. Each enzyme has a different substrate specificity and subcellular localization such as lysosome, Golgi and ER 10. Four of these genes, ARSC, ARSD, ARSE, and ARSF, encoding arylsulfatase C, D, E, and F, respectively, are located within the same chromosomal region (Xp22.3). They are probably the result of duplication events during evolution and because they share significant sequence similarity and a nearly identical genomic organization [27]. It is possible to divide the sulfatases in two main functional categories. The first category includes sulfatases involved in a catabolic function and they are localized into the lysosomes and their enzymatic activity act at

acidic pH. The second category includes the sulfatases involved in biosynthetic pathways and act at neutral pH and they are localized in other cellular compartments such as the ER and the Golgi apparatus [25-26]. The importance of sulfatases in human metabolism is highlighted by the identification of eight human monogenic diseases caused by the deficiency of individual sulfatase activities, six of them are lysosomal storage disorders. Among them there are five different types of mucopolysaccharidoses (MPS types II, IIIA, IIID, IVA, and VI) in which the deficiencies of sulfatases cause a block in the catabolism of glycosaminoglycans [21,24,33] and then there is metachromatic leukodystrophy (MLD), which is characterized by the storage of sulfolipids in the lysosomes of visceral tissues, central and peripheral nervous systems [34]. Moreover, there are two human diseases caused by deficiencies of non-lysosomal sulfatases. These include X-linked ichthyosis, a skin disorder due to steroid sulfatase (STS/ARSC) deficiency, and chondrodysplasia punctata, a disorder affecting bone and cartilage due to arylsulfatase E (ARSE) deficiency [35].

In the multiple sulfatase deficiency (MSD), a rare autosomal recessive lysosomal storage disorder, all sulfatase activities are simultaneously defective and for this reason the clinical phenotypes, multisystemic, combine the features observed in individual sulfatase deficiencies. MSD is due to a loss of function mutations in the gene of SUMF1, with consequent defects in the sulfatases posttranslational modification and in their activation [30,36].

5. Mucopolysaccharidosis type II (Hunter syndrome)

MPS II (Hunter syndrome) is a rare, recessive X-linked lysosomal storage disorder caused by a deficiency of the lysosomal enzyme iduronate-2-sulfatase (Ids). This enzyme catalyzes the catabolism of GAGs by cleaving the O-linked sulfate from dermatan sulfate and heparan sulfate [37-38] (Fig. 3). Up to now, more than 300 mutations have been identified in the gene encoding the protein iduronate-2-sulphatese, responsible for the Ids enzyme deficiency, and include point mutation, missense and nonsense mutations but also insertions or deletions in the gene located on chromosome X at the locus 28 (Xq28) [19,39-41]. The clinical phenotype of MPS II is characterized by the progressive pathological accumulation of GAGs (dermatan and heparan sulphates) in the lysosome of the cells of tissues and organs, with consequent cellular vacuolization and at last by organ dysfunction that manifests as various chronic and progressive patterns of clinical severity [19,21,42]. The estimated incidence of the MPS II is approximately 1 in 162,000 live births and occurs nearly exclusively in males, although females that can carry one abnormal copy of the Ids gene can sometimes be affected [43]. Usually, the measurement of urinary GAGs (heparan and dermatan sulphates) is the first screening test for MPS II followed by measuring Ids activity in serum, white blood cells, or fibroblasts from skin biopsy. In some people with Hunter syndrome, analysis of the Ids gene can determine clinical severity. Prenatal diagnosis is routinely available by measuring Ids enzymatic activity in amniotic fluid or in chorionic villus tissue [19,44].

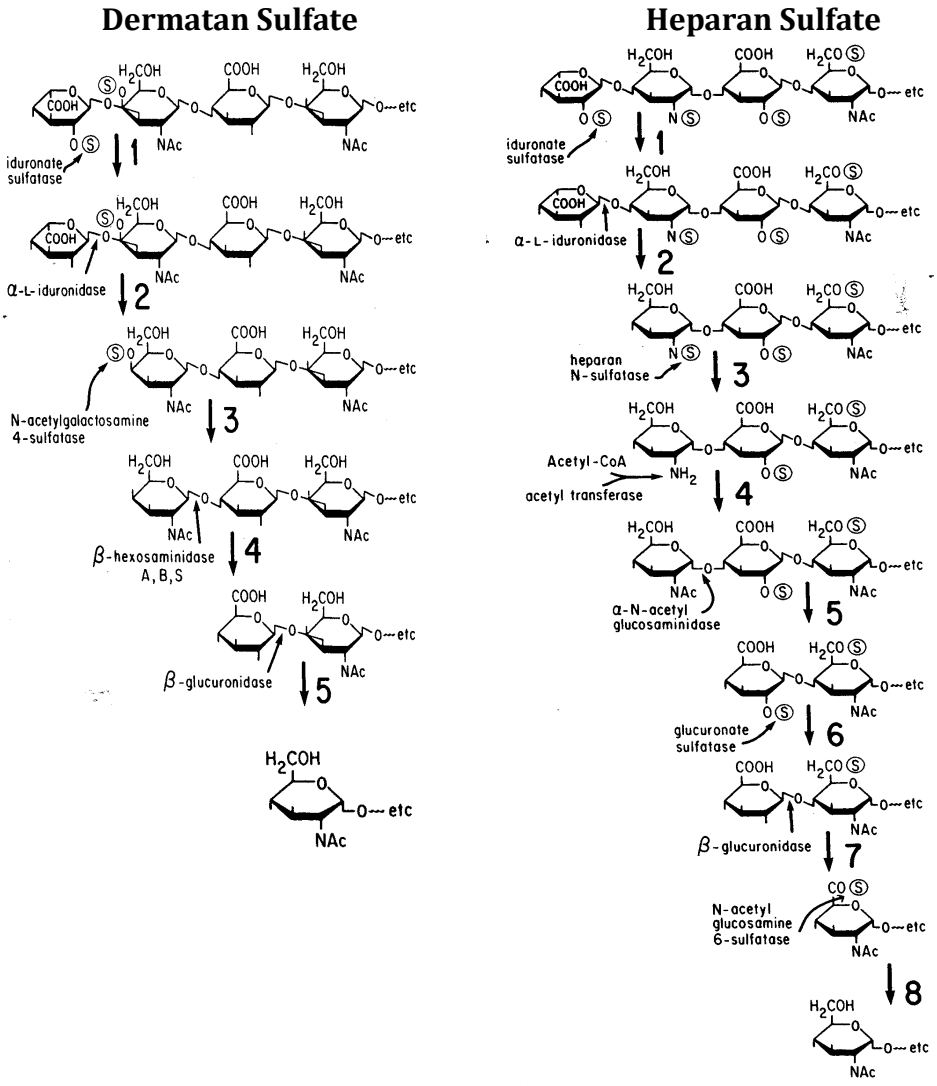

Figure 3: Catabolism of Dermatan sulfate and Heparan sulfate. Iduronate-2-sulfatase (Ids) catalyze the first step of the degradation of both GAG

5.1. General phenotype of MPS II patients

The progressive accumulation of dermatan sulfate and heparan sulfate within tissues and organs is responsible for the clinical manifestations of the disease. The MPS II affects multiple organs and system, including the liver, spleen, heart, bones, joints and central nervous system, with a variable age of onset of signs and symptoms and a variable rate of progression [21,38,42]. The clinical spectrum of Hunter syndrome covers a wide range, from a mild to a severe phenotype. Patients usually appear normal at birth and this causes a delay in the diagnosis of the disease. In the most severely

affected patients, signs and symptoms typically begin to appear between 2 and 4 years of age. All affected patients, including those with a mild phenotype show a progressive somatic involvement, including enlarged liver and spleen, skeletal and joint involvement resulting in reduced joint range of motion and contractures and heart and airway disease.

Patients affected by severe form of MPS II have, in addition, a neurological involvement that results in severe cognitive impairment and progressive neurodegeneration, and death occurs in the second decade of life [19,2138,42]. Instead, MPS II patients affected by an attenuated phenotype demonstrate normal intelligence and usually survive into adulthood, although with a shortened life span [46]. As, mentioned above, there are two clinically forms of mucopolysaccharidosis type II: the severe form called MPS II A and the mild form, called MPS II B.

5.2. Mucopolysaccharidosis type II A (MPS II A)

Patients affected by the severe form of MPS II (MPS II A) present progressive central nervous system involvement with early cognitive impairment. Patients with a severe phenotype typically have an earlier onset of signs and symptoms (in the first few years of life) compared to ones with milder phenotype [19,42,45,47] (Figure 4). The profound cognitive impairment results in a developmental delay, with an onset in early childhood. Developmental skills plateau between 4 and 6 years of age and decline thereafter. These patients often exhibit severe behavioral problems, including hyperactivity, obstinacy, and aggression, beginning in the second year of life and continuing into late childhood. Behavior may later appear to improve, with a decrease in hyperactivity and aggression, but this change is due to continuing neurodegeneration [47]. Late stage disease is characterized by a neurodegenerative state often associated with seizures and lack of mobility. The patients can present

hydrocephalus which may contribute to the behavioral problems, as well as seizures [48-49] and severe retinal degeneration. Physical characteristics include a large head, a distinctive coarseness in their facial features and an enlarged tongue (Figure 4 A). The progressive storage of GAGs in cells can lead to organs being affected in important ways [19,21,42]. The thickening of the heart valves along with the walls of the heart can result in progressive decline in cardiac function. The walls of the airway may become thickened as well, leading to breathing problems while sleeping (obstructive airway disease). People with Hunter syndrome may also have limited lung capacity due to pulmonary involvement. The MPS II A patients can present an increase in the volume of the spleen and liver (hepatosplenomegaly) (Figure 4 B). Moreover, all major joints (including the wrists, elbows, shoulders, hips, and knees) may be affected, leading to joint stiffness and limited motion. Progressive involvement of the finger and thumb joints results in decreased ability to pick up small objects (Figure 4 C). The effects on other joints, such as hips and knees, can make it increasingly difficult to walk normally. The bones themselves may be affected, resulting in short stature (Figure 4 D). In addition, pebbly, ivory-colored skin lesions may be found on the upper arms and legs and upper back of some people with the severe form of MPS II A resulting in death occurs before the 15 years of age.

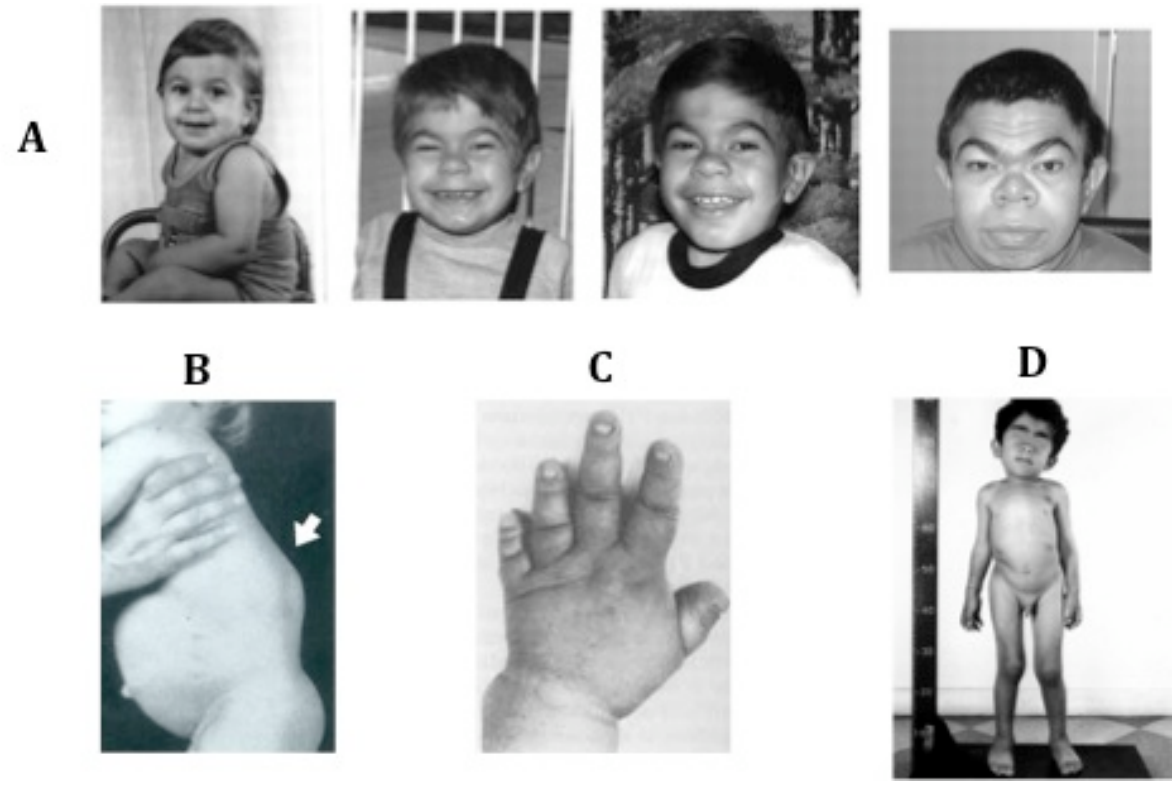

Figure 4: Patients affected by MPS II A. (A) A series of photographs showing the progression of the characteristic facial features of the severe form of Hunter syndrome. **(B-C)** Hepatosplenomegaly and skeleton deformities **(D)** Short stature: in this picture show a boy 10 years old.

5.3. Mucopolysaccharidosis type II B

The mild form of mucopolysaccharidosis type II is called MPS II B. Patients affected by of MPS II B present less wasting and progress at a much slower rate compared to MPS II A, and indeed, the diagnosis is often made in the second decade of life [19,21,46,50]. Physical characteristics include hearing loss, poor peripheral vision, diarrhea, and sleep apnea. Skeletal problems may be less severe, but carpal tunnel syndrome and joint stiffness can restrict movement and height is smaller compared to a normal person. Moreover, some patients can develop cardiac and respiratory problems. Intellect and social development are not affected and the average life span in the 50s or beyond. The quality of life remains high in a large number of people.

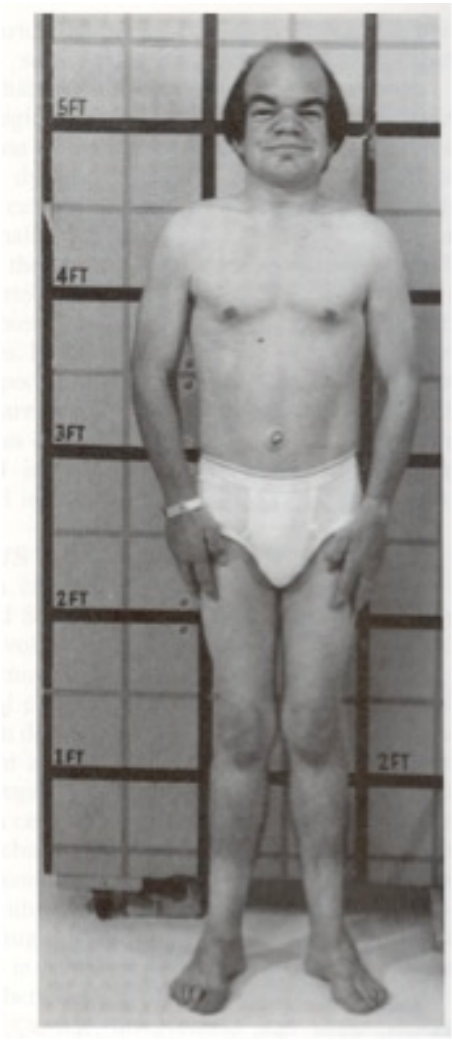

Figure 5: Patient affect by MPS II B.

6. The Enzyme Replacement Therapy

Enzyme replacement therapy (ERT) is a therapeutic treatment in which a specific enzyme that is deficient or absent in patients, is replaced with functional recombinant enzyme produced in the lab. Usually this is done by an intravenous (IV) infusion containing the enzyme to the affected person [51-53]. The recombinant enzyme that is injected diffuses from the bloodstream to cells of tissues where it is taken up via receptor system and translocated to the lysosome.

In the last decade, enzyme-replacement therapy was considered as a therapeutic option for patients affected by lysosomal storage diseases and in fact was used in numerous preclinical and clinical trials. Most of the enzymes used for ERT are produced in an in vitro system by Chinese hamster ovary (CHO) cells as these cells are easy to grow and carry out and have similar post-translational modifications as do human cells. Moreover, the overexpression of a human cDNA for a lysosomal protein in CHO cells not only is trafficked to the lysosomes, but also most of the recombinant human enzyme is selectively secreted into the culture media, thereby facilitating large-scale production of the required enzyme [54-56].

The discovery that intracellular and secreted lysosomal glycoproteins are delivered to the lysosome by the mannose-6-phosphate (M6P)-receptor-mediated pathway provided the rationale to modify by addition of the mannose 6-phosphate all the recombinant enzyme used to treat LSDs [57-58].

Usually, the half-life of many lysosomal enzymes used for ERT is short because of rapid clearance in liver by carbohydrate-recognizing receptors, particularly the mannose receptor and the mannose-6-phosphate receptor (M6PR) that is highly expressed on Kupfer cells [59].

At present, there are six ERT products currently used for LSD patients. Each is specific for a single disease: Mucopolysaccharidosis I (Hurler disease),

Mucopolysaccharidosis II (Hunter disease), Mucopolysaccharidosis VI (Maroteaux-Lamy syndrome), Fabry's disease, Gaucher Type I and Pompe disease [60-65]. It is important to note that ERT is a symptomatic treatment; in fact, does not treat the disease and, for this reason, it is a lifelong therapy. At the moment, protocols of ERT are effective in lysosomal storage diseases in which there are no neurological symptoms; it has not yet proven to be beneficial in the diseases that have an involvement of central nervous system such as the severe form of Niemann-Pick B disease, Hurler's syndrome and Hunter's syndrome, since the replacement enzymes is reported do not efficiently cross the blood-brain barrier.

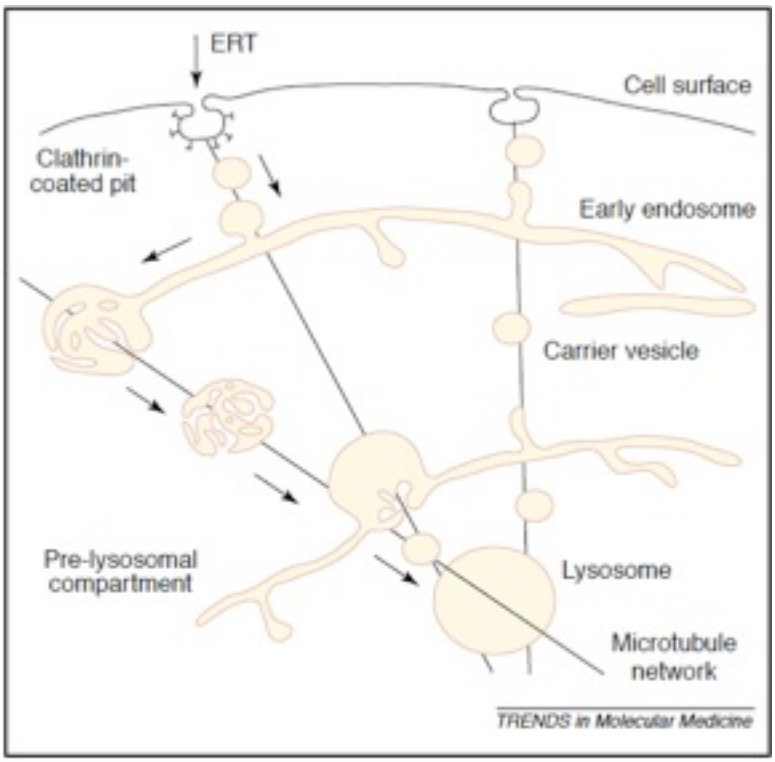

Figure 6: Enzyme-replacement therapy (ERT) and enzyme uptake.
During ERT, the infused enzyme is internalized from circulation via the cell surface, by receptor mediated uptake (for example by Mannose 6-phosphate receptor). The enzyme is translocated through different endosome compartments including and late and early endosomes towards its final destination, the lysosome.

6.1. ERT for MPS diseases

ERT is clinically available for several lysosomal storage diseases, including MPS I [66-68], MPS II [69-70] and MPS VI [71]. Those protocols of ERT have resulted in marked improvement in the visceral organs but little or no improvement in bones and in the brain because the enzymes are not delivered to these tissues effectively. Most of the enzyme-based drugs are delivered to major visceral organs like the liver and spleen and only a small amount of enzyme is delivered to the bones and is able to reach the brain. The major obstacle to translocation of enzyme injected intravenously is the presence of blood brain barrier (BBB), although, ERT at high doses in mouse models of α-mannosidosis (MPSVII) and of metachromatic leukodystrophy leads to the crossing of BBB by enzymes, thereby partially reversing the storage in brain tissues [72-73]. Patients affected by MPS I (phase I/II clinical trial) treated with weekly infusions of 0.53 mg/kg of recombinant α-L-iduronidase (IDUA) showed a dramatic decrease of GAG excretion and decreases in liver and spleen volumes to almost normal values. Moreover, the treatment showed significant improvements in pulmonary function and motor activity.

MPS VI patients are treated with a weekly injection of 1.0 mg/kg galsulfase. The treatment was well tolerated, and produced significant decreases in urinary GAG excretion and improvements in motor performance.

6.2. ERT for MPS II

Hunter syndrome (mucopolysaccharidosis II) is one of these mucopolysaccharidosis for which there is a protocol of ERT available using the human recombinant enzyme idursulfase [70] (Elaprase®, Shire Human Genetic Therapies, Inc., Cambridge, MA, USA). Patients affected by the severe form of MPSII develop progressive neurodegeneration [19,42,45,47-49], ultimately affecting cognitive function and limiting

lifespan. Unfortunately, intravenous administration of ERT does not allow for sufficient enzyme to cross the blood–brain barrier and reach the central nervous system, and patients only show an improvement or stabilization of some somatic signs and symptoms [42].

A protocol of ERT with the recombinant Ids was used to treat a mouse model of MPS II. The results showed that with a weekly dose of idursulfase 0.5 and 1.0 mg/kg for 5 weeks, the MPS II mice had a reduction in urine and tissue GAG levels in a dose dependent manner, although no amelioration was seen in the brain [75].

Based on results obtained in mouse model, a clinical trial of ERT with the recombinant human Ids enzyme was designed for MPS II patients. In a phase I/II clinical trial of 12 patients (double-blind, placebo-controlled trial) three different dosage regimens were used. The enzyme intravenously injected for 24 weeks was well tolerated and produced a significant decrease in urinary GAG, liver and spleen sizes, and improvement in the performance in 6MWT(6 minutes walk test). During the clinical phase II/III study, 96 patients were treated with two dosage regimens, for 1 year double-blind, placebo-controlled trial, using a composite endpoint, including 6MWT, to evaluate efficacy. Once again, the treatment was well tolerated, the patients showed a significative improvement in urinary GAGs levels, a decrease in liver and spleen volumes and increase in 6MWT performance. The results also showed that treatment with idursulfase 0.5 mg/kg weekly produced significantly more improvement than biweekly infusions of the same amount of enzyme.

6.3. The Immuno Response To ERT

One of the major adverse effects of ERT is the immunoresponse or the hypersensitivity reactions to the infused recombinant enzyme [76-79].

In fact, LDS patients do not produce the normal protein, thus, the large dose of normal

lysosomal protein infused in the bloodstream can be recognized as foreign and induce antibodies against itself. Some of the common adverse infusion-related reactions during an ERT include itching and redness at the IV site, edema, hives, and allergic-like symptoms, such as nasal discharge, watery eyes, and generalized itching. Other commonly reported events are chills, rigors, and fatigue. More significant events including chest tightness, respiratory distress, and cardiac arrhythmia could be signs of anaphylaxis.

Decreasing the rate of the infusion together with antihistamines can usually control reactions to the infused enzyme. However, as ERT has only been for available since few years, the long-term adverse effects have not been defined, even though many patients with Gaucher's disease treated with ERT for 15-20 years did not show any significant protein-related adverse events. Patients who have reaction to the infusion of recombinant enzyme can develop two types of antibodies: the IgG and IgE [21,76]. IgG antibodies bind to the recombinant protein and increase the chance for mild to moderate infusion reactions. IgE antibodies, on the other hand, increase the risk for more serious anaphylactic reactions. Some patients who initially improve during therapy may seem to later regress/redevelop previously resolved symptoms.

ERT treatment for all of three MPS disorders is generally well tolerated [76,80]. Except for Gaucher's disease (12%), the percentage of patients that develop antibodies against any of the recombinant enzymes is ≥50%, these IgG antibodies are usually not associated with typical allergic reactions. In only one case, a patient with MPS I, treatment been interrupted for a significant period of time as a result of a severe infusion-related adverse reaction. Except for Gaucher's disease the percentage of people receiving ERT who become IgG antibody positive ranges from 50% - 90%. The conversion rate in MPS I (Aldurazyme) is 59%-90%; MPS II [81] (Elaprase) is 50%, and MPS VI (Naglazyme) is 90%.

7. MPS II mouse model

The knock-out mouse model ($Ids^{y/-}$) of MPSII was created by replacing a portion of the Ids gene (exon 4 and part of exon 5 were deleted) with the neomycin resistance gene [82-83]. Disruption of the Ids gene resulted in a loss of Ids enzyme activity, high urinary GAG levels and GAGs accumulation in visceral tissues and in the brain, compared to wild type mice. The onset of the gross morphological phenotype was clearly manifested at 3–4 months of age, and it became progressively severe through their adult lives; the affected mice usually died by 60–70 weeks of age. This phenotype includes skeletal abnormalities, craniofacial abnormalities, such as thickened digits, swollen hocks, and distorted faces (Figure 7). This mouse model mimics the severe form of human MPS II.

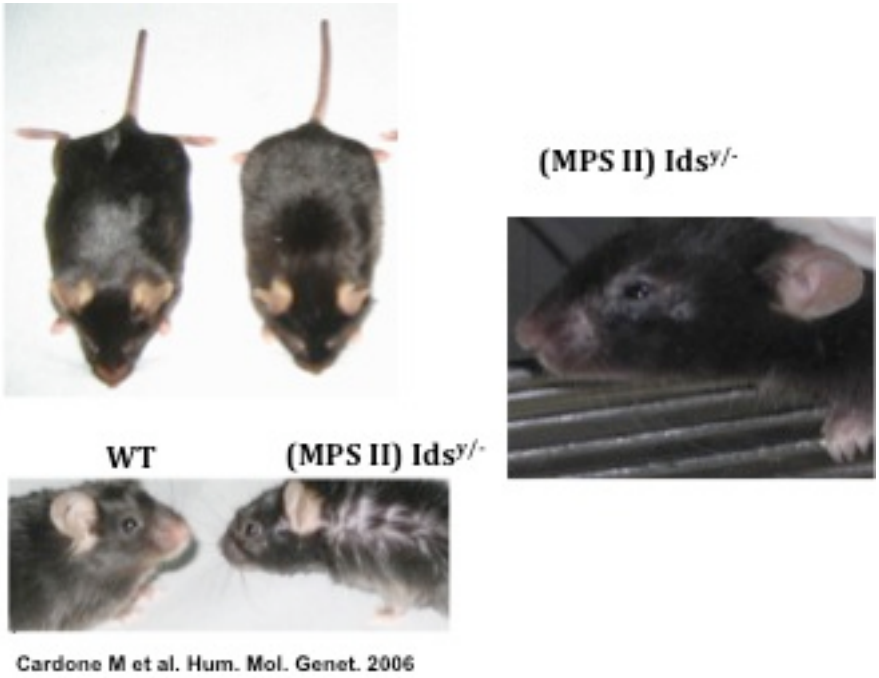

Figure 7: Phenotype of MPS II mouse model

MATERIALS AND METHODS

1. Animals

Female heterozygous MPSII mice were used, as described previously (83)

2. Blood and tissue collection

Blood (50 µl) was collected in EDTA at different times after the injections (months 1, 3, 5 and 7; T1, T3, T5 and T7) of the treated mice and the untreated MPSII ($Ids^{y/-}$) and wild-type (control) mice. Injected human Ids (Elaprase) was kindly provided by Shire Human Genetic Therapies, Inc., Cambridge, MA, USA. The blood was centrifuged at 10 000×g for 10 min at 4°C, and the serum (supernatant) was used for enzyme assays. Tissues were collected at the end of each treatment from the treated mice and in parallel from the untreated MPSII and wild-type mice. The mice were anesthetized and sacrificed by cardiac perfusion: the left ventricle was cannulated, an incision was made in the right atrium and the mice were perfused with 40 ml of phosphate-buffered saline (PBS). The organs were collected, and half of each was fixed (for Alcian blue staining and immunohistochemistry or immunofluorescence), and the other half of each was frozen in dry ice before being processed for the Ids activity assay.

3. Ids activity assay

The tissues for analysis were homogenized in water. Serum and tissue protein concentrations were determined using the Bio-Rad colorimetric assay (Bio-Rad, Hercules, CA, USA). The Ids assay was performed using 50 µg total protein extract was incubated with 20 µl of the fluorogenic substrate, 4-methylumbelliferyl-α-iduronide-2-sulfate (Muscerdam Substrates), for 4 h at 37°C. Then, 10 µl purified α-iduronidase from rabbit liver (Muscerdam Substrates) and 40 µl McIlvain's buffer (0.4 M Na-phosphate/0.2 M Na-citrate, pH 4.5) were added to the reaction mixture,

which was then incubated for an additional 24 h at 37°C. The reaction was stopped by adding carbonate stop buffer (0.5 M $NaHCO_3$/0.5 M Na_2CO_3, pH 10.7), and the fluorescence of the 4-methylumbelliferone liberated was measured using 365 nm excitation and 460 nm emission in a fluorimeter (BIO-RAD VersaFluor Fluorometer). The enzyme activities were expressed as nmol/4 h/mg protein, as calculated through the standard curve of the fluorogenic substrate, 4-methylumbelliferyl-α-iduronide (Sigma-Aldrich).

4. Alcian blue staining

After the perfusion of the mice with PBS, the tissues were collected and fixed in methacarn solution (30% chloroform, 60% methanol and 10% acetic acid) for 24 h at 4°C. The next day, the tissues were embedded in paraffin (Sigma-Aldrich) after their dehydration through a 70–100% ethanol gradient. Finally, the tissues were sectioned into 7 μm thick serial sections. The tissue sections were stained with 1% Alcian blue (Sigma-Aldrich) in hydrochloric acid. The counterstaining was performed for 2 min with Nuclear-Fast red (Sigma-Aldrich).

5. Immunohistochemistry and immunofluorescence

Mice brains were collected after PBS perfusion and fixed with 10% neutral buffered formalin, pH 7.0, for 12 h at 4°C. Then the brains were embedded in paraffin (Sigma-Aldrich) and dehydrated through a 70–100% ethanol gradient. Immunohistochemistry and immunofluorescence analyses were performed on 7 μm thick serial sections. The specimens were incubated for 1 h with blocking solution [Tris-buffered saline, 0.2% Tween-20 (Sigma-Aldrich) and 10% normal horse serum, Vectastain Elite ABC kit] before incubation overnight with the primary antibodies.

For immunohistochemistry analyses of Lamp2 and ubiquitin of the paraffin-

embedded, formalin-fixed brains, the avidin-biotin complex (ABC) method was used (Vectastain Elite ABC kit). A monoclonal rat antibody against murine Lamp2 (diluted 1:100; Santa Cruz Biotechnology, Inc., CA, USA) and a polyclonal rabbit antibody against murine ubiquitin (diluted 1:50; Abcam, Cambridge, UK) were used. Then, secondary biotinylated horse anti-rat and anti-rabbit IgG and streptavidin–biotin–peroxidase complex (Vectastain Elite ABC kit) were used for 1 h of incubation (for anti-Lamp2 and ubiquitin). The color was developed using the ABC Elite Vector Staining kit and the horseradish peroxidase substrate (Vector Laboratories, Inc., Burlingame, CA, USA). For the detection of apoptotic cells in the brain sections, TUNEL staining kits (Chemicon International) were used, according to the manufacturer's instructions.

Immunofluorescence analyses were carried out for the detection of NeuN, GFAP and CD68 and for the co-localization signal of Lamp2-hIds. A monoclonal mouse antibody against murine NeuN (diluted 1:200; Abcam), a monoclonal rabbit antibody against murine GFAP (diluted 1:400; Sigma-Aldrich), a monoclonal rat antibody against murine CD68 (diluted 1:250; AbD Serotec) and an antibody against human Ids (hIds, Shire Pharmaceuticals, Boston, MA, USA) were used for the detection of co-localization signals between Lamp2-hIds. After washing, the sections were incubated for 1 h with secondary antibodies (Molecular Probes, Invitrogen, CA, USA). Stained sections were mounted with Vectashield with DAPI (Vector Laboratories, Inc.).

6. Staining quantification

All analyses were conducted blindly with no knowledge of the genotype of the animals. A series of sections (every sixth section throughout the rostrocaudal extent of the brain except olfactory bulb) with a random start to ensure an equal probability of being chosen for sampling was labeled with antibodies to Ubiquitin, GFAP, Tunel, NeuN. The staining signals were processed in imageJ software. For the For the

quantification of Purkinje cells of the cerebellum, serial parasagittal sections were stained with antibody to Calbindin and the number of Calbindin-positive Purkinje cells were counted in 40th section over the entirety of each cerebellar.

7. Electron microscopy

The cerebellum was excised from 10-month-old treated mice and untreated MPSII and wild-type mice and fixed in 1% glutaraldehyde in 0.2 M HEPES buffer. Then small blocks of the cerebellum tissue were cut and post-fixed in uranyl acetate and in OsO_4. After dehydration through a graded series of ethanol, the tissue samples were cleared in propylene oxide, embedded in the Epoxy medium (Epon 812) and polymerized at 60°C for 72 h. From each sample, semi-thin sections were cut with a Leica EM UC6 ultramicrotome and mounted on glass slides for light microscopic inspection to identify the Purkinje and granular cell layers. Ultrathin (70 nm thick) sections of the area of interest were obtained. Electron microscopic images were acquired from thin sections using an FEI Tecnai-12 electron microscope equipped with an ULTRA VIEW CCD digital camera (FEI, Einhoven, The Netherlands). Quantification of the lysosome-like organelle dimensions was performed using the AnalySIS software (Soft Imaging Systems GmbH, Munster, Germany).

8. Quantitative analysis of GAG accumulation in the urine

Urine from individual mice was collected in metabolic cages at the end of each treatment and from the untreated MPSII and wild-type mice. GAG levels in the urine were determined using the dimethylmethylene-blue-based spectrophotometry of GAGs[84]. These were normalized to the creatinine content. Urine creatinine was measured using Creatinine Assay kits (Quidel Corporation, San Diego, CA, USA). Absorbance was read at 490 nm. Urinary GAG was expressed as milligram

GAG/milligram creatinine.

9. Open-field and rotarod tests

The motor and the exploratory behaviors of treated mice were assessed in an acrylic open arena, as described previously[84]. The open-field test was performed (between 09:00 and 11:00 h) using the open-field apparatus (60 cm × 60 cm × 40 cm). The floor of the wooden arena was divided equally into squares marked by red lines. In this test, the treated mice and the untreated MPSII and wild-type mice were placed individually in the center of the arena and allowed to explore freely. The number of crossings (squares crossed with all paws) and rearings (rising of the front paws) was recorded during the test period of 10 min. This apparatus was cleaned with a detergent and dried after occupancy by each mouse.

The rotarod test is designed to assess the sensory motor coordination, balance, equilibrium and motor learning [85]. The treated mice and the untreated MPSII and wild-type mice were placed on top of the rotating rod facing away from the experimenter, in the orientation opposite to that of the rod rotation. The latency times for the mice to fall from the rod were recorded automatically by the apparatus. For the first day of the test, the mice were placed on the rotating rod set at the steady slow speed of 4 rpm and trained to remain on the rod for 60 s. After this habituation trial, each mouse was tested in four trials per day, for 3 consecutive days, with an inter-trial interval of 30 min. The rotarod apparatus (Ugo Basile, Italy) accelerates gradually from 4to 40 rpm. The cut-off time was 600 s for the trials.

10. Electroretinograms recordings and Magnetic Resonance Imaging

These experiments were performed in collaboration with Dr. Surace at Tigem.

ERGs were performed on MPSII and WT mice. Briefly, the animals were dark adapted

for 3 hours and then anesthetized and placed in a stereotaxic apparatus under dim red light. ERGs were evoked by flashes of different light intensities ranging from 10^{-4} to 20 cd · m^{-2} · s^{-1} generated through a Ganzfeld stimulator (Lace Elettronica, Pisa, Italy). To minimize the noise, three different responses evoked by light were averaged for each luminance step (the time interval between light stimuli was 4 to 5 minutes). The electrophysiological signals were recorded through gold plate electrodes inserted under the lower eyelids. Electrodes in each eye were referred to a needle electrode inserted subcutaneously at the level of the corresponding frontal region. The different electrodes were connected to a two-channel amplifier. Amplitudes of a- and b-waves were plotted as a function of increasing light intensities. After completion of responses obtained in dark-adapted conditions, the recording session continued with the purpose of dissecting the cone pathway mediating the response to light. For this purpose, the ERG in response to light of 20 cd · m^{-2} was recorded in the presence of a continuous background light set at 15 cd · m^{-2}. The amplitude of the b-wave for each eye was plotted as a function of luminance (transfer curve) under scotopic and photopic conditions. For each group, the mean b-wave amplitude was plotted.

The experiments of MRI were performed in collaboration with Prof. Brunetti, II Policlinico di Napoli,

11. Statistical analyses

The statistical significance was determined for the measurements compared by the analysis of variance (one way or two way ANOVA) test.

RESULTS

1. Longitudinal characterization of neuropathological features in MPS II mice.

Patients affected by the severe form of MPS II are characterized by a dramatic CNS phenotype. Indeed, they show mental retardation, hydrocephalus and progressive neurodegeneration in all brain regions. Our laboratory has already reported on the histopathological features of MPS II mice ($Ids^{y/-}$) [82]. In the present study, we analyzed the time course of the neurodegenerative process in MPS II animals. To do this we sacrificed groups of animals at different ages, specifically we analyzed MPS II mutants and WT littermates at 1, 3, 6 and 12 month of age (Figure 8 A-B). Paraffin serial sections (7mm) were prepared and processed for immunohistological analyses. The analyses reported in these studies were performed in two major structures; the cortex and the cerebellum. The Alcian Blue staining, which labels GAGs storages in lysosomes, revealed an already strong accumulation of GAGs in 1 month-old mice independent of the brain region tested; these GAGs aggregates were dramatically aggravated as mice aged (Figure 8 A).

GAGs aggregates in neurons lead to blockade of the proteasome and in an increase in protein ubiquitination. Ubiquitin positive neurons started to be detected in 1 month-old cortex of MPSII mice; which by 12 months contained 95% of ubiquitin-positive neurons (Figure 8 A-B). In addition, we observed a gradual increase of gliosis as shown by immunostaining using anti-GFAP antibodies, a marker of astrocytes. Indeed, in 1-month-old mice we quantified a 13% increase of GFAP-positive cells in the cortex, which in 12-month-old mice reached 90% increase, as compared to WT littermates. In parallel to gliosis, we observed a strong increase of apoptotic cells in MPSII mice, as indicated by Tunel-staining of brain sections. Apoptosis was first detected in 3 month-old mice and became dramatic by 12 month, where 75% of cells were Tunel-positive.

To quantify the number of neurons in MPS II mice, we stained serial sections with an antibody that specifically recognizes neuronal nuclei, NeuN. Quantification of NeuN-positive cells in the cortex of MPSII mice, showed that starting at 1 month of age, these mice had a 10% reduction of neurons as compared to WT mice; this percentage increases to 78% in 12 month-old mice (Figure 8 A-B).

We then analyzed a second brain structure, the cerebellum by analyzing the only output neurons of the cerebellar cortex, the Purkinje cells (PCs). We followed the decrease in the number of Purkinje cells in MPS II mice by immunostaining, using the anti-Calbindin antibody. At 3 months of age, we observed a decrease of 20% in the number of PCs, which reached 65% in 12 month-old mice (Figure 9 A-B).

A

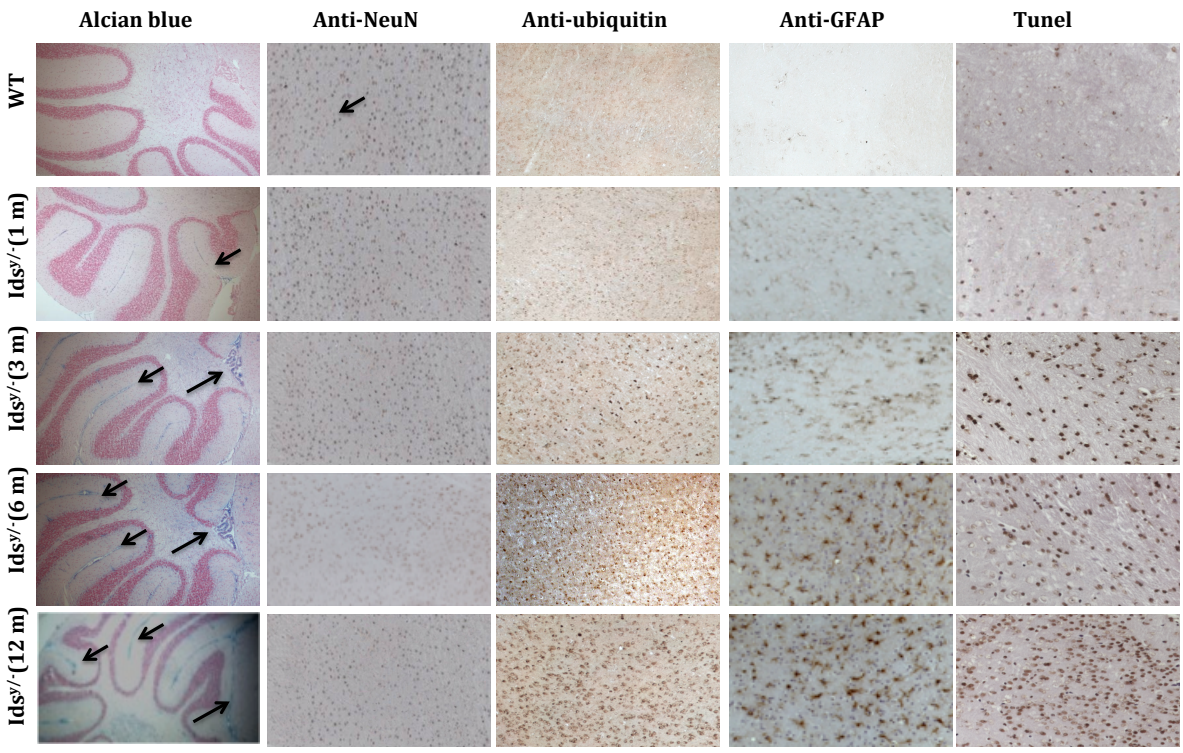

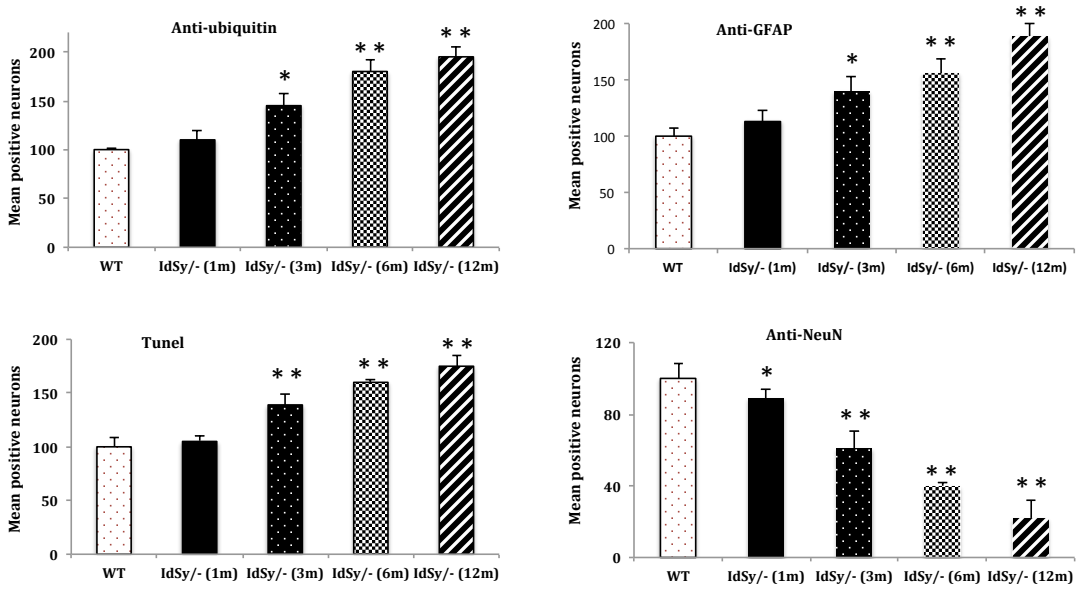

Figure 8: Histopathological characterization of brain of MPS II mice.
Longitudinal analysis of GAGs accumulation and CNS marker expression in serial brain sections of 1, 3, 6 and 12 month old MPS II (*Ids*$^{y/-}$) and control WT mice (n=8 per age group) **(A)** Representative pictures of: i) Alcian Blue staining (cerebellum) revealing a progressive GAGs accumulation in the MPS II (Ids$^{y/-}$) mice; ii) Progressive loss of NeuN-positive cells in the cortex in MPS II mice as compared to littermates; iii) Representative pictures (cortex) of immunostainings performed using anti-ubiquitin, anti-GFAP and Tunel. These analyses show a progressive increase with time of ubiquitinated proteins, gliosis and apoptotic cells in most of the region analysed in MPS II mice as compared to WT. Magnification 10X **(B)** Quantification of immunostainings shown in (A) using the ImageJ software (NIH)(statistics were performed by ANOVA; p: * <0.05 **<0.01).

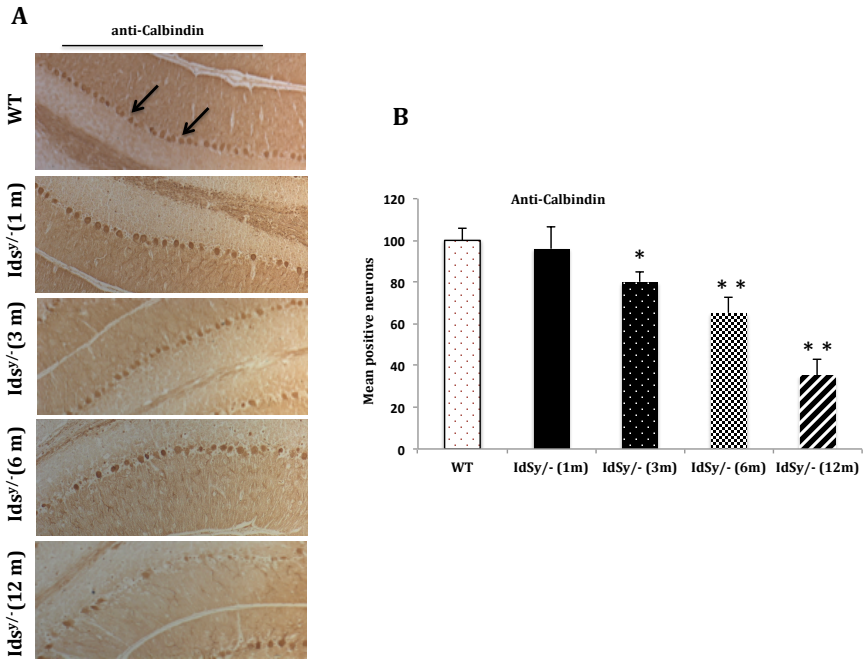

Figure 9: MPS II show a progressive loss of Purkinje cells.

(A) Representative images of immunostaining performed using the anti-Calbindin antibody on serial brain sections from 1,3,6 and 12 month-old MPS II (*Ids*$^{y/-}$) and control WT mice (n=8 per age group) (B) Quantification of PC number in the cerebellum lobi. in MPSII mice as compared to WT littermates at the different time point. Stainings revealed a progressive reduction of the numbers of PCs with time. PC number decreased with age, from 20% in 3 month old to 65% in 12 month old MPS II mice as compared to age-matched WT siblings (ANOVA; p: * <0.05 **<0.01).

2. MPS II mice are characterized by motor impairments.

To investigate whether the progressive neurodegeneration affects the behavioral phenotype of MSPII mice, we subjected these mice together with their WT littermates to different behavioral paradigms.

First, we analyzed motor performances, by testing MPS II mice at two different time points, 3 and 6 months of age using the rotarod and the open field tests [84-85] (Figure 10 A-C). We did not analyze older animals since the neurodegenerative process is so elevated and widespread that the behavioral deficits can no longer be assigned only to CNS impairments, but also to other systems.

The rotarod test is a behavioral test that measure motor coordination and motor learning. A good performance in this test excludes cerebral and cerebellar defects.

Animals were exposed to the rotarod for 4 consecutive 10 minutes sessions and the better performance was used to analyze the behavior; furthermore, to analyze motor learning, animals were tested on the rotarod for 3 consecutive days.

6 month-old MPS II mice showed a latency to fall time significantly lower compared to WT mice, indicating that MPS II animals at this time point had an evident motor deficit as well as a poorer motor learning. Interestingly, this motor impairment was absent in younger mice (3 month-old), indicating a late-onset of the motor deficit. When these same groups were tested in the open-field to test the overall locomotor activity (Figure 10 B-C), we found, similarly to the rotarod results, a clear phenotype in 6-month-old, but not in younger mice. MPS II mice (6-month-old) showed a strong impairment in the horizontal and vertical activities; MPS II animals showed an average 32% decrease of motor activity than control littermates (Figure 10 B-C).

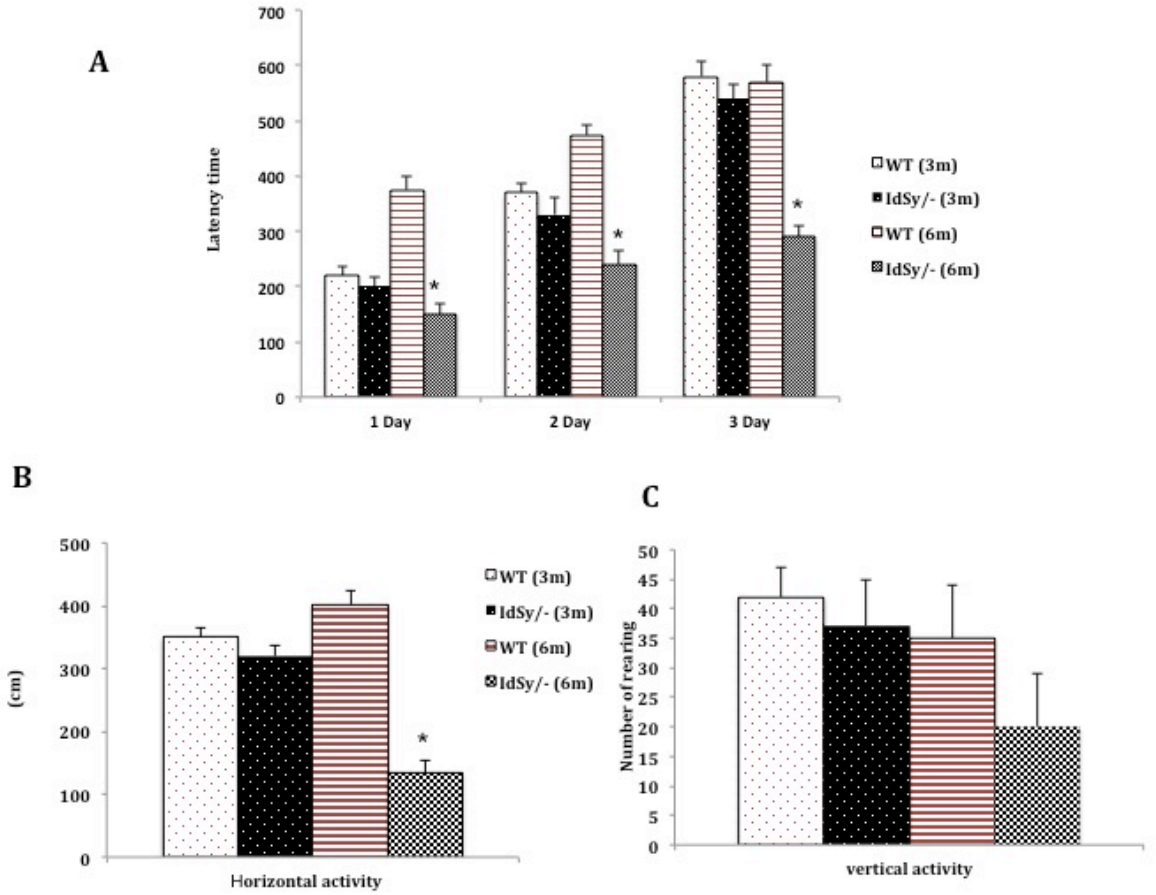

Figure 10: Behavioral characterization of MPS II mice.

Motor behavior in 3 and 6 month old WT (n = 8) and MPS II mice ($Ids^{y/-}$) (n = 8 for group) was analyzed by the rotarod **(A)** and the open field **(B-C)** tests. **(A)** The rotarod test was performed for 3 consecutive days and revealed, in 6 month old MPS II mice, a clear motor deficit shown by lower latency to fall as compared to WT animals. **(B)** In the open-field test, the number of crossings **(B)** and rearings **(C)** were evaluated. 6 month old MPS II mice showed impairment in horizontal (B) and vertical (C) activities as compared to the littermates. The error bars indicate standard deviations. (ANOVA; p: * <0.05).

3. MPS II mice present a progressive reduction of retinal functions.

MPS II A patients, during the progression of the disease, show a gradual retinal degeneration that eventually leads to the blindness [19,42,45]. To assess the retinal function of MPS II mice, we exposed 3-6-12 month-old mice to a single-flash electroretinograms (ERGs) [86]. ERGs recordings allow the assessment of the electrical responses of a number of cell types, which include rods on bipolar cells (scotopic b-waves), rods (dark adapted a-waves) and cones on bipolar cells (photopic b-waves). This analysis was conducted in collaboration with Dr. Surace at TIGEM.

In all time points analyzed, scotopic ERGs b-wave and a-wave amplitudes were significantly reduced in the MPS II mice as compared to age-matched controls, across a wide range of stimulus intensities (Figure 11). These data indicate a severe decrease (approximately 45%) in retinal functions in MPS II mice at 3 months of age compared to wild type mice. The photoreceptor dysfunction became gradually more severe to finally reach a 75% reduction in 12 month-old mice as compared to control siblings.

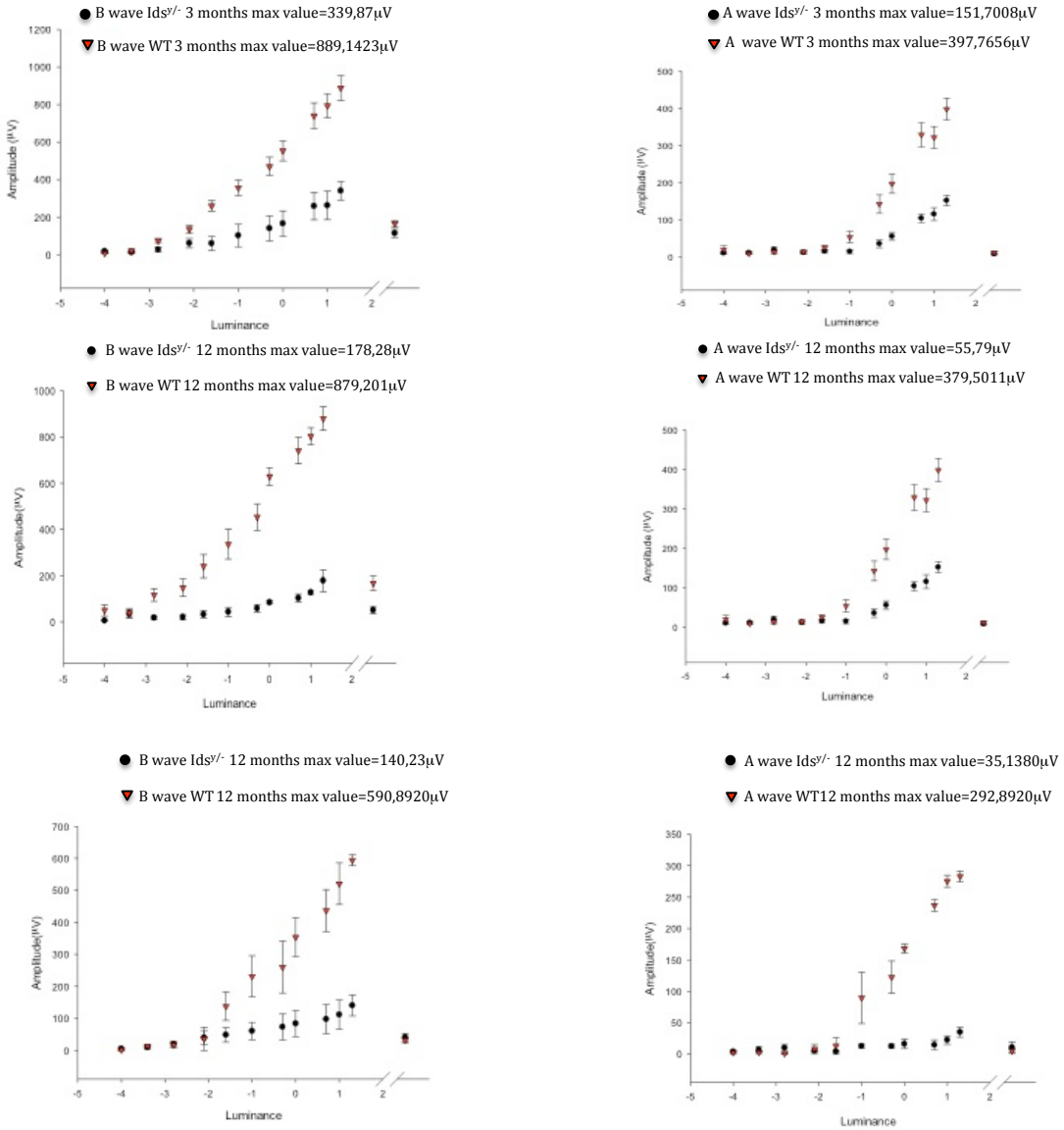

Figure 11: Representative ERGs recorded from MPS II (Ids$^{y/-}$) mice and WT mice at 3, 6 and 12 month-old. In 3-month-old mice, the dark-adapted b-wave amplitudes of the (Ids$^{y/-}$) mouse decrease of 45% as well as the a-wave amplitudes as compared to the age-matched control. In 12-month-old mice, the dark-adapted b-wave a-wave amplitudes of MPS II (Ids$^{y/-}$) mouse are dramatically reduced compared to WT mice.

4. MPS II mice present ventricular atrophy.

Hydrocephalus is a condition found in MPS II patients with a consequent ventricles enlargement and atrophy of brain regions [48-49]. To study whether MPS II mice showed the same pathological feature, 12 month-old mice were subjected to MRI.

The result of MRI showed dilatation and atrophy in the lateral and IV ventricles of MPS II mice as compared to wild type mice (Figure 12). Analysis performed on younger animals did not show significative difference between MPS II and control littermates.

Altogether, these data indicate that the MPS II mouse is a good animal model for the human MPS II A disorder. Thereby, they represent a useful model to test therapeutic approaches in preclinical studies.

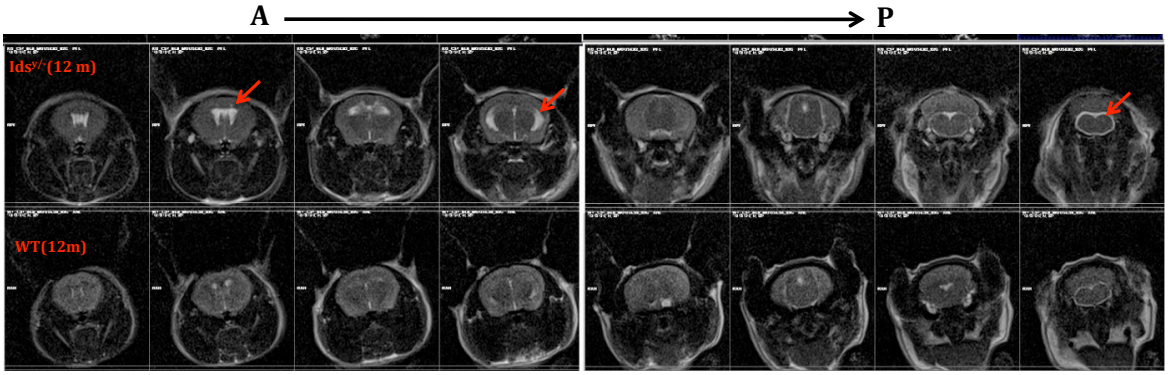

Figure 12: MPS II mice present ventricular atrophy. MRI analyses showed ventricular enlargment of the brain of 12 month old MPS II mice as compared to WT mice.

5. From characterization to therapy: Ids activity can be partially rescued in the brain of MPSII mice using the enzyme replacement therapy (ERT).

ERT has been used to treat MPSII patients, although to date this approach is unable to rescue the brain defects because the infused Ids is unable to cross the blood brain barrier (BBB) [42]. It is thus imperative to develop an efficient therapy to treat the CNS symptoms. Ideally, having circulating Ids that crosses the BBB would be highly preferred and would provide treatment of both visceral and CNS defects, simultaneously. The BBB is formed by a layer of endothelial cells of the brain microvasculature that regulates the passage of molecules between the blood and the CNS. Tight junctions block the passage of most molecules, except some specific substances that cross the BBB via receptor-mediated transport.

Thus, we tested different ERT protocols to study if systemic infusion of Ids (idursulfase Elaprase®)enzyme can deliver the enzyme through the BBB to the brain and prevent or cure the CNS degeneration. Since high doses of the infused enzyme can generate toxicity and immunoresponses, these treatments used in my study were designed to identify the minimal Ids dose and the longest treatment-interval time sufficient to treat the CNS phenotype of MPSII mice.

We used four protocols of ERT (A-D): (A) adult MPSII mice at 2 months of age were injected via the tail vein with human Ids doses at 10, 5 or 1.2 mg/kg, every other day (indicated as 1–2 in Table 1), for a total period of 1 month. Groups of untreated, age-matched, MPSII and wild-type mice were used as controls. (B) Adult MPSII mice at 2 months of age were injected via the tail vein with human Ids at dose 1.2 mg/kg, once every 4 days (1–4 Table 1) and once every 7 days (1–7 Table 1), for a total period of 1 month. Groups of untreated, age-matched, MPSII and wild-type mice were used as controls. (C) Adult MPSII mice at 7 months of age were injected via the tail vein with human Ids at dose 10 mg/kg via the tail vein, every other day (1–2 Table 1), once

every 4 days (1–4 Table 1) and once every 7 days (1–7 Table 1), for a total period of 3 months. Groups of untreated, age-matched, MPSII and wild-type mice were used as controls. (D) Adult MPSII mice at 3 months of age were treated for 7 months (the longest period) with injection, via the tail vein, of human Ids at doses of 1.2 mg/kg, once every 7 days (1–7 Table 1). Groups of untreated, age-matched, MPSII and wild-type mice were used as controls.

During the treatment times, the plasma Ids activity was measured in of all treated mice every other month from T1 to T7 (months 1, 3, 5 and 7) four hours after the last injection. The Ids plasma activity in the MPS II treated mice was extremely high, even higher than the activity measured in the wild type control mice. Interestingly, group D animals treated with Ids for the longest time, after 7 months showed very high plasma Ids activity compared to wild-type control (8.7-fold higher in treated MPS II versus WT mice) (Table 1). Then, we measured, in all groups, the plasma Ids activity 48 h after each injection. The results showed that the Ids activity was higher (from 4- to 11-fold, depending on treatments) than in the untreated MPSII mice and comparable to levels measured in the untreated wild-type mice (Table 2). The Ids activity returned to the level measured in the untreated MPSII mice 72 hours after the last injection of each treatment protocol (Figure 13). These results clearly show that Ids enzyme is very stable and remains at high levels for a long time in the plasma of the MPSII treated animals.

Plasma IDS activity (nmol/4h/ mg) - after 4h	1 Month	3 Month	5 Month	7 Month
wt	320 ± 27	243 ± 32.1	220 ± 36.2	198 ± 18.9
Ids $^{y/-}$	27± 1.5	24 ± 0.6	18 ± 1.1	20 ± 1.3
Ids $^{y/-}$+ 10 mg/kg IDS (1-2)	10938 ± 779			
Ids $^{y/-}$+ 5.0 mg/kg IDS (1-2)	7500 ± 447			
Ids $^{y/-}$+ 1.2 mg/kg IDS (1-2)	2790 ± 226			
Ids $^{y/-}$+ 1.2 mg/kg IDS (1-4)	1810 ± 151			
Ids $^{y/-}$+ 1.2 mg/kg IDS (1-7)	1877 ± 136			
Ids $^{y/-}$+ 10 mg/kg IDS (1-2)	9292 ± 611	6957 ± 557		
Ids $^{y/-}$+ 10 mg/kg IDS (1-4)	7471 ± 118	6459 ± 301		
Ids $^{y/-}$+ 10 mg/kg IDS (1-7)	6642 ± 389	6633 ± 390		
Ids $^{y/-}$+ 1.2 mg/kg IDS (1-7)	2828 ± 198	2551 ± 215	2212 ± 26	1724 ± 193

Table 1. Plasma Ids activities according to mouse treatment groups, 4 h after last treatment. Ids activity was measured at different time-points (T1-T3-T5-T7) (1, 3, 5, 7 months during the treatments, respectively), 4 hours after the administration of hIds protein, in the plasma of wt (*n* = 5), *Ids*$^{y/-}$ (*n* = 5) and *Ids*$^{y/-}$ injected with 10, 5.0, 1.2 mg/kg one other days (*n* = 7 for each treatment), *Ids*$^{y/-}$ injected with 1.2 mg/kg one each 4 and each 7 days (*n* = 7 for each treatment), *Ids*$^{y/-}$ injected with 10 mg/kg one other day, one each 4 and each 7 days (*n* = 7 for each treatment), *Ids*$^{y/-}$ injected with 1.2 mg/kg one each 7 days (*n* = 4) treated mice.

IDS activity (nmol/4h/mg)	T1	T3	T5	T7
wt	320 ± 27	243 ± 32.1	220 ± 36.2	198 ± 18.9
Ids $^{y/-}$	27 ± 1.5	24 ± 0.6	18 ± 1.1	20 ± 1.3
Ids $^{y/-}$+10 mg/kg IDS (1-2)	271 ± 74			
Ids $^{y/-}$+5.0 mg/kg IDS (1-2)	296 ± 54			
Ids $^{y/-}$+1.2 mg/kg IDS (1-2)	217 ± 38			
Ids $^{y/-}$+1.2 mg/kg IDS (1-4)	105 ± 27			
Ids $^{y/-}$+1.2 mg/kg IDS (1-7)	116 ± 46			
Ids $^{y/-}$+10 mg/kg IDS (1-2)	208 ± 11	192 ± 12		
Ids $^{y/-}$+10 mg/kg IDS (1-4)	204 ± 10	183 ± 10		
Ids $^{y/-}$+10 mg/kg IDS (1-7)	210 ± 30	156 ± 37		
Ids $^{y/-}$+1.2 mg/kg IDS (1-7)	214 ± 90	216 ± 94	169 ± 46	159 ± 38

Table 2. Plasma Ids activities according to mouse treatment groups, 48 h after last treatment. Ids activity was measured at different time-points (T1-T3-T5-T7) (1, 3, 5, 7 months during the treatments, respectively), 4 hours after the administration of hIDS protein, in the plasma of wt (*n* = 5), *Ids*$^{y/-}$ (*n* = 5) and *Ids*$^{y/-}$ injected with 10, 5.0, 1.2 mg/kg one other days (*n* = 7 for each treatment), *Ids*$^{y/-}$ injected with 1.2 mg/kg one each 4 and each 7 days (*n* =

7 for each treatment), *Ids*$^{y/-}$ injected with 10 mg/kg one other day, one each 4 and each 7 days (*n* = 7 for each treatment), *Ids*$^{y/-}$ injected with 1.2 mg/kg one each 7 days (*n* = 4) treated mice.

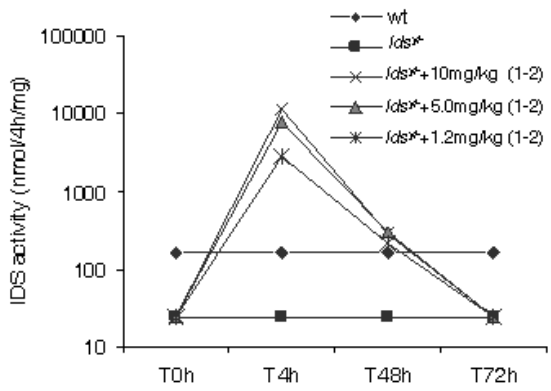

Figure 13: Determination of the half-life of the Ids enzyme after ERT. Plasma Ids activity in MPS II mice following ERT, analyzed 4, 48 and 72 hr after the last injection. The Ids activity returned to the level measured in the untreated MPSII mice 72 hours after the last injection of each treatment protocol.

6. Ids supplied by ERT crosses the blood brain barrier.

To investigate if the ERT protocols used were able to deliver Ids in the brain through the blood brain barrier and restore Ids activity in brains of the treated MPS II mice (groups A–D), these animals and the controls (MPS II untreated and wild-type mice) were sacrificed 4 h after the final administration of Ids of each treatment protocol (Figure 14 A-D).

The animals of group A showed brain Ids activities that decreased in parallel with the concentrations of Ids injected. Interestingly, with the administration of the lower dose of Ids (1.2 mg/kg), some enzymatic activity was still detected in the brains of the treated MPSII mice (Figure 14 A). It is important to note that in the animals of group B, treated with the lower dose 1.2 mg/kg for longer time intervals of treatment, every 4 and 7 days showed levels of Ids activities comparable to those measured in the mice of group A injected every other day (Figure 14 B). Mice belonging to the protocol treatment C showed that the infusion of higher dose (10 mg/kg) of enzyme in older

MPSII mice allowed to detect some Ids activity in the brain, although these animals received the enzyme only once every 7 days for 3 months (Figure 14 C). Moreover, MPSII mice of group D treated every 7 days with lower dose of enzyme (1.2 mg/kg) for 7 months showed Ids activity in their brains although the activity was not very high (Figure 14 D). Thus, these data showed that all of the ERT protocols used were effective, because in each of them it was possible to detect a higher Ids activity than in MPS II untreated animals indicating that infused Ids crossed the blood brain barrier. Interestingly, even in MPSII mice treated with the lowest Ids dose (1.2 mg/kg) once every 7 days, the Ids activity measured in the brains was higher than that of untreated MPS II littermates. It is important to note that, as expected, the Ids activity in the brain in all the treated groups was lower than that measured in wild-type mice.

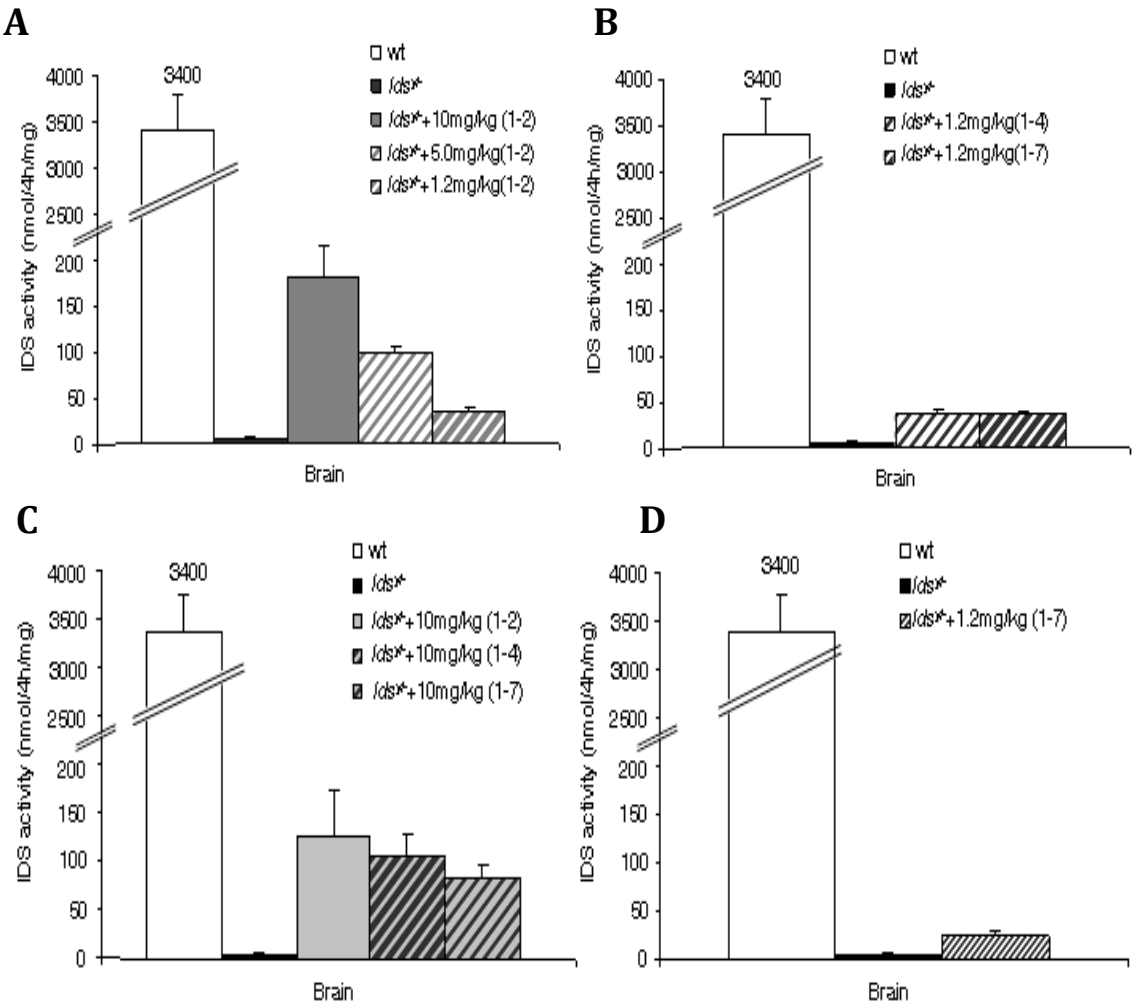

Figure 14: Ids activity measured in the brain homogenates of *Ids*$^{y/-}$ mice following ERT. **(A-D)** Ids activity was measured in the protein extracts of wt (n = 5), *Ids*$^{y/-}$ (n = 5), *Ids*$^{y/-}$+10, 5.0, 1.2 mg/kg; 1-2 days) (n = 7 for each treatment), *Ids*$^{y/-}$+1.2 mg/kg; 1-4, 1-7 days (n = 7 for each treatment), *Ids*$^{y/-}$+10 mg/kg; 1-2, 1-4, 1-7 days (n = 7 for each treatment), *Ids*$^{y/-}$+1.2 mg/kg; 1-7 days (n = 4) mice injected via tail-vein with hIds protein and sacrificed respectively 4 hours after the last administration. The duration of treatments was of 1 month in 2 month-old *Ids*$^{y/-}$ mice **(A, B)**, of 3 months in 7 month-old *Ids*$^{y/-}$ mice **(C)** and of 7 months in 3 month-old *Ids*$^{y/-}$ mice **(D)**. The error bars indicate standard deviations. $P < 0.05$ (with ANOVA test).

7. Ids activity is present in all visceral tissues after ERT.

We measured the Ids enzyme activity in homogenates of visceral tissues (liver, kidney, lung, spleen, heart and skeletal muscle) of the MSP II treated mice and of the controls untreated MPSII and wild-type mice, belonging to all the ERT protocols used (Figure 15 A-D). This analysis showed that the tissue Ids enzymatic activity was always higher than that measured in the untreated MPSII mice. Surprisingly, Ids activity in

peripheral organs was also higher than that measured in the tissues of the wild-type siblings, with the exception of the muscle.

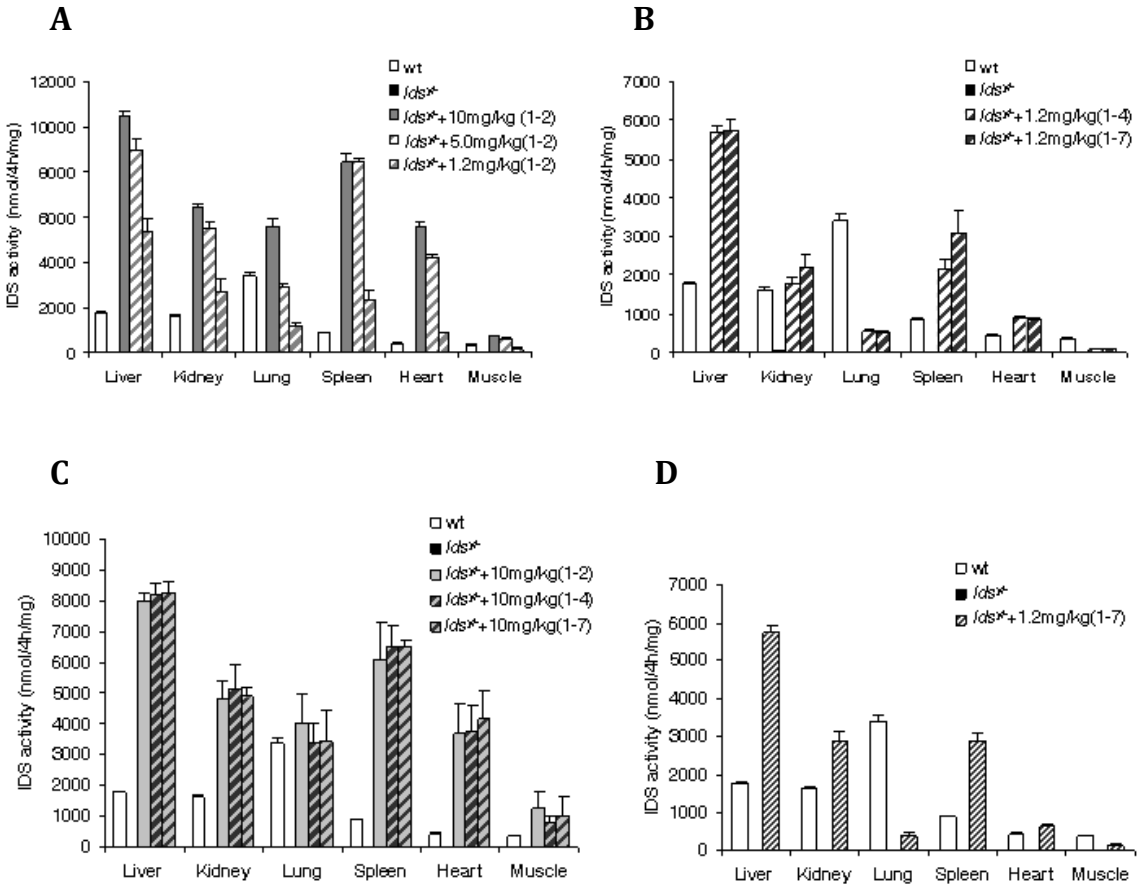

Figure 15: Ids activity measured in the visceral tissues of *Ids*$^{y/-}$ treated mice following ERT. (A-D) Ids activity was measured in the protein extracts of wt (n = 5), *Ids*$^{y/-}$ (n = 5), *Ids*$^{y/-}$ +10, 5.0, 1.2 mg/kg; 1-2 days (n = 7 for each treatment), *Ids*$^{y/-}$+1.2 mg/kg; 1-4, 1-7 days (n = 7 for each treatment), *Ids*$^{y/-}$+10 mg/kg; 1-2, 1-4, 1-7 days (n = 7 for each treatment), *Ids*$^{y/-}$+1.2 mg/kg; 1-7 days (n = 4) mice injected via tail-vein with hIDS protein and sacrificed 3 hours after the last administration. The duration of treatments was respectively of 1 month in 2 month-old *Ids*$^{y/-}$ mice **(A, B)**, of 3 months in 7 month-old *Ids*$^{y/-}$ mice **(C)** and of 7 months in 3 month-old *Ids*$^{y/-}$ mice **(D)**. The error bars indicate standard deviations. $P < 0.05$ (with ANOVA test).

8. The Ids enzyme co-localizes with lysosome markers in the brain.

To confirm the presence of the Ids enzyme in the brain of treated mice, we performed a co-immunostaining using anti-lamp2 antibody, a marker of the lysosome storage, and anti-human Ids antibody on brain sections of MPSII treated mice belonging to groups A-D. These analyses showed the presence of Ids in the brains of treated mice, where it was possible to detect co-localization of Lamp2 and hIds in all cells (Figure 16 Groups A-D).

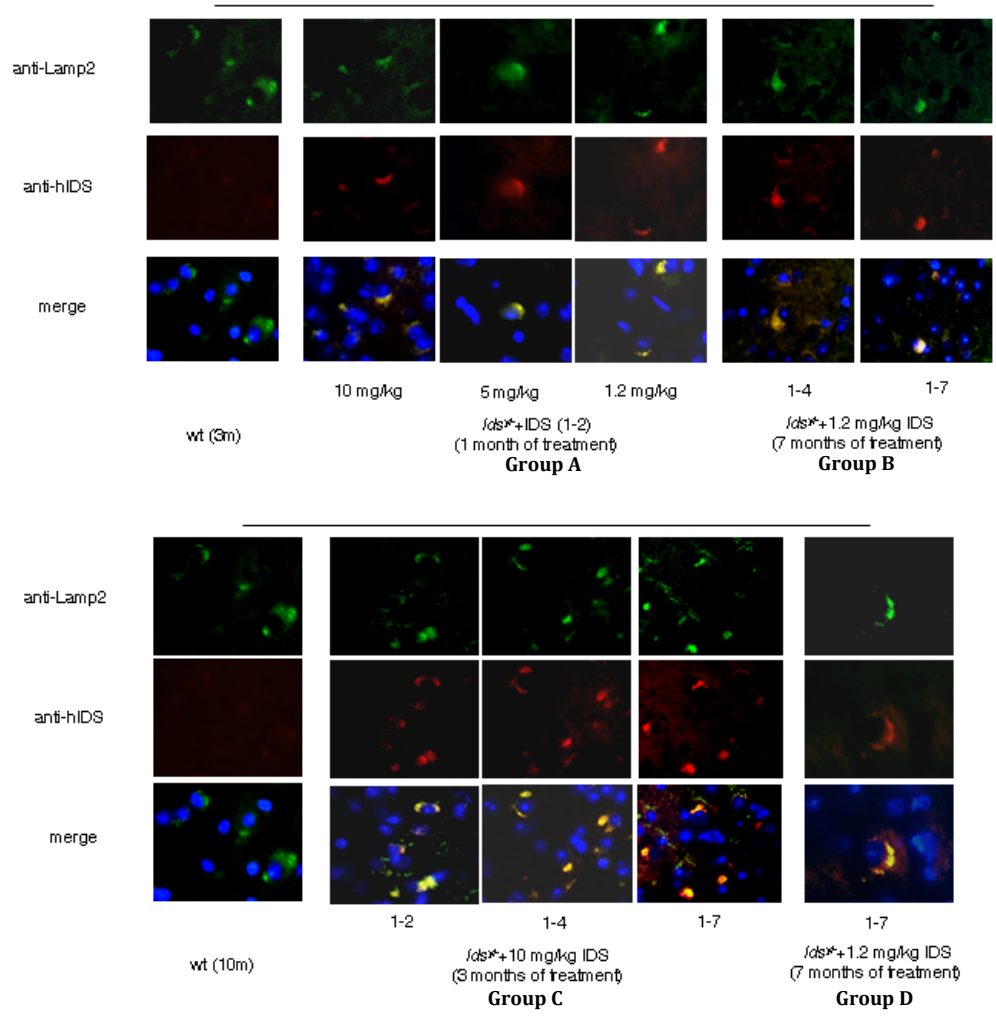

Figure 16: The Ids enzyme co-localizes with lysosome markers in the brain.

Co-localization of hIds protein (anti-hIds) with the lysosomal marker (anti-Lamp2) in the brain of, as indicated, *Ids*$^{y/-}$ treated mice belonging to all protocols of ERT (A-D). Magnification was 40x in the anti-CD68 IF, 100x in the double anti-Lamp2/anti-hIds IF and 20x in all the other IF and IHC reactions.

9. ERT allows clearance of lysosomal GAGs accumulation in the brains and tissues of MPS II treated mice.

In order to investigate whether the ERT protocols allowed GAGs clearance in the brains and visceral tissues of all groups of MPS II treated mice, we analyzed by Alcian blue staining, sections of these tissues from treated, untreated MPSII and wild-type mice.

Analyses of the brain of group A and B animals, showed an almost complete clearance of GAGs accumulation, no matter of the dose and intervals of treatment used. Figure 17 shows a dramatic reduction of GAGs accumulation in the choroid plexus of the third and fourth ventricles as well as in the cortex and thalamus as compared to the untreated MPSII mice (Figure 17 A). Interestingly, even the lower dose of Ids (1,2 mg/kg) administered with the longer interval time of treatment (once every 7 days) allowed to obtain a good clearance of GAGs in all of the regions of the brain analyzed not only in animals treated for 7 months, but also in those injected for just 1 month (group B and D) (Figure 17 A-B). Furthermore, in group C the administration of the higher dose of enzyme (10 mg/kg) in older MPS II mice was sufficient to correct partially the GAGs storage in the brain (Figure 17 B).

These data showed that both short and prolonged ERT protocols were efficient to correct lysosomal GAGs accumulation, in particular, the lower dose of Ids in young mice and the higher dose in the older ones.

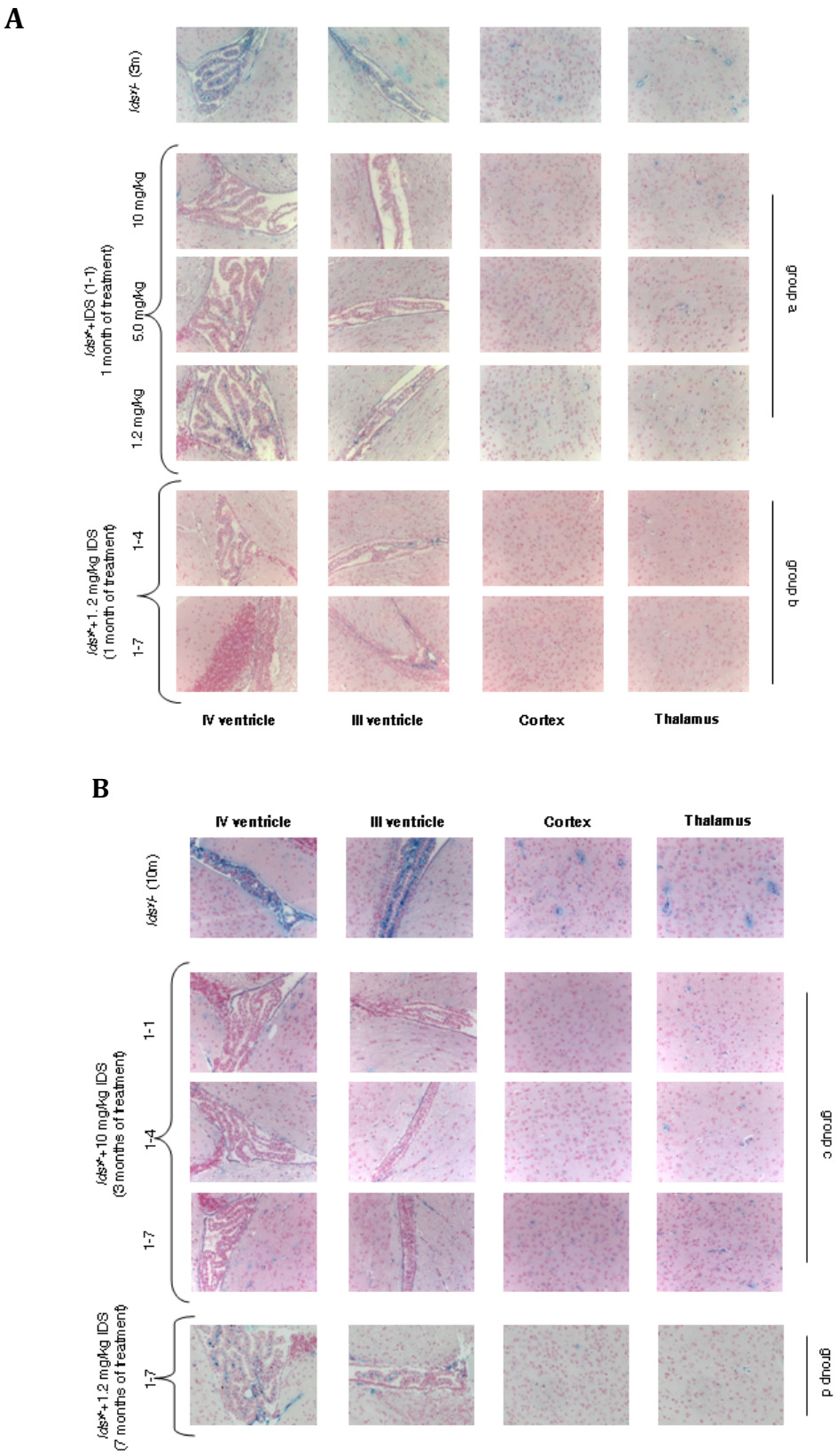

Figure 17: Rescue of GAGs accumulation in brain of *Ids*$^{y/-}$ treated mice. Representative GAG accumulation following ERT, measured by Alcian blue staining of sections of different regions of the of, as indicated, treated (Groups A, B, C, D) animals and of control wild type and untreated mice. **(A)** Almost total rescue of GAGs accumulation was seen in MPS II (*Ids*$^{y/-}$) mice of groups A and B **(B)** Partial rescue of GAGs accumulation was found in all regions of *Ids*$^{y/-}$ treated brain analyzed. Magnification was 20x.

Importantly, all the ERT protocols used allowed a total clearance of GAGs in all of the visceral tissues (Figure 18) and in the urine (Figure 19 A-B).

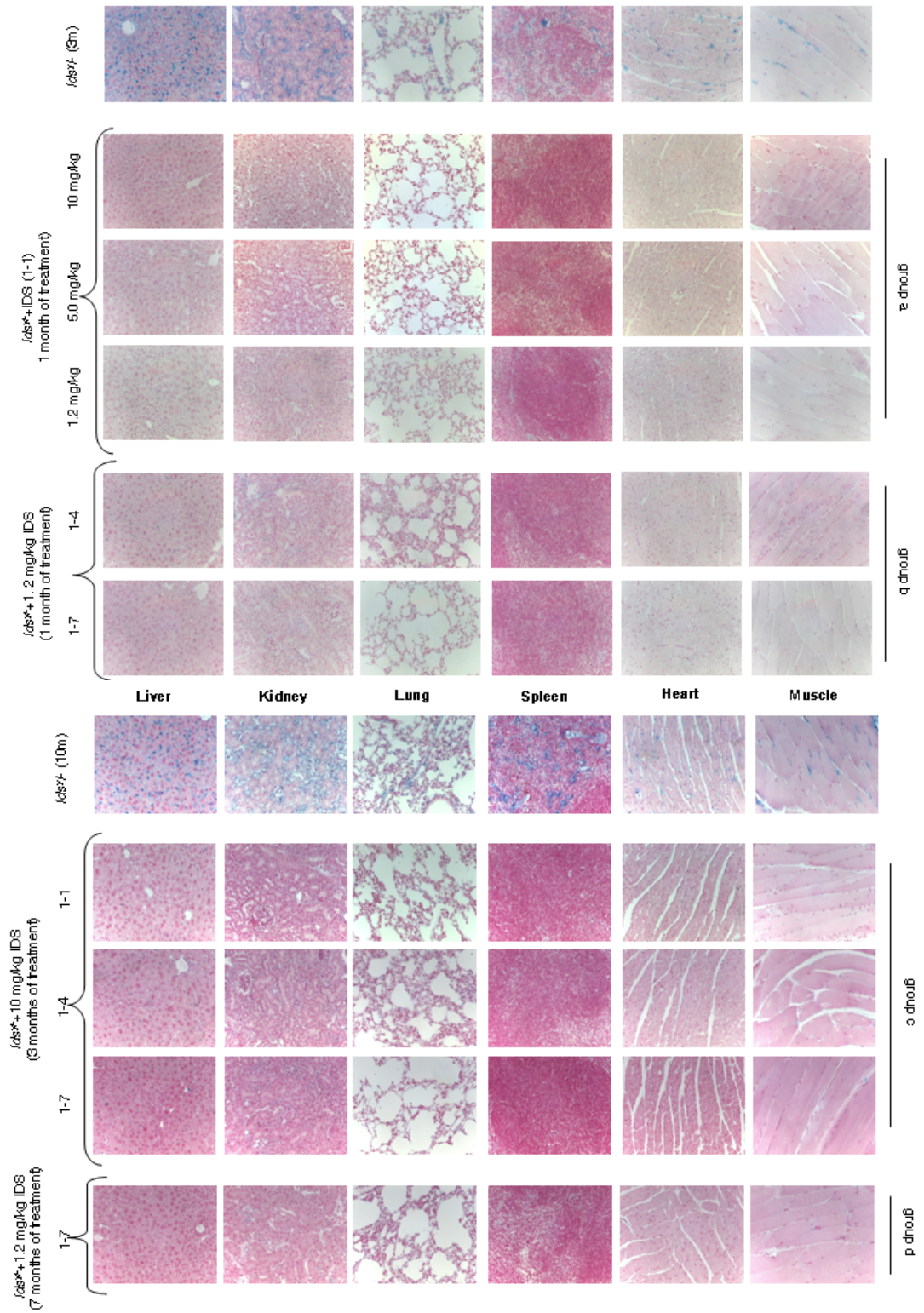

Figure 18: Total rescue of GAGs accumulation in the visceral tissues of *Ids*$^{y/-}$ mice treated. Representative GAGs accumulation following ERT, measured by Alcian blue staining of sections of different visceral tissues of untreated MPSII (Idsy/-) mice (3 and 10 months old) and groups A-D treated MPSII mice (as indicated).Magnification was 20x.

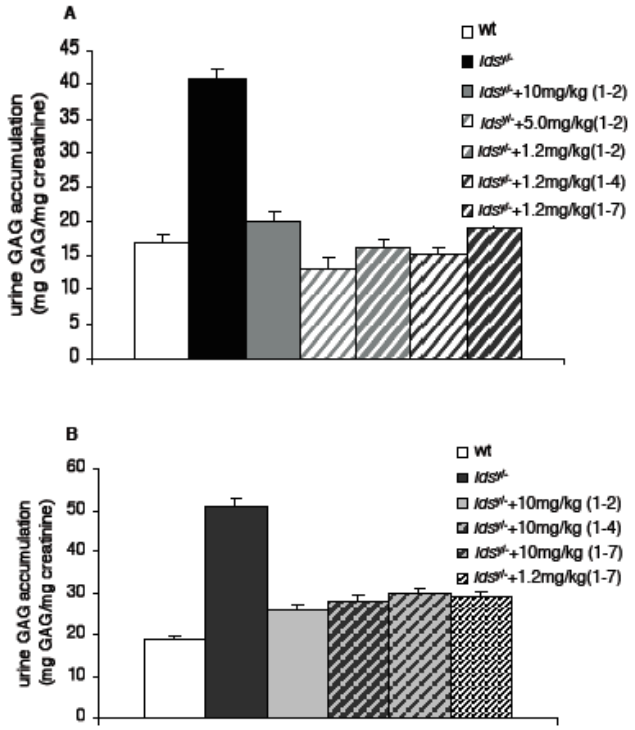

Figure 19: Clearance of urine GAGs accumulation after ERT. Urine GAG accumulation was evaluated at the end of each treatment ERT protocol, in the wt (n = 5), *Ids*$^{y/-}$ (n = 5) and *Ids*$^{y/-}$+10, 5.0, 1.2 mg/kg;1-2 days (n = 7 for each treatment), *Ids*$^{y/-}$+1.2 mg/kg; 1-4, 1-7 days (n = 7 for each treatment) **(A)**, *Ids*$^{y/-}$+10 mg/kg; 1-2, 1-4, 1-7 days (n = 7 for each treatment), *Ids*$^{y/-}$+1.2 mg/kg; 1-7 days (n = 4) **(B)** treated mice. The GAG concentrations were normalized against the urine creatinine contents. The error bars indicate standard deviations. $P < 0.05$ (with ANOVA test).

10. Ultrastructural analyses of the brain of MSPII mice following ERT.

The clearance of lysosome storage after ERT was also evaluated by ultrastructural analysis**.** Ultrastructural analysis of thin sections from the cerebellum of wild-type mice revealed electron-dense membrane structures with morphological features of lysosomes in Purkinje cells (Figure 20 A). These lysosomal organelles were mainly electron-dense with a few translucent areas in the lumen, and they usually ranged from 300 to 1000 nm in diameter. In contrast, the cytoplasm of Purkinje cells from the MPSII mice contained large lysosome-like organelles (Figure 20 B) which in some cases reached even 3000 nm in diameter and were, on average, more than twice the

diameter of those of the wild-type mice Purkinje cell lysosomes (Figure 20 D), as revealed by the morphometric analysis. The lumen of these organelles was filled with the heterogeneous material, part of which looks like 'fuzzy flakes' that resemble GAGs. Taken together, these ultrastructural features suggest that the degradation processes in these organelles are impaired, which results in GAGs storage. We analyzed the Purkinje cells of the group C treated mice (the oldest mice) by ultrastructural analysis and found significant improvement of the above-described MPSII phenotype. Indeed, for all the Ids treatments, the average diameters of the lysosome-like structures decreased (although they remained greater than that in the untreated wild-type mice (Figure 20 C-D). The overall population of the lysosomes was also highly variable in terms of the content. Some lysosomal organelles in the treated mice showed heterogeneous material in the lumen, as seen for the Purkinje cells from the untreated MPSII mice (Figure 20C black arrows), whereas others more resembled the electron-dense lysosomes for the Purkinje cells from the untreated wild-type mice (Figure 20 C black arrowhead). Thus, the ultrastructural analysis confirmed that the Ids cleared GAGs storage in the lysosomes. Interestingly, this was also seen for the group of older mice that had the more severe GAG-storage phenotype.

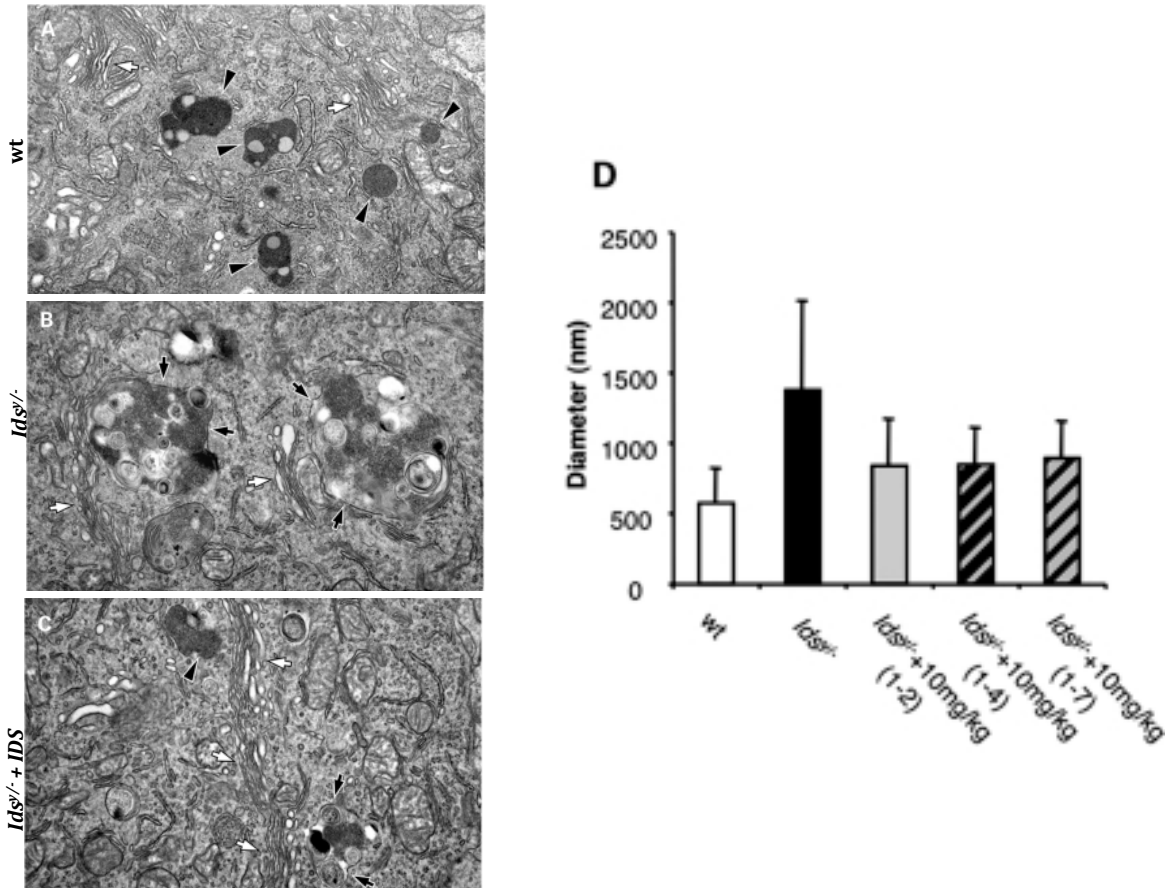

Figure 20: Clearance of lysosome storage after ERT as evaluated by ultrastructural analysis. The ultrastructure of the lysosome-like organelles in MPSII treated mice (group C). The ultrastructure of the lysosome-like organelles in the Purkinje cells was investigated in thin sections of cerebellum from wt **(A)**, *Ids*$^{y/-}$ **(B)** and *Ids*$^{y/-}$ treated (10mg/kg; 1-7 days) **(C)** mice. In all cases Purkinje cells sectioned through their central area (judged on the basis of the presence of the Golgi membranes, white arrows) were analyzed to ensure most representative sampling. The cells from control mice exhibited relatively small electron dense lysosome-like organelles **(A**, black arrowheads**)**. Huge vacuolar structures containing heterogeneous material **(B**, black arrows**)** were detected in cell from *Ids*$^{y/-}$ mice. Similar vacuoles with heterogeneous content **(C**, black arrows**)** were found also in treated mice, although their size were significantly smaller. The lysosomes with regular size and morphology (black arrowhead) were frequently detected as well. **(D)** Quantification of the lysosome diameter (average ± S.D., n = 80 lysosomes) reveals its significant increase in *Ids*$^{y/-}$ mice and reduction in result of all treatments (10mg/kg 1-2, 1-4, 1-7 days). Scale bar, 1000 nm **(A-C)**.

11. Ids activity and GAGs clearance in the brains and tissues of treated and control mice, sacrificed 4 days after the final Ids infusion

To investigate if after prolonged periods of time from the last Ids administration, it was still possible to measure Ids enzyme activity and GAGs clearance, a group of adult MPSII mice (aged 2 months) were treated with an enzyme dose of 1.2 mg/kg, once every 7 days (group E) for 1 month, and sacrificed 4 days after the last enzyme injection and compared to WT controls. The results of the experiment showed that 4 days after the last Ids administration, there was still Ids activity in the brains and the visceral tissues of the MPS II treated mice (Figure 21 A-B) and this was translated into a persistent GAGs clearance in the different brain areas and in the tissues (Figure 21 C-D). These data illustrate that the Ids enzyme is very stable, indeed it can be found in the brain and peripheral tissues for long time. The residual levels of enzymatic activity appear to be sufficient to maintain a good clearance of GAG accumulation in tissues. This is the reason for which the administration of Ids enzyme once every 7 days appears to be sufficient to correct the brain and the tissue defects.

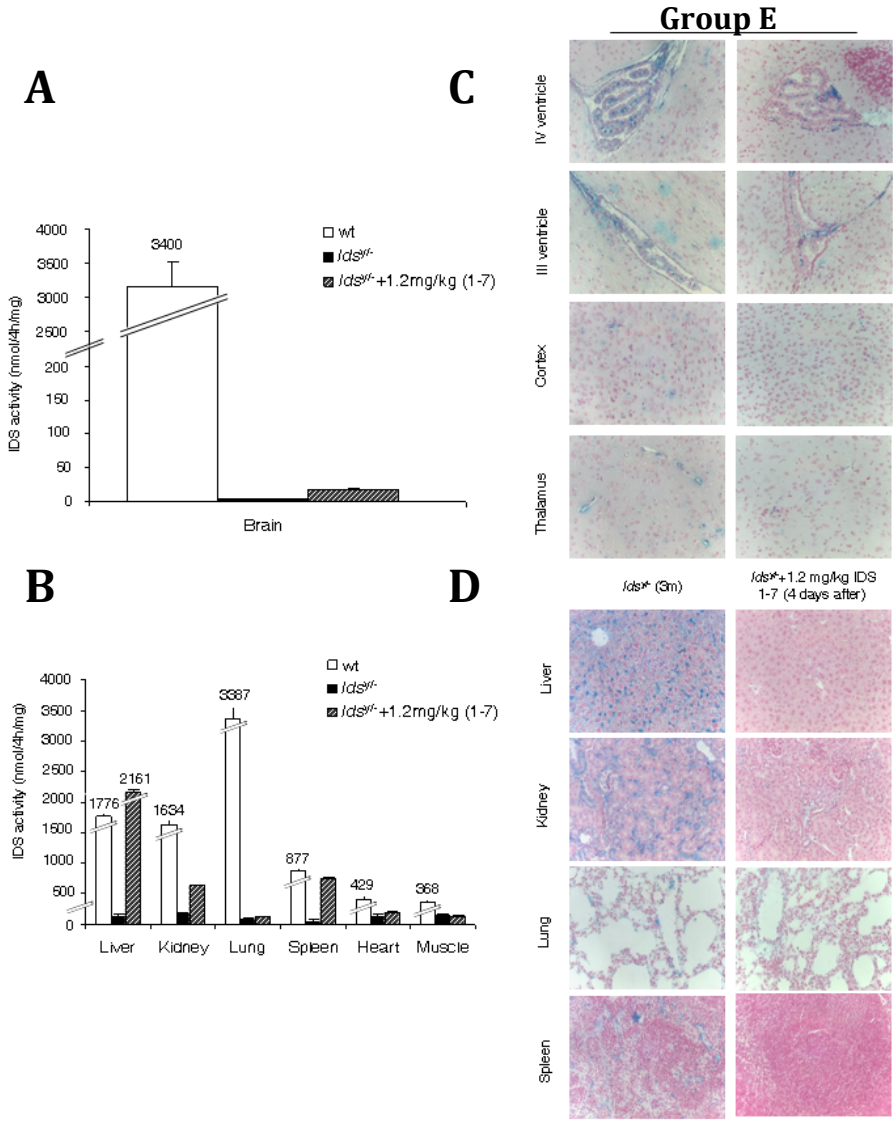

Figure 21: Residual levels of Ids activity are sufficient to maintain clearance of GAGs accumulation in brain and visceral tissues. Ids activity and GAG accumulation in the brains and visceral tissues of MPS II (*Ids*$^{y/-}$) mice treated as indicated and sacrificed 4 days after the last administration of hIDS protein. **(A, B)** IDS activity was measured in the protein extracts of wt (n = 5), *Ids*$^{y/-}$ (n = 5), *Ids*$^{y/-}$+1.2 mg/kg; 1-7 days (n = 4) injected mice. The duration of treatment was of 1 month. The error bars indicate standard deviations. $P < 0.05$ (with ANOVA test). **(C, D)** Alcian Blue stained sections of brains and visceral tissues of wt, *Ids*$^{y/-}$, *Ids*$^{y/-}$+1.2 mg/kg; 1-7 days treated mice. Magnification was 20x.

12. Partial correction of the brain defects in the treated MPS II mice

To investigate whether the ERT protocols used were efficient to treat the brain defects in MPS II mice, we analyzed brain sections of treated and control mice by immunostainings for several markers of neurodegeneration.

For groups A and B the staining anti-Lamp2 showed a clear reduction in the lysosomal GAGs accumulation compared to the untreated MPSII mice (Figure 22 A). Moreover, a marked decrease in the neurodegeneration was also evident in the treated mice belonging to all groups, as revealed by the reduction in anti-ubiquitin and TUNEL signals in neurons of the thalamus (Figures 22 A-B) as well as in the cortex and in other regions of the brain. In animals of treatment groups A, B and D we also found an increases in neuron density, showed by comparison of the anti-NeuN immunostaining between treated and untreated MPSII mice (Figures 22 A-B). For the animals of protocol C, in which older mice were treated with higher dose of Ids enzyme (10 mg/kg), as expected, there was only a small increase in neuron density in several brain areas (Figure 22 B); indeed, the treatment of 7 month-old mice was not as efficient as earlier time points. This is likely due to the fact that the therapy was started too late, when the neurodegeneration was already too advanced. In addition, mice belonging to all the ERT protocols showed a clear amelioration in the astroglyosis, as revealed by anti-GFAP, in several regions of the brain as in the thalamus, cortex and brain stem (Figures 22 A-B). We analyzed the inflammatory responses in the thalamus, cortex and brain stem, by performing anti-CD68 antibody staining, a marker for the infiltration of activated macrophages. The treated mice showed significant reduction in macrophage infiltration in all of the regions of brain analyzed as compared to untreated MPSII mice that instead showed a severe inflammation (Figures 22 A-B). Together these data demonstrate that ERT is a great approach that allows to obtain a partial correction of neuropathological defects in

MPS II brain and importantly, this is true even for the treatment of the older mice. Indeed, old mice (group C) even when treated once every 7 days showed definite amelioration of the brain phenotype. It is interesting to note that the lower dose of infused Ids enzyme (1.2 mg/kg) with the longest interval time of treatment (once every 7 days), administrated for a prolonged period (7 months of treatment; group D) was also efficient to lead to an improvement in the CNS phenotype of these treated adult mice.

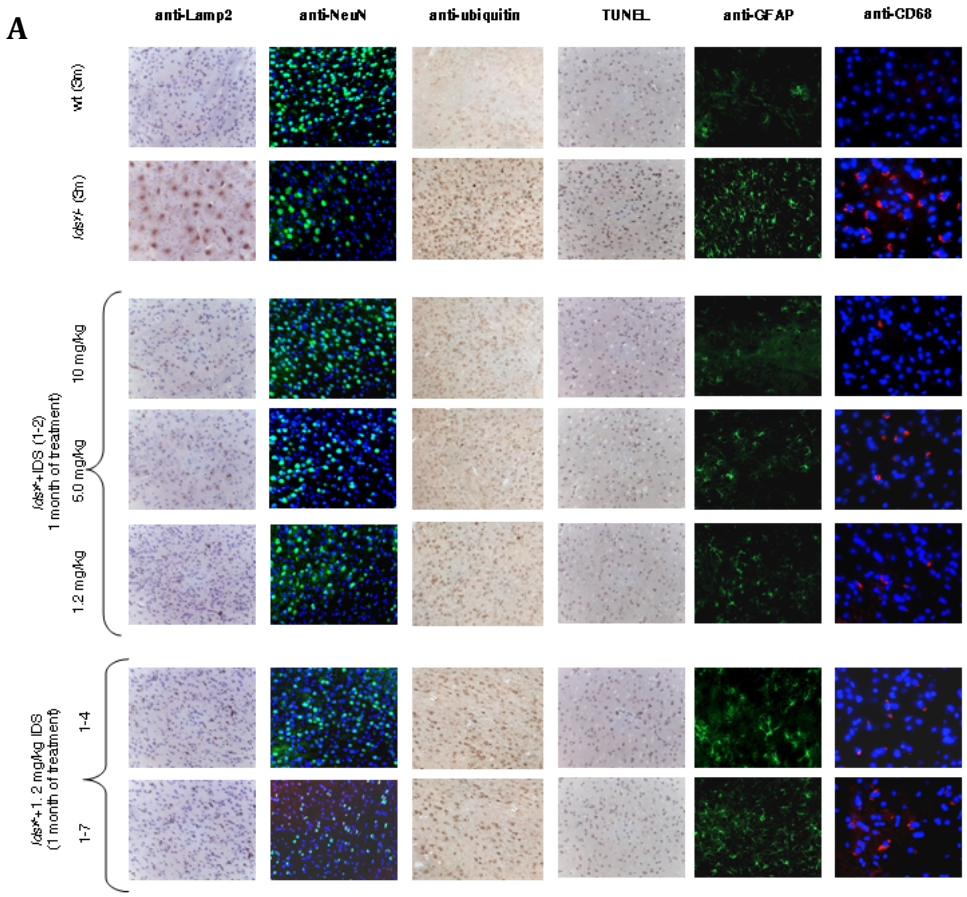

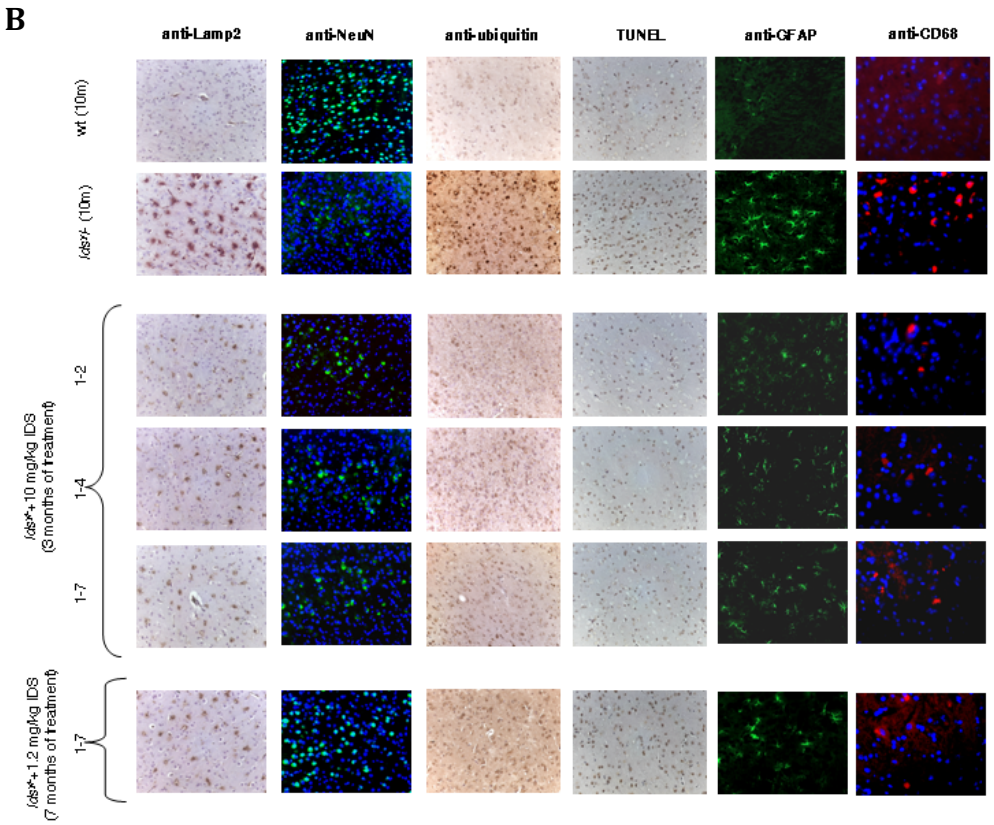

Figure 22: Rescue of the CNS markers after ERT in MPS II mice

(A) Analysis of the CNS marker rescue after ERT in groups A and B of mice Immunohistochemistry (IHC) and immunofluorescence (IF) of CNS markers on brain sections of *Ids*$^{y/-}$ mice treated as indicated and of control wild type and untreated mice. Rescue of storage was seen with anti-Lamp2 IHC, neuron density was evaluated with the anti-NeuN IF, rescue of ubiquitination with anti-Ubiquitin IHC, rescue of apoptosis with the TUNEL assay, rescue of gliosis with the anti-GFAP IF and rescue of macrophage infiltrations with the anti-CD68 IF. **(B)** Analysis of the CNS marker rescue after ERT in groups C and D of mice. IHC and IF of different CNS markers (anti-Lamp2, anti-NeuN, anti-Ubiquitin, TUNEL, anti-GFAP and anti-CD68) on the brain sections of WT, *Ids*$^{y/-}$ and *Ids*$^{y/-}$ treated mice, as indicated. Partial rescue of storage was seen with anti-Lamp2 IHC, neuron density was evaluated with the anti-NeuN IF, partial rescue of ubiquitination, of gliosis and of macrophage infiltration was evaluated with anti-ubiquitin, anti-GFAP IFs and anti-CD68 IHC, rescue of apoptosis was seen with the TUNEL assay.

13. Treated MPSII mice show improved sensorimotor coordination in the open-field and rotarod tests.

To assess whether the ERT would allow an improvement of the behavioral phenotype of MPS II mice, we tested the mice belonging to groups C and D in the open-field and rotarod tests. These neurobehavioral tests were carried out only in these two groups because the clear phenotype measured by these two tests can be seen only in MPSII mice from about 5 to 6 months of age [83]. The ability to explore, the locomotion and the anxiety to move of the treated mice were determined through the open-field test. As shown in Figure 23, the performance in the open field test showed both the vertical and horizontal activities to be fully corrected in the treated mice and to be comparable to the untreated wild-type mice (Figure 23 A, B, D and E). The rotarod test, as mentioned before, evaluates the sensorimotor coordination and the motor learning in rodents, functions associated to the cerebellum. We used this test to determine if ERT allowed the rescue of these cerebellum defects in the treated mice. The treated mice significantly improved their performances when compared with the untreated MPSII mice; indeed, in both groups, the fall latency time of the treated mice were almost comparable to those of the untreated wild-type mice (Figure 23 C and F). In addition, both groups of animals showed an improvement of motor learning. These data show that by systemic ERT, the MPSII brain defects can be functionally rescued, confirming the importance of this therapeutic approach for the treatment of the MPSII disease.

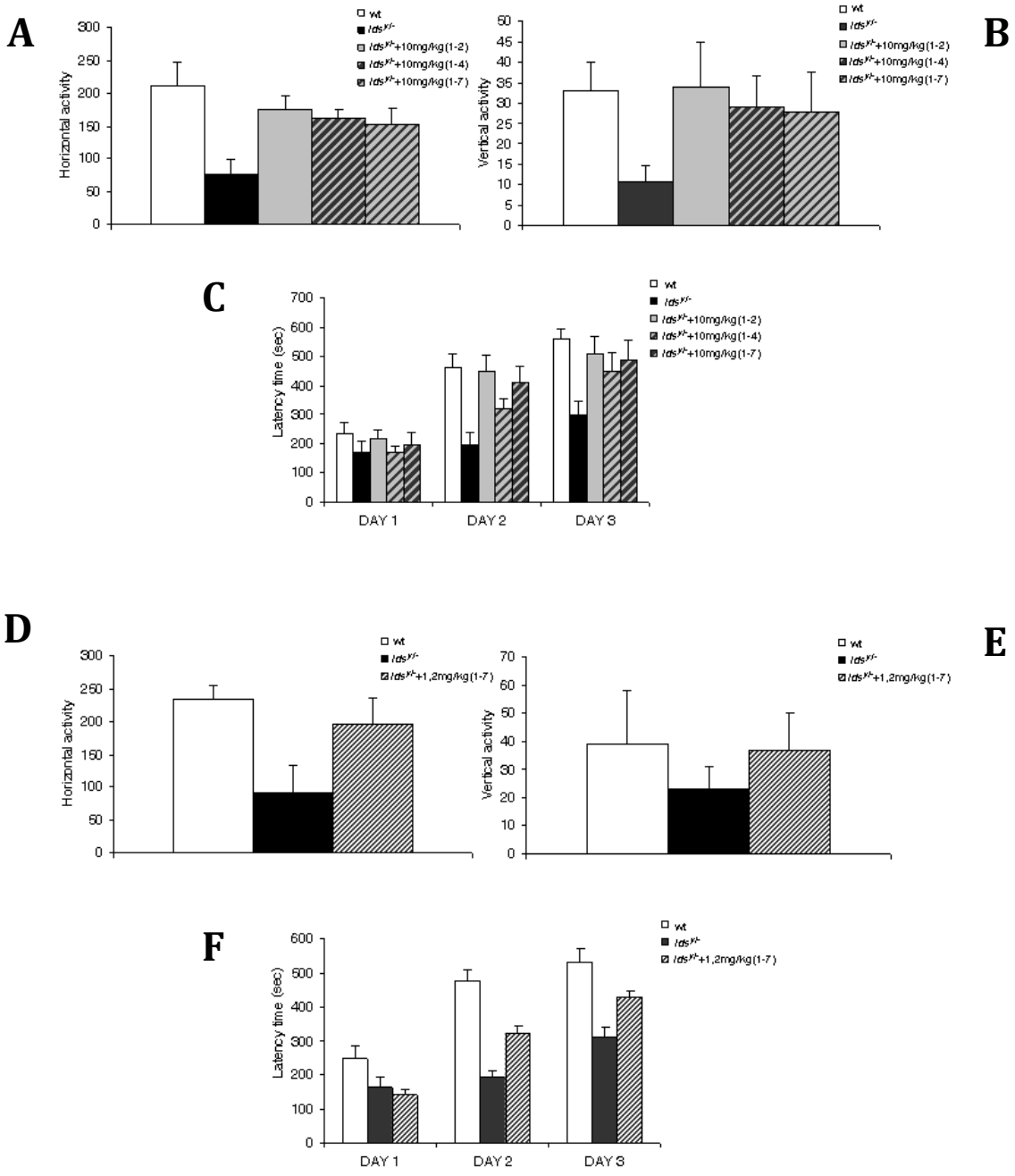

Figure 23: Rescue of behavioural phenotype in groups C and D of *Ids*$^{y/-}$ treated mice after ERT. WT (n = 5), *Ids*$^{y/-}$ (n = 5), *Ids*$^{y/-}$+10 mg/kg; 1-2, 1-4, 1-7 days (n = 7 for each treatment) **(A, B, C)** and *Ids*$^{y/-}$+1.2 mg/kg; 1-7 days) (n = 4) **(D, E, F)** mice were analyzed with the open field and the rotaroad tests at 10 months of age after 3 months of treatment **(A, B, C)** and 7 months of treatment **(D, E, F)**. In the open-field test, the number of crossings **(A, D)** and rearings **(B, E)** were evaluated, in the in the rotarod test **(C, F)** the latency time was measured. The error bars indicate standard deviations. $P < 0.05$ (with ANOVA test).

DISCUSSION

The mucopolysaccharidosis type II (MPS II) also called Hunter syndrome is a lysosomal storage disease, caused by deficiency of the lysosomal enzyme iduronate-2 sulphatase (Ids). This enzyme catalyzes the catabolism of GAGs as dermatan and heparan sulphate and its inactivity results in the progressive GAGs accumulation within lysosomes of various tissues and organs with consequent vacuolization and cell death, and at last organ dysfunction. Age of onset, disease severity, and rate of progression vary significantly. There are two clinical forms of MPS II: the mild and the severe form. In the severe disease the patients are characterized by a strong CNS involvement (manifest primarily by progressive cognitive deterioration), progressive airway disease, and cardiac disease that usually result in death in the first or second decade of life. In mild disease the CNS is not affected (or is minimally affected), there is survival into adulthood with normal intelligence, although the effect of GAGs accumulation in visceral organs may be severe as in patients affected by the severe form of MPS II. To date, the only therapy available to treat MPSII patients is ERT using the recombinant form of human iduronate 2-sulfatase, Idursulfase (Elaprase®), that it is approved in the United States and in the European Union for the treatment of MPS II [70]. This therapeutic approach is demonstrated to be effective to ameliorate certain systemic defects and in the management of the clinical symptoms [42,63,74,87-88]. Nonetheless, the ERT protocol used is only able to partially rescue the visceral phenotype of MPSII patients, but not the central nervous system one. Progressive neurodegeneration, in the severe form of MPSII disease, is a devastating feature leading to dramatic intellectual impairment including seizures, dementia, hydrocephalus and brainstem dysfunction in patients. Thus, it is very important to establish an ERT protocol for patients affected by the severe MPS II form that might lead to amelioration of the CNS symptoms, in addition to the visceral phenotype.

We first investigated the neurodegenerative progression in MPS II mice analyzing neuropathological features within the CNS. Then, we set up a novel protocol of ERT using the human recombinant Ids enzyme that allowed to cross the blood brain barrier and treat, in addition to visceral defects, also the brain ones. The longitudinal characterization of brain phenotype of MPS II mice, revealed: i) a progressive lysosomal GAGs accumulation; ii) a decrease in neural density and iii) an increased gliosis and apoptosis starting during the first months of the mouse life.

In addition, we observed by MRI analysis, ventricular atrophy in old animals as well as defective ERGs recordings, which highlighted a progressive and severe retinal degeneration starting already in 3 month-old mice. In contrast, behavioral tests showed a motor deficit only in adult animals indicating a late onset of the behavioral phenotypes. Our phenotypic characterization confirmed that MPS II mouse model reproduces the features of the severe form of the human disease and for this reason is useful to study novel therapeutic approaches to treat the disease.

We focused our attention in the development of novel ERT protocols, in which the Ids enzyme is able to reach the brain and correct or prevent its defects as well as visceral ones. At present, MPSII patients are treated with an infusion of 0.5 mg/kg recombinant human Ids once a week [63,74,89], but at this dose there has been no neurological improvement. In our study we found that in young mice, the systemically infused low dose (1.2 mg/kg) of human Ids, administered once every 7 days for short as well as for prolonged treatment periods is sufficient to ameliorate and apparently prevent progression of the CNS defects in MPSII mice. Thus one of the important observations of our study is that as opposed to much higher doses of other enzymes needed for ERT (such as β-glucuronidase in MPSVII mice, arylsulfatase A in metachromatic leukodystrophy mice and α-mannosidase in α-mannosidasis mice) to obtain only minor improvements in the CNS phenotypes [72-73,89]. In this study, we

have a scenario in which a dose that is very close to that used already in the clinic is sufficient to improve the CNS phenotype of MPSII mice. Remarkably, a clear improvement in the disease phenotype is also seen in the 7-month-old mice when a high dose (10 mg/kg) of Ids was administered once every 7 days for 3 months, showing that even when the central nervous system impairment is clearly manifested, ERT can be effective to ameliorate the disease.

This could be explained by the slow clearance in the plasma of Ids, reason for which we found the Ids in the brain even with low infused doses. Moreover, Ids contains N-linked glycosylation sites, and the circulating enzyme is highly sialylated [90-91]. This was considered important to mask immune reactivity and to reduce receptor recapture, resulting in a high amount of circulating Ids and therefore reduced clearance. In contrast, other lysosomal enzymes currently used in ERT protocols also contain N-linked oligosaccharides; however, their clearance is much faster.

How the Ids crosses the blood–brain barrier and reaches the brain remains a mystery at present, and it will be extremely interesting to analyze this further. Indeed, the stability of the Ids enzyme in the plasma leads us to conclude that it is an important parameter for the crossing of the blood–brain barrier. Whether high circulating levels of Ids are required for its delivery through receptor-mediated uptake or via different routes remains an open question.

For example, in MPS VII mouse model, β-glucuronidase fused to the HIV Tat peptide was shown to be taken up by absorptive endocytosis, which was mediated by binding to heparan sulfate on the cell surface [92]. Similarly, the exposure of brain capillaries to high levels of circulating enzyme might lead the heparan sulfate of the BBB endothelial cells of MPSII mice to facilitate Ids delivery to the brain. Finally, we cannot exclude also an injection-dependent hydrodynamic effect, due to the high volume of Ids infused. Thus, further studies to address the mechanism of the barrier

crossing will perhaps be important to modify the Ids enzyme so as to promote an increase in its uptake into the brain. Indeed, although we saw relatively low activity of the Ids enzyme in brain homogenates after these treatments, this activity appeared to be sufficient to greatly ameliorate the CNS markers and neurobehavioral symptoms in the treated mice. Importantly, we clearly obtained clearance of GAGs storage in the lysosomes after Ids uptake. This is an additional important characteristic of Ids, i.e. how a low amount of this enzyme is already sufficient to ameliorate the phenotype.

In truth, however, whether these therapeutic approaches will indeed be sufficient to treat or prevent neurodegeneration in MPSII patients is difficult to predict at present. First of all, patients are currently treated when the disease is already clearly manifest, and secondly, and unfortunately, they can also show high and variable immune responses against the infused Ids [42,63,74]. It will be important to direct future studies toward minimizing any immune response that might be mounted in the MPSII patients, perhaps also by modifying some of the epitopes of the Ids protein. As we clearly showed that the CNS lysosomal storage of MPSII mice can be normalized with a little enzymatic activity, this might well happen also in the future attempts of CNS treatment of the MPSII patients. An amelioration of the CNS phenotype in the patients might be obtained if they will be treated very early and before the neurodegeneration already impaired their cognitive functions. An optimization of the ERT protocol by adjusting the Ids dose and administration timing to a level that can be beneficial for the treatment of the CNS is however needed.

In conclusion, these studies clearly show that the systemic infusion of Ids in MPSII mice is an effective treatment for the CNS phenotype, and this work now opens up hope for effective treatment and/or prevention of the CNS defects in young and adult MPSII patients.

References:

1. Kornfeld, S. & Mellman, I. The biogenesis of lysosomes. Annu. Rev. Cell Biol. **5**, 483–525 (1989)

2. Kornfeld, S. Lysosomal enzyme targeting. Biochem. Soc.Trans. 18, 367–374 (1990).

3. Braulke T, Bonifacino JS Sorting of lysosomal proteins. Biochim Biophys Acta 1793:605-614(2009).

4. D. Lazzarino CG Mannose processing is an important determinant in the assembly of phosphorylated high mannose-type oligosaccharides. J Biol Chem 264 5015–5023(1989).

5. C. de Duve The lysosome turns fifty, Nat. Cell. Biol. 7 847–849(2005).

6. Scriver, C. R. et al. (eds) The Metabolic and Molecular Bases of Inherited Diseases (2001).

7. Wilcox WR. Lysosomal storage disorders: the need for better pediatric recognition and comprehensive care. J Pediatr 144: S3–S14 (2004).

8. Hopwood JJ, Brooks DA. An introduction to the basic science and biology of the lysosome and storage diseases. In: Organelle Diseases, edited by Applegarth DA, Dimmick JE, Hall JG. (New York: Chapman and Hall, p. 7–35) (1997).

9. Ballabio A, Gieselmann Lysosomal disorders: from storage to cellular damage V.Biochim Biophys Acta.;1793(4):684-96. (2009) Review.

10. Futerman AH, van Meer G The cell biology of lysosomal storage disorders. Nat Rev Mol Cell Biol 5:554-565(2004).

11. Wraith JE Lysosomal disorders. Semin Neonatol 7:75-83(2002).

12. Meikle PJ et al . Prevalence of lysosomal storage disorders. J Am Med Assoc; 281: 249–254(1999).

13. Poupetov´a H et al . The birth prevalence of lysosomal storage disorders in the Czech Republic: comparison with data in different populations. J Inherit Metab Dis; 33: 387–396 (2010).

14. Staretz-Chacham O. et al. Lysosomal storage disorders in newborn. Pediatrics.;123(4):1191-207. (2009) Review.

15. Hemsley KM, Hopwood JJ. Emerging therapies for neurodegenerative lysosomal storage disorders - from concept to reality J Inherit Metab Dis. 34(5):1003-12 (2011) Review.

16. Dunder U, Kaartinen V, Valtonen P et al. Enzyme replacement therapy in mouse model of aspartylglycosaminuria. FASEB J14:361–367(2000).

17. Hawkins-Salsbury JA, Reddy AS, Sands MS. Combination therapies for lysosomal storage disease: is the whole greater than the sum of its parts? Hum Mol Genet.;20(R1):R54-60 (2011) Review.

18. Urbanelli L et al., Recent developments in therapeutic approaches for lysosomal storage diseases. Recent Pat CNS Drug Discov;6(1):1-19 (2011).

19. Neufeld EU, Muenzer J. The mucopolysaccharidoses In: Scriver CR, ed. The Metabolic and Molecular Bases of Inherited Disease. New York: McGraw-Hill,:3421_52 (2001).

20. Tomatsu S, Okamura K, Maeda H et al. Keratan sulphates levels in mucopolysaccharidoses and mucolipidoses. J Inherit Metab Dis;28:187_202(2005).

21. Muenzer J. Overview of the mucopolysaccharidoses. Rheumatology (Oxford). 50 Suppl 5:v4-v12 (2011).

22. Esko JD, Kimata K, Lindahl U. Proteoglycans and Sulfated Glycosaminoglycans. Chapter 16 Cold Spring Harbor (NY). (2009).

23. Gandhi NS and Mancera R L. The Structure of Glycosaminoglycans and their Interactions with Proteins. Chem Biol Drug Des; 72: 455–482 (2008).

24. Coutinho MF, Lucia Lacerda L and Alves S. Glycosaminoglycan Storage Disorders: A Review. Biochemistry Research International (2012).

25. Parenti G, Meroni G, Ballabio A The sulfatase gene family. Curr Opin Genet Dev 7:386-391(1997).

26. Hopwood JJ, Ballabio A (2001) Multiple sulfatase deficiency and the nature of the sulfatase family. In: Scriver CR, Beaudet AL, Valle D, Sly WS (eds) The metabolic and molecular basis of inherited disease. Mc Graw- Hill, New York, pp 3725-3732

27. Meroni G et al., Characterization of a cluster of sulfatase genes on Xp22.3 suggests gene duplications in an ancestral pseudoautosomal region. Hum Mol Genet 5:423-431(1996)

28. Bond CS et al., Structure of a human lysosomal sulfatase. Structure 5:277-289. (1997).

29. Lukatela G et al., Crystal structure of human arylsulfatase A: the aldehyde function and the metal ion at the active site suggest a novel mechanism for sulfate ester hydrolysis. Biochemistry 37:3654-3664 (1998).

30. Cosma MP et al., The multiple sulfatase deficiency gene encodes an essential and limiting factor for the activity of sulfatases. Cell 113:445-456 (2003).

31. Ferrante P et al., Molecular and Biochemical characterisation of a novel sulphatase gene: Arylsulfatase G (ARSG). European Journal of Human Genetics 10:813-818 (2002).

32. Morimoto-Tomita M Cloning and characterization of two extracellular heparindegrading endosulfatase in mice and humans. The Journal of Biological Chemistry 277:49175-49185 (2002).

33. Graciana Diez-Roux and Andrea Ballabio Sulfatases and human diseases Annu. Rev. Genomics Hum. Genet. 2005. 6:355–79 (2005) Review.

34. Von Figura K, Gieselmann V, Jaeken J Metachromatic leukodystrophy. In: Scriver CR, Beaudet AL, Sly WS, Valle D (eds) The metabolic and molecular basis of inherited disease. Mc Graw-Hill, New York, pp 3695-3724(2001).

35. Franco B et al., A cluster of sulfatase genes on Xp22.3: mutations in chondrodysplasia punctata (CDPX) and implications for warfarin embryopathy. Cell 81:15-25 (1995).

36. Dierks T et al., Multiple Sulfatase Deficiency Is Caused by Mutations in the Gene Encoding the Human C(alpha)-Formylglycine Generating Enzyme. Cell 113:435-444 (2003).

37. Bach G et al., The defect in the Hunter syndrome: deficiency of sulfoiduronate sulfatase. Proc Natl Acad Sci;70:2134 –2138 (1973).

38. Martin R, et al., Recognition and diagnosis of mucopolysaccharidosis II (Hunter syndrome). Pediatrics;121:e377– e386 (2008).

39. Goldenfum SL et al., Mutation analysis in 20 patients with Hunter disease. Hum Mutat 7:76–78(1996).

40. Li P, Bellows AB, Thompson JN Molecular basis of iduronate-2-sulphatase gene mutations in patients with mucopolysaccharidosis type II (Hunter syndrome). J Med Genet 36:21–27(1999).

41. Moreira da Silva I et al., Molecular basis of mucopolysaccharidosis type II in Portugal: identification of four novel mutations. Clin Genet 60:316–318 (2001).

42. Wraith JE et al., Mucopolysaccharidosis type II (Hunter syndrome): a clinical review and recommendations for treatment in the era of enzyme replacement therapy. Eur J Pediatr 167:267–277(2008).

43. Baehner F. et al., Cumulative incidence rates of the mucopolysaccharidoses in Germany, J. Inherit. Metab. Dis. 28 1011–1017 (2005).

44. de Jong JG Measuring urinary glycosaminoglycans in the presence of protein: an improved screening procedure for mucopolysaccharidoses based on dimethylmethylene blue Clin Chem. Jun;38(6):803-7 (1992).

45. Young ID, Harper PS The natural history of the severe form of Hunter's syndrome: a study based on 52 cases. Dev Med Child Neurol 25:481–489 (1983).

46. Young ID et al., A clinical and genetic study of Hunter's syndrome. 2. Differences between the mild and severe forms. J Med Genet 19:408–411 (1982).

47. Young ID, Harper PS. Psychosocial problems in Hunter's syndrome. Child Care Health Dev 7:201–209(1981).

48. Fowler GW et al., Communicating hydrocephalus in children with genetic inborn errors of metabolism. Child's brain 1:251-254 (1975).

49. van Aerde J et al. Hydrocephalus in Hunter syndrome. Acta Paediatr Belg 34:93–96 (1981).

50. Spranger J The systemic mucopolysaccharidoses. Ergebnisse der inneren Medizin und Kinderheilkunde 32:165-265 (1972).

51. Brady, R.O. et al. Replacement therapy for inherited enzyme deficiency: use of purified glucocerebrosidase in Gaucher's disease. N. Engl. J. Med. 291, 989–993(1974)

52. Burrow TA et al. Enzyme reconstitution/replacement therapy for lysosomal storage diseases. Curr Opin Pediatr;19(6):628-35 (2007).

53. Brady RO. Enzyme replacement for lysosomal diseases. Annu Rev Med;57:283-96 (2006).

54. Bijvoet, A. G. et al. Human acid α-glucosidase from rabbit milk has therapeutic effect in mice with glycogen storage disease type II. Hum. Mol. Genet. 8, 2145–2153 (1999).

55. Miranda, S. R. et al. Infusion of recombinant human acid phingomyelinase into Niemann–Pick disease mice leads to visceral, but not neurological, correction of the pathophysiology. FASEB J. **14**, 1988–1995 (2000).

56. Cramer, C. L. et al. Bioproduction of human enzymes in transgenic tobacco. Am. NY Acad. Sci. 792, 62–71 (1996).

57. Kornfeld, S. Lysosomal enzyme targeting. Biochem. Soc. Trans. 18, 367–374 (1990).

58. Hille-Rehfeld, A. Mannose 6-phosphate receptors in sorting and transport of lysosomal enzymes. Biochim. Biophys. Acta 1241, 177–194 (1995).

59. Achord DT, Brot FE, Bell CE, and Sly WS. Human β-glucuronidase: *in vivo* clearance and *in vitro* uptake by a glycoprotein recognition system on reticuloendothelial cells. *Cell*;15:269–278 (1978).

60. Barton NWet al. Replacement therapy for inherited enzyme deficiency–macrophage targeted glucocerebrosidase for Gaucher's disease. *N Engl J Med.*;**324**:1464–1470(1991).

61. Lim-Melia ER, and Kronn DF. Current enzyme replacement therapy for the treatment of lysosomal storage diseases. *Pediatr Ann.*;**38**:448–455 (2009).

62. Kakkis ED et al. Enzyme-replacement therapy in mucopolysaccharidosis I. *N Engl J Med.*;344:182–188 (2001).

63. Muenzer J, et al. A phase II/III clinical study of enzyme replacement therapy with idursulfase in mucopolysaccharidosis II (Hunter syndrome) *Genet Med.*;**8**:465–473 (2006).

64. Xia H, Mao Q, and Davidson BL. The HIV Tat protein transduction domain improves the biodistribution of β-glucuronidase expressed from recombinant viral vectors. *Nat Biotechnol.*;19:640–644 (2001).

65. Shunji Tomatsu et al, Enhancement of Drug Delivery: Enzyme-replacement Therapy for Murine Morquio A Syndrome Mol Ther. 18(6): 1094–1102 (2010).

66. L. A. Clarke, J. E. Wraith, M. Beck et al., "Long-term efficacy and safety of laronidase in the treatment of mucopolysaccharidosis I," Pediatrics, vol. 123, no. 1, pp. 229–240, (2009).

67. H. Harada, H. Uchiwa, M. Nakamura et al., "Laronidase replacement therapy improves myocardial function in mucopolysaccharidosis I," Molecular Genetics and Metabolism, vol. 103, no. 3, pp. 215–219 (2011).

68. A. Tylki-Szymanska, J. Marucha, A. Jurecka, M. Syczewska, and B. Czartoryska, "Efficacy of recombinant human **α**-Liduronidase (laronidase) on restricted range of motion of upper extremities in mucopolysaccharidosis type i patients,"
Journal of Inherited Metabolic Disease, vol. 33, no. 2, pp. 151– 157 (2010).

69. Burrow T. A. and Leslie N. D., "Review of the use of idursulfase in the treatment of mucopolysaccharidosis II," Biologics, vol. 2, pp. 311–320 (2008).

70. Bagewadi S. Home treatment with Elaprase and Naglazyme is safe in patients with mucopolysaccharidoses types II and VI, respectively. J Inherit Metab Dis 31:733–737(2008).

71. Harmatz P., et al., "Longterm follow-up of endurance and safety outcomes during enzyme replacement therapy for mucopolysaccharidosis VI: final results of three clinical studies of recombinant human N-acetylgalactosamine 4-sulfatase," Molecular Genetics and Metabolism, vol. 94, no. 4, pp. 469–475 (2008).

72. Matzner U. et al. Enzyme replacement improves ataxic gait and central nervous system histopathology in a mouse model of metachromatic leukodystrophy. Mol. Ther., 17, 600–606 (2009).

73. Vogler, C. et al. Overcoming the blood–brain barrier with high-dose enzyme replacement therapy in murine mucopolysaccharidosis VII. Proc. Natl Acad. Sci. USA, 102, 14777– 14782 (2005).

74. Muenzer, J et al. A phase I/II clinical trial of enzyme replacement therapy in mucopolysaccharidosis II (Hunter syndrome). Mol. Genet. Metab., **90**, 329–337 (2007).

75. Garcia AR et al. Preclinical dose ranging studies for enzyme replacement therapy with idursulfase in a knock-out mouse model of MPS II. Molecular Genetics and Metabolism 91 183–190(2007).

76. Brooks DA. et al. Significance of immune response to enzyme-replacement therapy for patients with a lysosomal storage disorder. TRENDS in Molecular Medicine Vol.9 No.10 (2003).

77. Dickson P. et al. Immune tolerance improves the efficacy of enzyme replacement therapy in canine mucopolysaccharidosis I. J. Clin. Invest. 118:2868 2876 (2008).

78. Barton, N.W. et al. Replacement therapy for inherited enzyme deficiency macrophage targeted glucocerebrosidase for Gaucher's disease. N. Engl. J. Med. 324:1464–1470 (1991).

79. Brooks DA et al. Enzyme replacement therapy in mucopolysaccharidosis VI: evidence for immune responses and altered efficacy of treatment in animal models. Biochim Biophys Acta; 1361: 203–16 (1997).

80. Miebach E. et al. Management of infusion-related reactions to enzyme replacement therapy in a cohort of patients with mucopolysaccharidosis disorders. Int. J. Clin. Pharmacol. Ther. 47, pp. S100–S106 (2009)

81. Burton BK et al. Incidence and timing of infusion-related reactions in patients with mucopolysaccharidosis type II (Hunter syndrome) on idursulfase therapy in the real-world setting: a perspective from the Hunter Outcome Survey (HOS). Mol Genet Metab;103: 113_20 (2011).

82. Muenzer, J. Enzyme replacement therapy in mucopolysaccharidosis type II (Hunter syndrome): a preliminary report. Acta. Paediatr. Suppl., 91, 98–99 (2002).

83. Cardone, M. et al. Correction of Hunter syndrome in the MPSII mouse model by AAV2/8-mediated gene delivery. Hum. Mol. Genet., 15, 1225–1236 (2006).

84. Bronikowski, A.M et al. Open-field behavior of house mice selectively bred for high voluntary wheel-running. Behav. Genet., 31, 309–316 (2001).

85. Monville C. et al.. Comparison of incremental and accelerating protocols of the rotarod test for the assessment of motor deficits in the 6- OHDA model. J Neurosci Methods 158, 219-223(2006).

86. Lei B. et al. Ocular Phenotype in a Mouse Gene Knockout Model for Infantile Neuronal Ceroid-Lipofuscinosis. J. Neurosci. Res;84:1139–1149 (2006).

87. Muenzer J. The role of enzyme replacement therapy in severe Hunter syndrome-an expert panel consensus. Eur J Pediatr.;171(1):181-8 (2012).

88. Muenzer J et al. Long-term, open-labeled extension study of idursulfase in the treatment of Hunter syndrome. Genet Med.;13(2):95-101 (2011).

89. Blanz, J. et al. Reversal of peripheral and central neural storage and ataxia after recombinant enzyme replacement therapy in alpha-mannosidosis mice. Hum. Mol. Genet., 17, 3437–3445 (2008).

90. Archer, I.M. et al. Multiple forms of iduronate 2-sulphate sulphatase in human tissues and body fluids. Biochim. Biophys. Acta, 708, 134–140 (1982).

91. Parkinson-Lawrence, E Analysis of normal and mutant iduronate-2-sulphatase conformation. Biochem. J., 386, 395–400 (2005).

92. Orii, K.O. et al. Defining the pathway for Tat-mediated delivery of beta glucuronidase in cultured cells and MPS VII mice. Mol. Ther., 12, 345–352 (2005).

PART 2

Diabetes Mellitus type 1 induces cognitive dysfunction through tau-dependent mechanism

ABSTRACT

Growing evidence suggest comorbidity between diabetes mellitus (DM) and Alzheimer's disease (AD); indeed, diabetic patients show increased risk of developing AD and cognitive deficits, while, AD patients show impaired insulin function and glucose metabolism. However, the molecular mechanisms linking these two disorders are still not fully understood. Here, we hypothesize that DM induces tau hyperphosphorylation generating the cognitive decline observed in AD. Interestingly, our results show that induction of type 1 DM by streptozotocin (STZ) administration in WT mice support our hypothesis showing, in these mice, tau hyperphosphorylation, decreased activity of the Insulin Receptor (IR)/PI3K/AKT pathway and increased phosphorylation of glycogen synthase kinase 3β (GSK3β), a kinase strongly involved in the pathogenesis of AD. At the behavioral levels, WT-STZ mice showed learning and memory deficits. Importantly, when type 1 DM was induced in knockout mice lacking tau proteins (here referred as mtauKO STZ), the behavioral and cellular phenotypes found in WT-STZ mice were not observed. Associated with these cognitive deficits, WT-STZ mice displayed a significant decrease of synaptic markers. Overall, our results indicate that tau phosphorylation is a critical and essential molecular mechanism underlying the link between DM and AD.

INTRODUCTION

1. Diabetes Mellitus and risk of Alzheimer Disease.

The incidence and prevalence of age-related neurodegenerative and metabolic disorders is growing due to an increase of life expectancy of the human population [1-8]. Diabetes Mellitus (DM) is the most common metabolic disorder, characterized by hyperglycemia resulting from defective insulin secretion or insulin action. In non pathological conditions, the persistently elevated blood glucose levels cause the release of additional insulin from the pancreas, to stimulate glucose uptake in peripheral organs such as muscle and liver. [2-7].

DM arises from a combination of genetic and environmental factors causing the failure of pancreatic beta-cells to produce sufficient insulin, and thus maintain adequate insulin secretion to prevent hyperglycemia . There exist two major clinically defined forms of diabetes: Type I and II, which share similar diagnosis, symptoms, causes, and complications. Type I Diabetes, or insulin-dependent diabetes, is an autoimmune disease where the immune system attacks and destroys pancreatic beta-cells. 5-10% of diabetic patients are affected by type 1 diabetes, characterized by insulin deficiency. In type I, patients either completely stop making insulin or they only make a very small amount of the hormone [1-5-9].

Type II Diabetes or non-insulin-dependent diabetes tends to develop gradually in later life. It is also known as “maturity” or “adult-onset” diabetes. Diabetes Type II accounts for 90 percent of all people with diabetes [5,6,8]. Type 2 diabetes is characterized by the combination of peripheral insulin resistance and inadequate insulin secretion by pancreatic beta cells. Insulin resistance, attributed to elevated levels of free fatty acids in plasma, whose accumulation appears to interfere with insulin signaling, leads to decreased glucose transport into muscle cells, elevated

hepatic glucose production, and increased breakdown of fat. In this condition the β cells are no longer able to secrete sufficient insulin to overcome insulin resistance. The strongest factors or causes of type II diabetes are family history of diabetes and obesity. In North America, 80% of those diagnosed are overweight. Over 176 million people are affected with DM in the world and it is estimated to reach 366 millions in 2030, it is among the most common causes of death and disability in North America and Europe [9].

In diabetes mellitus the hyperglycemia is associated with microvascular and macrovascular complications, retinopathy, nephropathy, neuropathy and cardiovascular diseases, whose severity depends by type of diabetes and on the age of its onset. In cross-sectional studies, DM is known as risk factors for all vascular diseases, including vascular dementia [1-2]. In particular, in Type 1 diabetes the association between cognitive changes is shown by a mild to moderate slowing of mental speed and a diminished memory and mental flexibility and neuronal loss [3-5,7] , whereas in type 2 diabetes cognitive changes mainly affect learning and memory processing speed attention and psychomotor functions [4-8].

Epidemiological studies show that people affected by diabetes have higher risk to develop Alzheimer's disease (AD) compared to healthy ones [1,2,10-14]. Interestingly, late-onset of Alzheimer's disease is characterized not only by a cognitive and memory decline but also by vascular lesions, hyperglycemia, hyperinsulinemia, glucose intolerance and insulin signaling dysfunctions [15]. The association between these two disorders suggests that DM may contribute to AD.

2. Insulin signaling and its neural function

Insulin has important functions in the brain, including metabolic, neurotrophic, neuromodulatory and neuroendocrine actions [16-20]. Peripheral insulin is actively transported in the brain across the blood–brain barrier, but it is also produced locally in the CNS [17]. The insulin receptors (IRs) are tyrosine kinases that mediate a series of signaling events regulating a variety of biological processes, including cell growth, protein synthesis, and glucose transport [21-22]. IRs are widely present in the brain of rodents and humans, with high expression in the olfactory bulb, hypothalamus, pituitary, hippocampus and cortex. IRs located at the synapse regulate neurotransmitter release and receptors recruitment, suggesting a role for insulin in synaptic plasticity [23]. The abundance of IRs in regions of the brain involved in learning and memory, such as the hippocampus and cortex, indicates that insulin plays a critical role in cognitive functions. Indeed, insulin modulates neuronal firing via actions at K_{ATP} channels, as well as, synaptic plasticity, affecting both long-term potentiation (LTP) and and long-term depression (LTD). Insulin affects LTD by internalization of AMPA channels from synaptic membranes [23-25].

In the brain as in other organs, insulin acts through binding to its receptors; this triggers the autophosphorylation of the receptor's β-subunit, leading to binding and phosphorylation on tyrosine residues of multiple IR substrates, including insulin receptor substrate-1 (IRS-1) and 2 (IRS-2). Phosphorylated IRS proteins then activate downstream signaling pathways, including the phosphatidylinositol 3-kinase (PI3K) and extracellular signal-regulated kinase (ERK) cascades that directly regulate various physiological processes [26] (Figure 1). In the brain, Ras-ERK and MAPK pathways have an important role in synaptic plasticity and memory formation.

A downstream target of the ERK pathway is the cAMP response element binding

protein (CREB), whose activation induces structural changes associated with long-term memory formation [27]. Moreover, the expression of these protein kinases are positively associated with Aβ plaques and neurofibrillary tangles (NFTs) in AD., indeed, ERK1/2 and MAPK p38 co-localize with NFTs and Aβ in hippocampal and cortical regions in AD brains [28-29].

The other signaling pathway activated by the complex insulin/IR is the PI3K pathway. Activated PI3K converts membrane phospholipid, phosphatidylinositol 4,5-bisphosphate (PIP2) to phosphatidylinositol 3,4,5-trisphosphate (PIP3), thereby leading to the activation of AKT.

AKT phosphorylates a variety of biologically important substrates including glycogen synthase kinase (GSK) 3β and the mammalian target of rapamycin (mTOR). The phosphorylation on serine 9 by Akt inactivates GSK3β, which normally promotes cellular proliferation and survival [30]. Studies have shown that GSK3β regulates tau phosphorylation, the main component of NFT pathology in the AD brain [29-31]. Several studies also reported impaired activity of GSK3β in AD brains [31,37,39] .

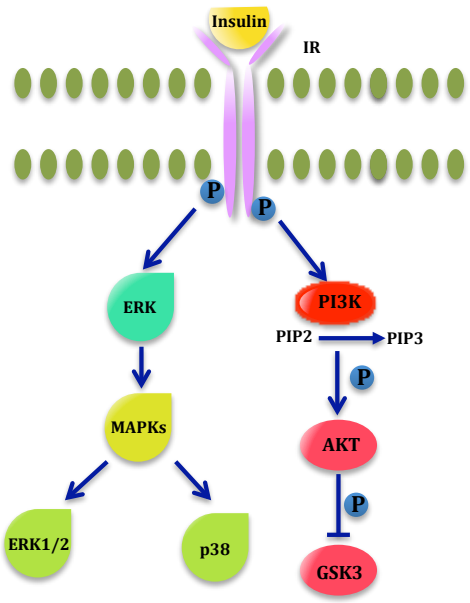

Figure 1. Insulin signaling pathway. Binding of insulin to insulin receptor activate two downstream signaling pathways including PI3K and ERK/MAPKs pathways

3. Alzheimer Disease and tau proteins

Alzheimer's disease (AD) is a neurodegenerative disorder characterized by progressive memory loss, spatial disorientation, deterioration of intellectual capacity and gradual neuronal loss [32]. This loss results in severe atrophy of the affected regions, including degeneration in the temporal lobe and parietal lobe, and parts of the frontal cortex and cingulate gyrus. AD is the most prevalent cause of dementia in humans with high incidence in the elderly population, affecting over 35 million people throughout the world [35]. All AD cases are marked by the accumulation of two lesions in the brain; "plaques", consisting by aggregates of ß-amyloid proteins, and "tangles", composed by hyperphosphorylation of tau with the consequent inflammation and loss of neurons [32-36]. Aβ peptides are natural products of amyloid precursor protein (APP) metabolism consisting of 36 to 43 amino acids. Monomers of Aβ40 are more prevalent than the aggregation-prone and damaging Aβ42 specie (Figure 2). The amyloid-β (Aβ) peptide is derived via proteolysis from APP, a type 1 transmembrane protein. APP can be processed by one of two proteolytic pathways: non-amyloidogenic and amyloidogenic pathway [32-33]. In the non-amyloidogenic pathway, APP is cleaved by a-secretase. Three enzymes with a-secretase activity have been identified, all belonging to the ADAM family. The activity of a-secretase releases two fragments, the larger ectodomain (sAPPa) and the smaller carboxy-terminal fragment (C83). The fragment C83 can also be cleaved by g-secretase to generate P3. In the non-amyloidogenic pathway, APP proteins are cleaved by the β-secretase BACE1 (β-site APP-cleaving enzyme 1), releasing an ectodomain (sAPPβ), and the fragment C99 that is subsequently cleaved 38–43 amino acids from the amino terminus to release Aβ, by the g-secretase, a protein complex with presenilin 1 or 2 at its catalytic core. This cleavage predominantly produces $A\beta_{1-40}$, and the more amyloidogenic $A\beta_{1-42}$ at a ratio of 10:1. β-amyloid spontaneously aggregates to form insoluble fibers of amyloid plaques or forms soluble oligomers that coalesce into

intermediate assemblies. Soluble oligomers and intermediate amyloids are the neurotoxic forms of Aβ. Mutations in one or more of the genes encoding APP, PS1 or PS2 are the cause of familial AD, although the 90% of AD are sporadic cases [32-33].

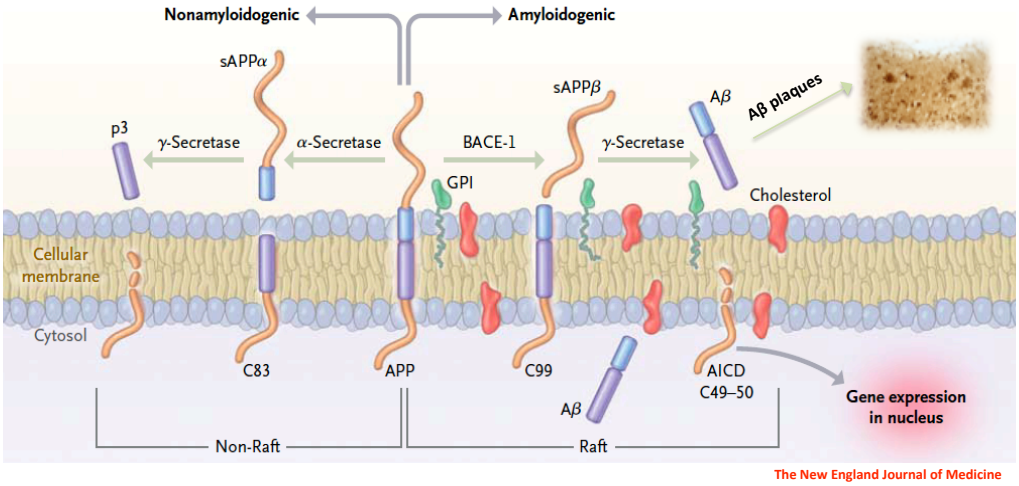

Figure 2. Metabolism of Amyloid Precursor Protein.

In the non-amyloidogenic cleavage via, bAPP protein is cleaved by a-secretase that releases a large amyloid precursor protein (sAPPa) and a fragment C-terminal that it is then digested by ghsecretase in the amyloid intracellular domain (AICD) and the fragment P3. In the amyloidogenic processing, bprocessing, processing,secretases : a:secretase, b secreatase and gasecretase that produce different fragments. Sequential cleavage by btsecreatase and g-secretase release several secretable Ab peptides including Ab $_{1\text{-}40}$ and Ab $_{1\text{-}42.}$

The other neuropathological feature of AD is the presence of neurofibrillary tangles (NTF), filamentous inclusions in pyramidal neurons of the hippocampus, composed by hyperphosphorylated tau protein [32]. Microtubule-associated protein tau (MAPs) is a soluble cytoskeleton protein that regulates neuronal development, promotes assembly and stability of microtubules and vesicles transport [34-35]. Tau protein exerts an essential role in the balance of microtubule-dependent axonal transport of organelles and biomolecules by modulating the anterograde transport by kinesin and the dynein-driven retrograde transport.

In physiological conditions almost 20% of tau are phosphorylated, however in pathological conditions, such as AD, the over-activation of some kinases or the

reduction in phosphatase activity can lead to tau hyperphosphorylation [34-36]. Tau can be phosphorylated by several serine/threonine kinases as MAPK, CAMKII, CDK5 and also glycogen synthase kinase 3β (GSK-3β) [32,37-39]. Hyperphosphorylated tau are insoluble, lack affinity for the microtubules and aggregate in paired helical filaments leading to the formation of toxic neurofibrillary tangles in the cell body and proximal dendrites of the neurons (Figure 3). The NFT alters intracellular trafficking and consequently leads to synapses dysfunctions, neuronal degeneration and cognitive decline [32,34-36]. Overall, Aβ and NFT accumulation causes synaptic failure with reduction in synaptic protein and dendritic spines, oxidative stress, mitochondrial dysfunction, inflammation and brain vascular abnormalities that lead to neurodegeneration and cognitive impairment [32].

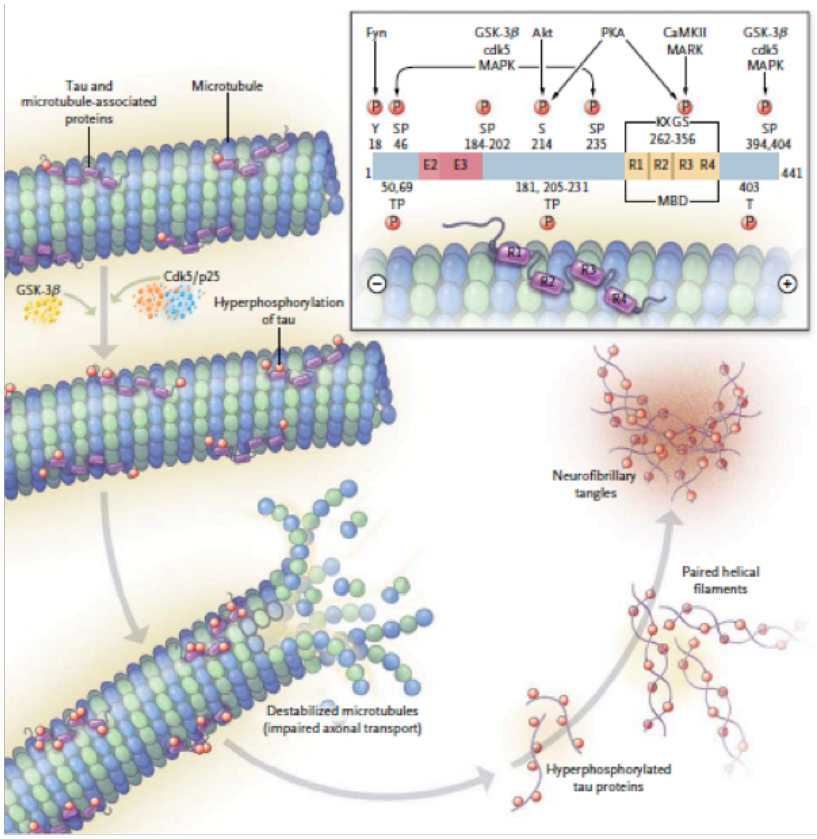

Figure 3. Tau structure and function.

Tau proteins are proteins that bind and stabilize the microtubules. Hyperphosphorilation of tau by aberrant kinases and/or phosphatases activities promote detachment of tau from microtubules, self-aggregate in paired helical filaments and microtubules destabilization.

4. Insulin signaling and Alzheimer Disease

There are increasing evidences to support a link between AD and insulin dysfunction. Several studies in rodents report that diabetes can increase the rate of formation of Aβ and NFT such as induction of diabetes mellitus (DM) exacerbates AD neuropathology in a mouse model of AD [37-47]. Moreover, DM and AD share several clinical and biochemical features such as oxidative stress, formation of advanced glycation end-products (AGEs), dysregulation in glucose metabolism and altered insulin signaling, suggesting a common pathogenic mechanism [48].

Data in vitro and in vivo indicate that insulin regulates the metabolism and the accumulation of β-amyloid (Aβ) and tau through phosphorylation by protein kinases including glycogen synthase kinase 3β (GSK-3β).

It has been proposed that insulin influences the clearance of Aβ in the brain of AD patients. Insulin-degrading enzyme (IDE) is involved in the degradation of insulin but also of extracellular Aβ. Therefore, by competition for IDE, insulin can inhibit Aβ degradation and increase the extracellular concentration of Aβ [49]. In addition, aberrant glucose metabolism can induce oxidative stress that is associated to Aβ accumulation and tau phosphorylation; which through MAPK stimulation, activates inflammatory pathways that lead to neuronal cell damage [48]. GSK-3β is a major player downstream of the insulin signaling pathway and its activity is downregulated by insulin. Moreover, numerous studies have reported that animal models of type 1 diabetes showed tau hyperphosphorylation associated to learning and memory deficit [42,45-47]. Thus, dysfunctions in insulin signaling pathway could cause activation of GSK3β or other kinases involved in tau hyperphosphorylation, thereby contributing to formation of NFTs. These evidence suggest that insulin could play an important role in the regulation of tau protein status in neurons. Thus, DM might be involved in the pathological scenario that lead to the development of neurofibrillary

lesions and amyloid plaques that are characteristic of AD brains. Nevertheless, the underlying mechanism for the association between AD and DM and their impact in cognition remains largely unexplored.

The aim of my project was to investigate the role of tau in the generation of a molecular link between DM Type 1 (DMT1) and AD. Wild-type mice (WT) and knock-out mice for the murine tau protein (mtauKO) were used to assess this hypothesis. DMT1 was modeled in both genotypes by intraperitoneal injection of streptozotocin (STZ; N-nitroso derivative of glucosamine), a drug that destroys pancreatic beta-cells causing insulin deficiency [9,47,50,51].

The absence of tau proteins in mtauKO mice was used as tool to explore the link between the tau protein and DM in AD. mtauKO mice have been previously characterized; they appear phenotypically normal, are able to reproduce and do not show any behavioral deficit compared to wild type mouse in all paradigms tested. Recent results suggest that non-tau MAPs (MAP1) can compensate the lack of the tau protein from these tau-deficient neurons [52-53].

MATERIAL AND METHODS

1. Transgenic mice

In this study, 4-month-old homozygous mtauKO and WT mice (10-13 (males and females) per genotype and treatment) were used. All animal procedures were performed in accordance with National Institutes of Health and University of California guidelines and Use Committee at the University of California, Irvine.

2. Behavioral Tests

Morris Maze

Mice were trained for the hidden Morris water maze test to swim to a 14 cm diameter circular Plexiglas platform submerged 1.5 cm beneath the surface of the water and invisible to the mice while swimming. The platform was located in a fixed position, equidistant from the center and the wall of the tank. Mice were subjected to four training trials per day. During each trial, mice were placed into the tank at one of four designated start points in a pseudorandom order per day. Mice were trained for as many days as needed to reach the training criterion of 25 seconds (escape latency). If mice failed to find the platform within 60 seconds, they were manually guided to the platform and allowed to remain there for 5 seconds. The probe trial was assessed 24 hours later to the last training session and consisted of a 60 second free swim in the pool without the platform. Performance was monitored with the EthoVision XT video tracking system [54].

3. Induction of DMT 1, glucose measure, insulin measure and LiCl treatment.

WT and mtauKO mice were injected i.p. with 150 mg/kg of streptozotocin (Sigma 1G), diluited in 100 μl of Na-Citrate buffer. After 3 days and 7 weeks, true-track glucose test strips measured glucose levels in the blood (Nitro diagnostic). For the LiCl experiment, 2 days after streptozotocin injection, animals were administered lithium daily (300μl of 0.6mol/L LiCl/mouse/day intraperitoneally) for a period of 4 weeks. The insulin concentration in the plasma was measured by ELISA assay (Millipore) after 7 weeks from streptozotocin injection .

4. Tissue preparation

After deep anesthesia with sodium pentobarbital (60mg/Kg), 4 month-old WT and mtauKO mice were perfused transcardially with 0.1M phosphate-buffered saline (PBS), pH 7.4. Half brain was fixed for 48 hours in 4% paraformaldehyde in 0.1M phosphate buffer saline, pH 7.4 and cryoprotected in 30% sucrose for immunohistochemical analysis, whereas the other half was frozen in dry ice for biochemical analysis. Thick (40 μm) free-floating sections were obtained using a freezing microtome (Leica SM 2010 R) and serially collected (each series contained sections that represented 1/7th of the total brain) in cold PBS and 0.02% sodium azide.

Protein extracts were prepared by homogenizing whole brain hemisphere samples in T-per (Pierce) extraction buffer (150mg/mL), complemented with proteases (Complete Mini Protease Inhibitor Tablets, Roche) and phosphatases inhibitors (5mmol/L sodium, sigma), followed by centrifugation at 100,000 x g for 1 hour. Protein concentration in the supernatant was determined using the Bradford assay.

5. Immunoblotting

Equal amounts of protein (20μg) were separated on 4-12% Bis-Tris gel (Invitrogen, Carlsbad, CA), transferred to nitrocellulose membranes. Membranes were blocked for 1 hour in 5% (w/v) suspension of nonfat milk in 0.2% Tween 20 Tris-buffered saline (pH 7.5). After blocking, the membranes were incubated overnight, at 4°C, with one of the following primary antibodies: anti-PSD95 (1:1000; Cell Signaling Technology, Danvers, MA, USA), anti-Synaptophysin (1:5000; Sigma Aldrich), anti-CREB (1:1000; Cell Signaling Technology, Danvers, MA, USA), anti-pCREB (ser133) (1:1000; Cell Signaling Technology, Danvers, MA, USA), anti-AT8 (1:1000; Pierce Biotechnology), anti-AT100 (1:1000; Pierce Biotechnology), anti-AT180 (1:1000; Pierce Biotechnology), anti-AT270 (1:1000; Pierce Biotechnology), anti-PHF1 (Dr. Peter Davies, Albert Einstein College of Medicine, Manhasset, NY, USA), anti-pIR(Tyr972) (1:1000; Millipore, Temecula, CA); anti-IR (1:1000; Millipore, Temecula, CA), anti-pPI3K(P85) (1:1000; Cell Signaling Technology, Danvers, MA, USA), anti-PI3K (1:1000; Cell Signaling Technology, Danvers, MA, USA), anti-pAKT(ser473) (1:1000; Cell Signaling Technology, Danvers, MA, USA), anti-AKT (1:1000; Cell Signaling Technology, Danvers, MA, USA), anti-pGSK3 β (ser9) (1:1000; Cell Signaling), anti-pGSK3 β (1:1000; Calbiochem), anti-Cdk5 (1:1000; Calbiochem), anti-C'-term p35 (1:200; Santa Cruz Biotechnology) for p25 and p35, anti-pERK1/2 (1:500; Santa Cruz Biotech), anti-ERK1/2 (1:500; Santa Cruz Biotech), anti-p-p38MAPK (1:1000; Cell Signaling Technology, Danvers, MA, USA), anti-p38MAPK (1:1000; Cell Signaling Technology, Danvers, MA, USA), anti-GAPDH (1:5000, Santa Cruz Biotechnology). The membranes were washed in tween-TBS for 20 min and incubated at 20ºC with the specific secondary antibody at a dilution of 1:10000 (Pierce Biotechnology) for 60 min. The blots were developed using Super Signal (Pierce Biotechnology).

6. Quantitative and statistical analyses

All immunoblot data were quantitatively analyzed using Image J 1.4 software. The data were subsequently analyzed by Student's *t*-test comparison or two-way analysis of variance (treatment vs genotype) followed by Bonferroni's comparisons using Graphpad Prism software (Graphpad Prism Inc., San Diego, CA, USA). The significance was set at 95% of confidence. All values are presented as mean ± SEM

RESULTS

1. STZ induces diabetes in WT and mtauKO mice

Streptozotocin (STZ) is one of most widely used drugs for induction of experimental diabetes (type I) in animals [9,47,50,51]. To induce type I diabetes, mice were intraperitoneal administrated with streptozotocin (Sigma, St. Louis, MO, USA) at the concentration of 150 mg/kg [55]. Hyperglycemia is a measure related with diabetes induction, thus diabetes was considered when mice developed glucose levels superior that 200mg/dL. To establish if hyperglycemia was obtained successfully as indicative of diabetes, 3 days and 7 weeks after STZ injection the blood glucose concentration was measured again in treated and untreated WT and mtauKO mice. The results showed a significant increase in glucose levels over 200mg/dL in WT and mtauKO mice treated with STZ as compared to controls (Table.1). Notably, similar glucose levels were detected in both WT-STZ and mtauKO-STZ mice which remained elevated after 7 weeks after the last injection (Table1). Furthermore, we measured the levels of insulin in the plasma 7 weeks after STZ administration by ELISA assay, which confirmed significative lower levels of insulin in treated WT and mtauKO mice as compared to controls (Table 1).

Genotype	N	Blood sugar (mg/dl) after 3 days from STZ injection	Final blood sugar (mg/dl) after 7 weeks from STZ injection	Plasma insulin after 7 weeks from STZ injection (ng/mL)
WT	13	114±7	136±6	0,8
WT-STZ	13	253±28***	315±24***	0,22*
mtauKO	10	134±10	146±7	0,9
mtauKO-STZ	10	261±12**	305±33***	0,24*

Table 1. Significant hyperglucemia and lower levels of plasma insulin in WT and mtauKO mice after STZ injection. Significant increases in glucose levels were observed in WT and mtauKO mice treated with STZ at 3 days and 7 weeks. The values represent the mean ± SEM (n=10-12). WT-STZ and mtauKO-STZ showed significant decrease in plasma insulin as compared to controls. A two-way ANOVA showed differences on treatment but not on genotype and no interaction. *Bonferroni's post hoc* comparisons revealed differences between STZ-treated and respectively untreated mice (* $p<0.05$ ** $p<0.01$, *** $p<0.001$)

2. The hippocampal cognitive deficit induced by the STZ treatment is tau dependent.

To assess the relevance of tau in diabetic condition on cognitive functions, vehicle and STZ-treated mice (WT and mtauKO) were tested in behavioral paradigms that analyze learning and memory. The brain structure strongly implicated in learning and memory processes is the hippocampus; whose functions are heavily challenged in AD [32,34,39]. Thus, we chose a hippocampal-dependent behavior test, the Morris water maze (MWM) to evaluate the presence of potential deficits. Tests were performed 7 weeks after the induction of diabetes. Mice were trained to reach criterion (escape latency <25 seconds) in the spatial reference version of the MWM to find the location of a hidden platform. Interestingly, significant, differences were observed during the learning process between the WT-vehicle and WT-STZ treated groups. In contrast, no differences were detected between mtauKO-vehicle and mtauKO-STZ treated mice. In addition, WT-vehicle mice reached criterion in 3 days, while mtauKO-vehicle and STZ-treated mice required 4 days and WT-STZ mice did not reach the criterion even after 5 days of training, indicating that the diabetic condition heavily impairs spatial learning, but importantly only in WT mice (Fig. 4A).

We then analyzed the effects of the STZ treatment on memory, by conducting probe trials with the different groups 24 hr after the last training trail. As with results obtained during the learning process, WT-STZ treated mice showed significant impairment of long-term memory (24 hours probe) as compared to WT-vehicle treated mice, as determined by the significant decrease in the time spent in the platform quadrant and the reduced number of crosses (Fig. 4B and C). By contrast, no differences were observed between the mtauKO-STZ and the mtauKO-vehicle treated groups. Interestingly, no statistically significant differences were noted among groups for swim speed and traveled distance (Fig. 4D and E) suggesting that the STZ treatment does not induce motor alterations. .These data indicate that the severe

learning and memory deficit observed in the WT-STZ treated mice is very likely induced by a tau-dependent mechanism(s).

To exclude the possibility that the impaired performance in the MWM could be due to visual deficits, we tested the visual acuity in all genotypes by performing the MWM test using a visible platform. In these conditions WT-STZ-treated mice performed as well as vehicle treated animals, indicating that the deficits are not dictated by visual loss.

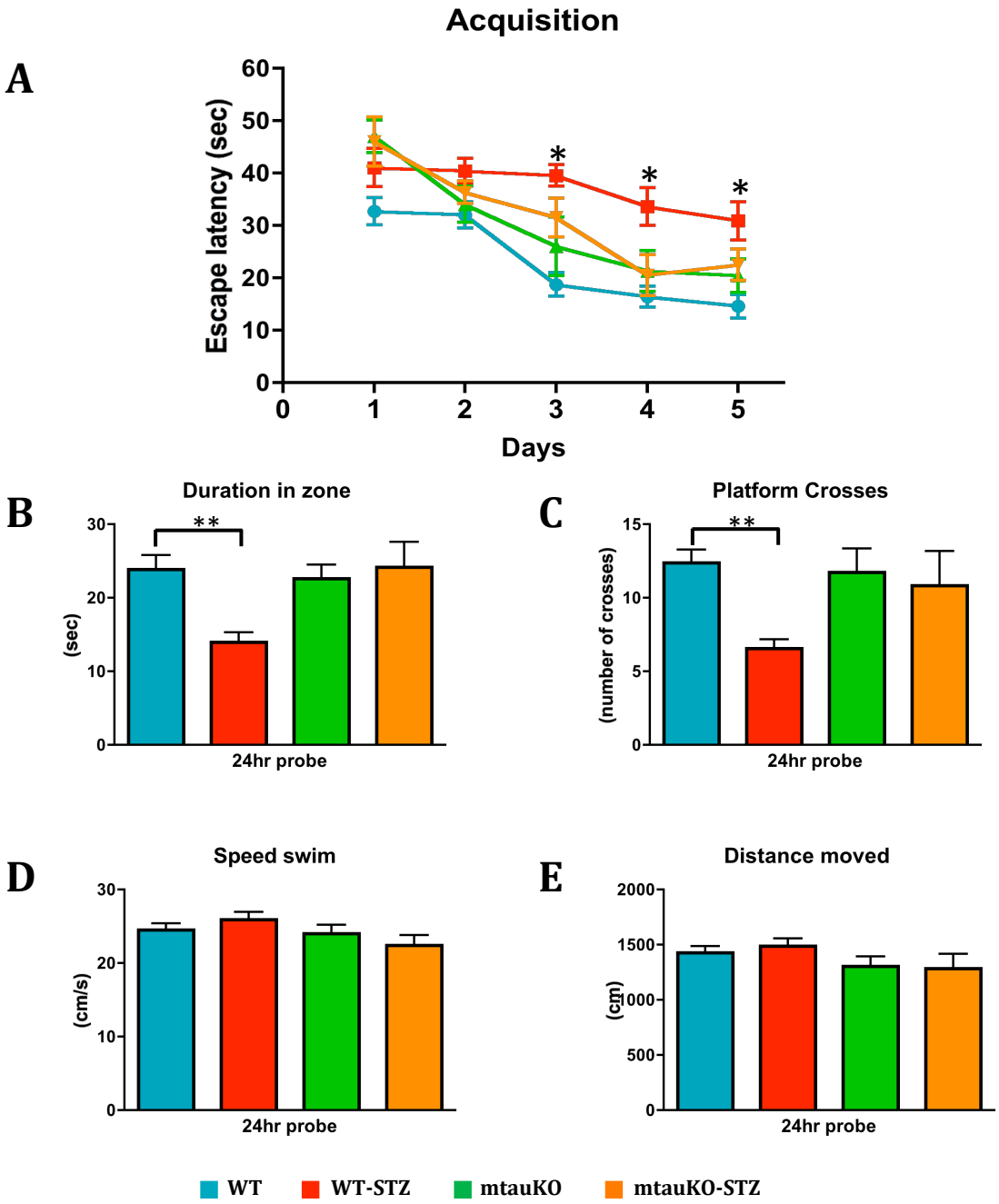

Figure 4. Streptozotocin treatment induces hippocampal cognitive impairment in WT mice through a tau dependent mechanism. Mice were trained on the spatial reference version of the Morris water maze (MWM; n=10-12 per group) at 4 months of age. Acquisition curves (**A**) are shown for the 5 days of training on the MWM. Significant differences in escape latency time were observed in WT-STZ group compared to WT mice. (**B-C**) Significant differences were observed between WT-STZ mice compared to WT mice, in the time spent in the target zone (58.48± 5.75 %, a two-way ANOVA showed no differences on treatment or genotype but strong interaction. A *Bonferroni's post hoc* comparison revealed differences between WT-STZ and untreated WT mice**p<0.01) (**B**) and in the number of platform crossings (52.89± 5.15 %, a two-way ANOVA showed no differences on treatment or genotype but strong interaction. A *Bonferroni's post hoc* comparison revealed differences between WT-STZ and untreated WT mice **p<0.01) (**C**). Notably, no differences were observed between mtauKO-STZ compared to mtauKO mice (*Bonferroni's post hoc* comparison. (**D-E**) In addition, two-way anovas revealed no statistic differences in speed swim (**D**) and in traveled distance (**E**) between groups. WT (blue); WT-STZ (red); mtauKO (green); mtauKO-STZ (orange). The values represent the mean ± S.E.M.

3. Cognitive deficits induced by the STZ treatment are correlated to a significant decrease of synaptic markers expression and of molecules involved in memory-related intracellular signaling.

To unravel the molecular mechanisms underlying the cognitive decline induced by diabetes in WT mice, we tested the level of expression of memory-related transcription factors, such as CREB (cAMP response element-binding) and of synaptic proteins, such as PSD-95 and synaptophysin, by western-blot. Changes of expression of these molecules have been associated with the memory impairments observed in some murine models of neurodegenerative disorders [56-57]. Our analysis revealed a significant decrease in the endogeneous levels of the synaptic proteins, PSD95 and synaptophysin in the WT-STZ compared to vehicle treated mice. Notably, analyses of these same molecules in mtauKO-vehicle compared to mtauKO-STZ-treated mice showed no differences (Fig. 5A and B).

Interestingly, a significant reduction of the phosphorylated form of CREB were found in WT-STZ compared to WT-vehicle mice (Fig. 5A and B); whereas, no difference was detected in mtauKO-vehicle compared to mtauKO-STZ treated mice (Fig. 5A and B). These results suggest that the memory and learning behavioral deficit observed in the MWM test in WT STZ-treated mice is very likely related with dysfunctions of synaptic functions and of transcription factors involved in memory formation.

We controlled in all genotypes and treatments that the behavioral and cellular phenotypes were not due to cell loss, by performing hematoxylin-eosin stainings of brain sections from WT, WT-STZ, mtauKO and mtauKO-STZ treated mice. Indeed, these analyses did not reveal the presence of macroscopic differences between the groups in all the regions of the brain analyzed (Figure 6).

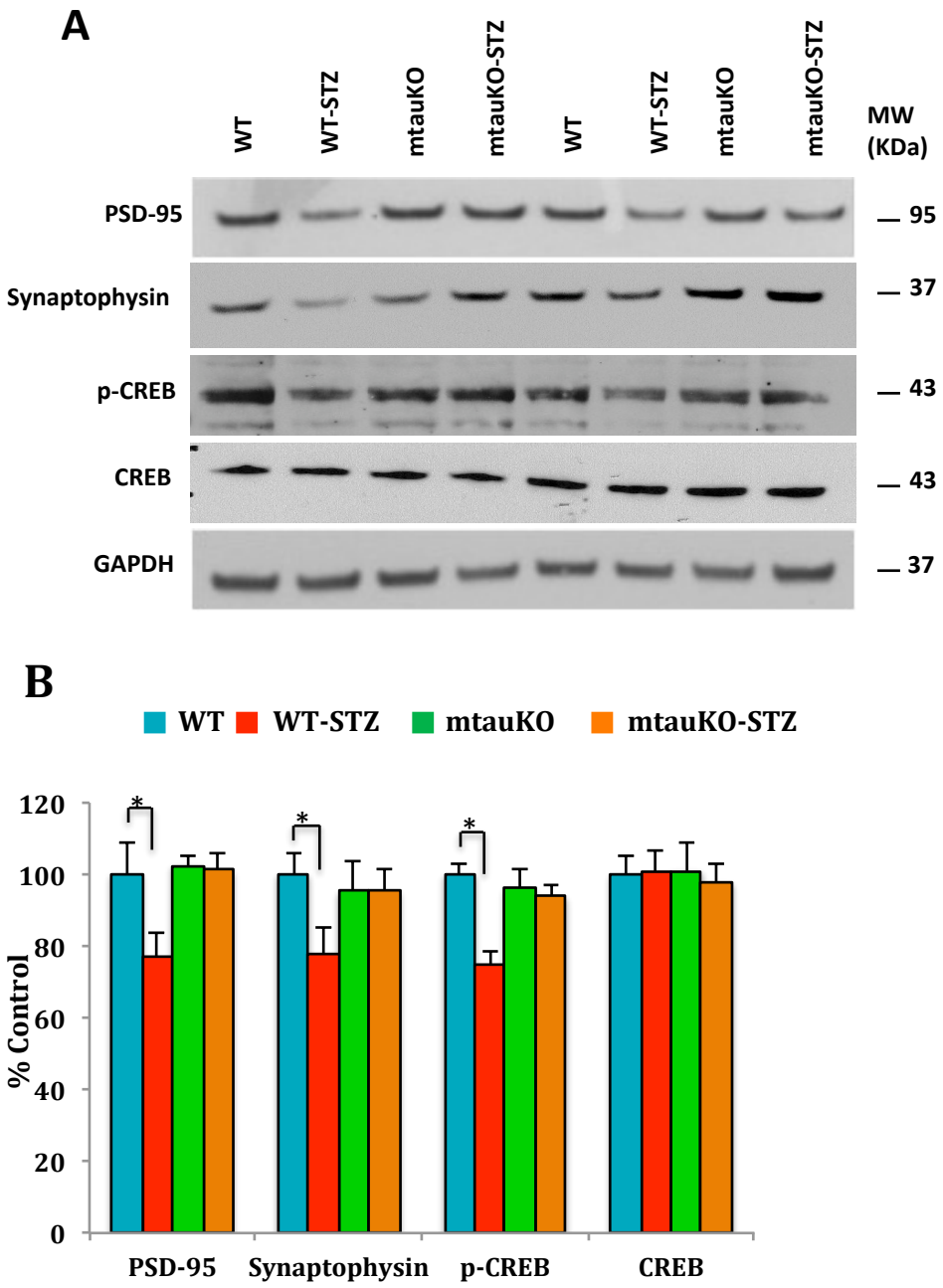

Figure 5. Streptozotocin treatment decreases the content memory-related intracellular signaling molecules and of synaptic-related proteins in WT mice. (A) Immunoblot analyses of PSD-95, synaptophysin, p-CREB and CREB levels in protein extracts from whole-brain homogenates of 5-month-old WT, WT-STZ, mtauKO and mtauKO-STZ treated (n=6) mice. **(B)** Quantification of band intensities shown in A) normalized to GAPDH and expressed as percentage of control showed significant decrease in PSD-95 (22.32 ± 8.05%, two-way ANOVA *p<0.05), synaptophysin (19.23± 9.2%, two-way ANOVA *p<0.05) and phosphorylated CREB expression (25.13± 3.52 %, two-way ANOVA **p<0.01) in WT-STZ compared to WT-vehicle treated mice. Quantification of CREB levels shows no differences between the different genotypes analyzed. The values represent the mean ± SEM

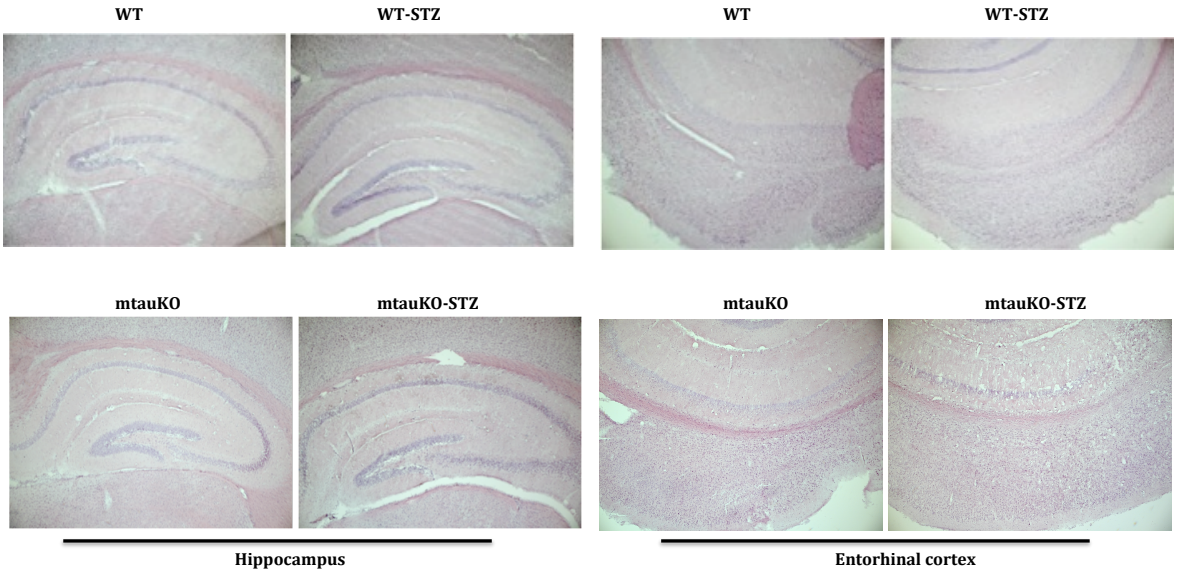

Figure 6: STZ treatment does not alter cellular composition in different brain structures. Representative pictures for H&E staining on brain section from WT, WT-STZ, mtauKO and mtauKO-STZ treated mice in two regions relevant for memory formation and storage, such as the hippocampus and the entorhinal cortex.

4. STZ treatment induces significant tau hyperphosphorylation in WT mice

It has been described in several previous studies that STZ induces hyperphosphorylation of tau [46,47,55]. Thus, we determined by western-blot analyses the level of phosphorylated tau in soluble homogenates of WT-vehicle treated or STZ treated mice (Figure 7A). We observed significant increases of tau phoshorylated levels at residues Ser202/Thr 205 (recognized by the AT8 antibody), Thr 231 (recognized by the AT180 antibody) and Ser396/404 (recognized by the PHF-1 antibody) in the WT-STZ compared to WT-vehicle treated mice (Figure 7B). In addition, a trend toward enhanced tau phosphorylation at residues Ser212/Thr214 (recognized by the AT100 antibody) and Thr181 (recognized by the AT270 antibody) was also observed in WT-STZ compared to WT-vehicle treated mice (Figure. 7B). Thus, STZ treatment leads to tau hyperphosphorylation at several epitopes with a biochemical pattern similar to that observed in Alzheimer's disease.

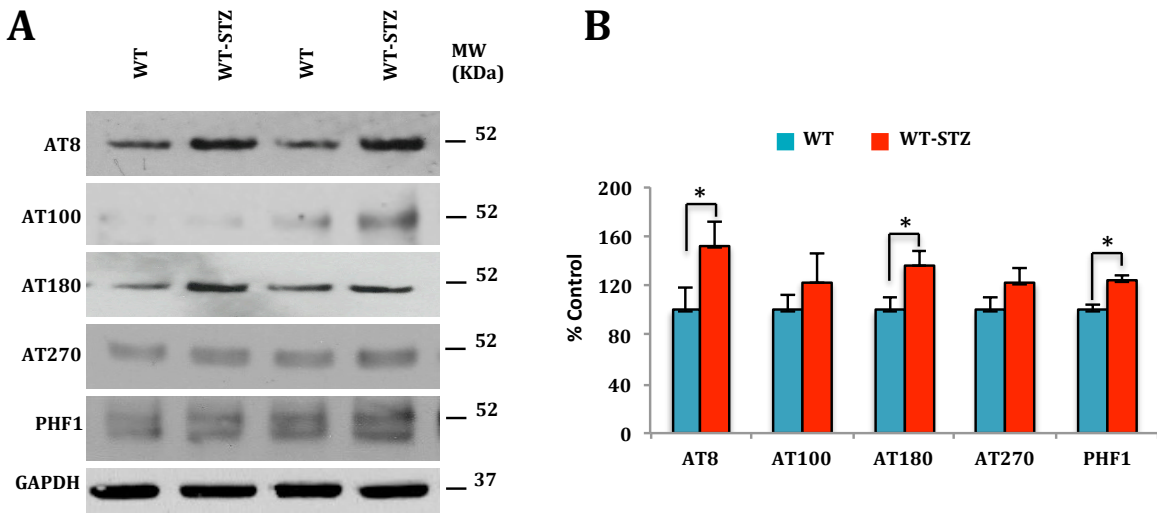

Figure 7. Streptozotocin treatment leads to tau hyperphosphorylation in WT mice. (A) Immunoblot analysis of phosphorylated-tau epitopes pSer199/202 tau (AT8), pSer212/Thr214 (AT100), pThr231 (AT180), pThr181 (AT270) and pSer396/404 (PHF-1) of protein extracts from whole-brain homogenates from 5 month-old WT and WT-STZ (n=6) mice, as indicated. **(B)** Quantification of protein levels shown in A) normalized to GAPDH and expressed as percentage of control. Note the significant increase in p-tau phosphorylation at pSer199/202 (52.06 ± 30.25%, *p<0.05, unpaired *t*-test), Thr231 (65.36±43.52%, *p<0.05, unpaired *t*) and Ser 396/404 (24.43± 3.21%, *p <0.05, unpaired *t*) residues in WT-STZ as compared to WT-vehicle treated mice. A trend toward tau phosphorylation at residues Ser212/Thr214 and Thr181 was found in WT-STZ compared to WT-vehicle treated mice. The values represent the mean ± S.E.M.

5. STZ treatment impairs IR/PI3K/AKT pathway with a consequent decrease of GSK3β [Ser9] phosphorylation level.

We have showed that STZ treatment induces tau hyperphosphorylation, so to further investigate the molecular mechanism underlying this effect, we analyzed the phosphorylated levels of molecules downstream of the IR-mediated pathway. This because changes in this pathway might reflect modulation of the activity of kinases responsive to the IR signaling and involved in tau phosphorylation.

The insulin receptor (IR) is the first step in the activation of the insulin pathway. Binding of insulin to its receptor induces the dimerization and autophosphorylation of the IRb-subunit. Therefore, total levels of IR and its phosphorylated form were investigated by western-blot. The results showed a severe decrease of steady-state level of phosphorylated IRb in both WT and mtauKO mice treated with STZ compared with their respective controls (Figure 8 A-B). In addition, no differences were observed in total IR levels, indicating that the significant decrease of phosphorylated IRb, induced by the STZ-treatment, is not associated with changes of total IR levels. Next, we investigated the phosphorylated levels of major downstream kinase components of the insulin pathway, including phosphoinositide 3-kinase (PI3K)/Akt/glycogen synthase kinase 3 beta (GSK3b) and MAPK pathways using antibodies directed against specific residues, whose phosphorylation is known to determine their activity. In this regard, we first analyzed PI3K and the regulatory subunit p85. This analysis showed a significant reduction of the phosphorylation of the regulatory subunit p85 in both WT and mtauKO mice treated with STZ compared to the respective controls; while no changes were observed in the total PI3K level (Figure 8 A-B). A similar significant decrease was observed in the level of phosphorylated AKT at Ser473 in WT and mtauKO mice STZ-treated, as compared to vehicle-treated mice. These results correlate well with the reduction of

phosphorylated GSK3b at Ser9 in WT and mtauKO mice STZ-treated, as compared to the respective controls. Similar to PI3K, no changes were observed in total AKT and GSK3b levels (Figure 8 A-B). In addition, no statistical differences were observed in total CDK5, ERK and p38 kinase levels or of their phosphorylated forms (Figure 9 A-B). These results suggest that the hyperphosphorylation of tau in WT mice treated with STZ is induced mainly by alterations of the PI3K/AKT/GSK3b pathway.

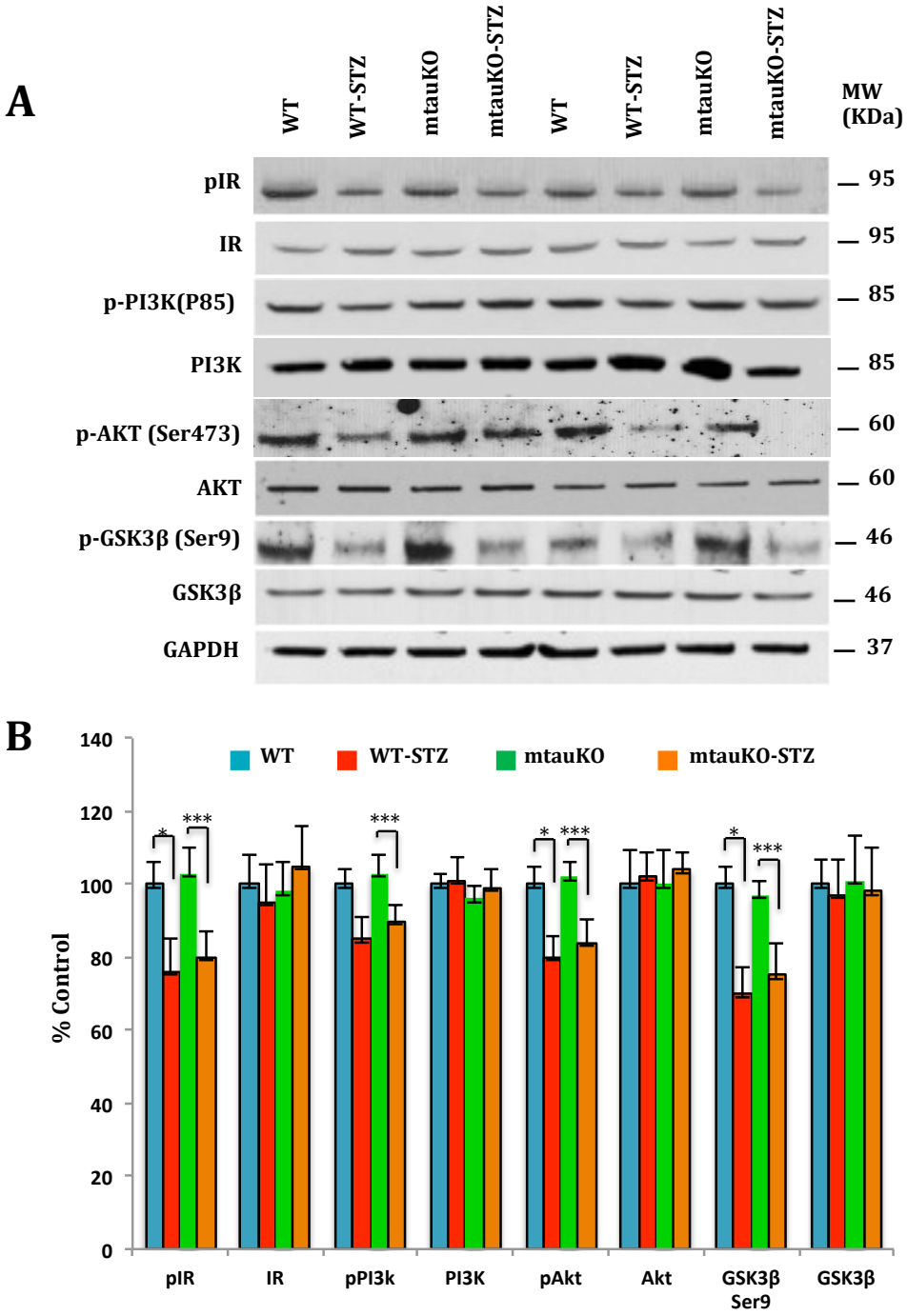

Figure 8. Streptozotocin treatment alters the IR/PI3K/AKT pathway in WT and mtauKO mice. (A) Immunoblot analyses of pIR, IR, pPI3k(p85), PI3k, pAKT(Ser473), AKT, GSK34 (Ser9) and GSK3β levels in protein extracts from 5-month-old WT, WT-STZ, mtauKO and mtauKO-STZ brains (n=6), as indicated. **(B)** Quantification of band intensities shown in A) normalized to GAPDH and expressed as percentage of control. A statistically significant decrease was observed in the level of phosphorylated IR between WT-STZ (25.55±7.36%, pairwise comparison *p<0.05) and mtauKO-STZ (21.3±7.29% pairwise comparison*p<0.05) with respect to control mice. WT-STZ and mtauKO-STZ showed significant decrease in the phosphorylated level of AKT [Ser473] (26.45± 6.01% pairwise comparison *p<0.05) in WT-STZ and mtauKO-STZ (14.6±4.5%, pairwise comparison *p<0.05) versus WT and mtauKO extracts; similarly, levels of phosphorylated GSK3β-Ser9 were different between WT-STZ and mtauKO-STZ versus WT and mtauKO extracts (30.4± 6.08% pairwise comparison *p<0.05 for WT-STZ and 24.7±45.1%, pairwise comparison *p<0.05 for mtauKO-STZ). Quantifications of IR, PI3K, AKT and GSK3β total levels showed no difference between the different genotypes

analyzed, indicating that reduction of these markers are presumably related with their activity. All two-way ANOVAs showed no differences. The values represent the mean ± SEM

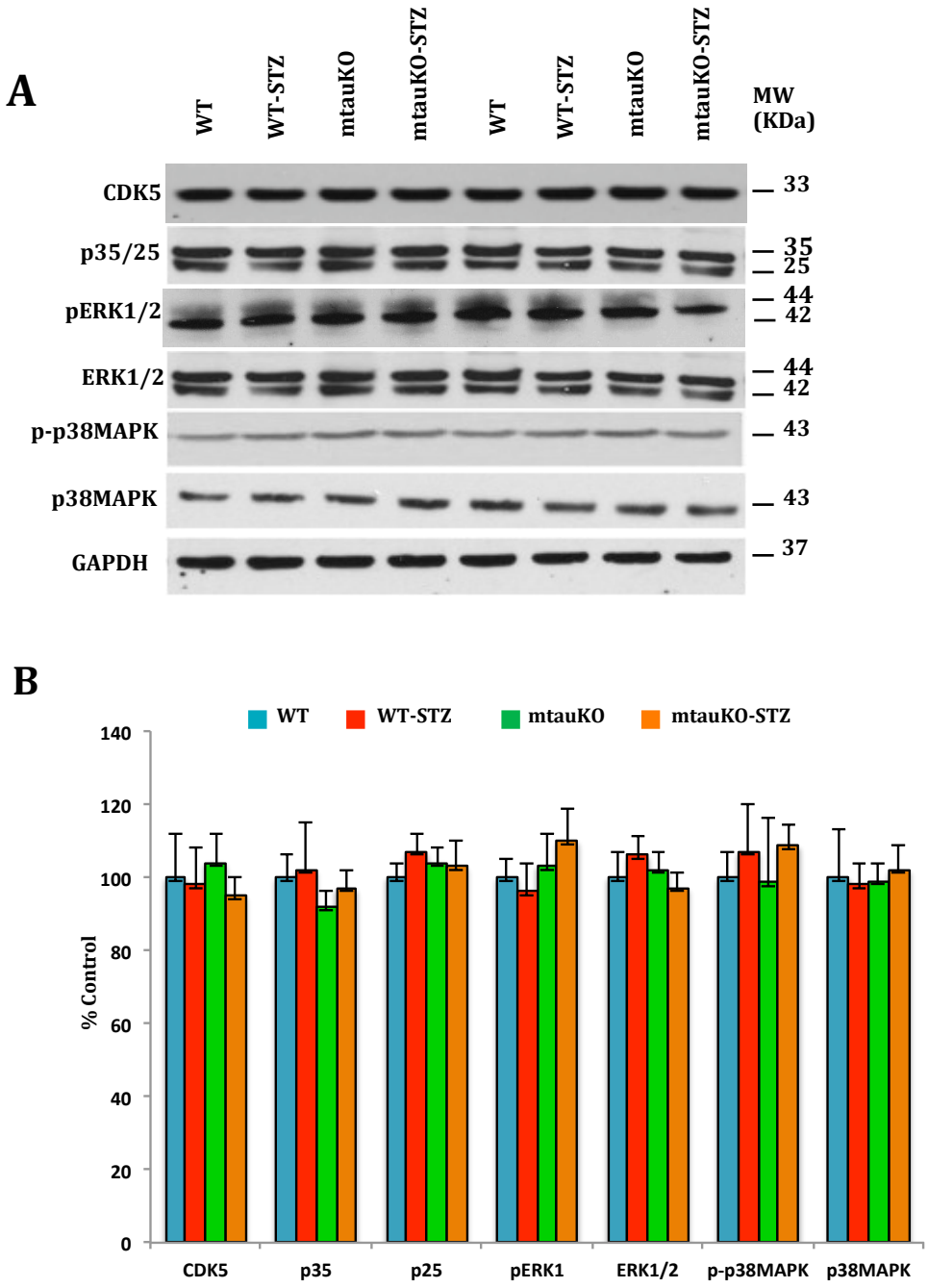

Figure 9. Streptozotocin treatment did not affect Cdk5, ERK and p38MAPK total content or phosphorylated levels. **(A)** Immunoblot analysis of total content of cdk5, p25/p35, ERK1/2, and of phosphorylated ERK1/2, p38MAPK and p38MAPK in protein extracts from whole-brain homogenates from WT, WT-STZ, mtauKO and mtauKO-STZ treated 5-month-old mice (n=6), as indicated. **(B)** Quantification of samples shown in A) normalized to GAPDH and expressed as percentage of control values. Similar levels of each kinase (cdk5, Erk and p38MAPK) and their phosphorylated forms (p35/p25, pErk and p-p38MAPK) were observed. The values represent the mean ± SEM. Data were analyzed by Two-way ANOVA, which showed no differences among groups.

6. Cognitive deficits induced by STZ treatment in WT mice are reversed by Lithium treatment.

Our results suggest that impaired insulin signaling in WT mice induces a cognitive deficit mediated by tau hyperphosphorylation, very likely through the activation of GSK-3β. Lithium is one of the most widely used drugs for treating bipolar disorders, which is well tolerated in humans. Several studies have reported that lithium Chloride (LiCl) inhibits GSK-3β activity [58-59]. Thus, we hypothesized that lithium treatment by blocking GSK-3β, might reduce tau hyperphosphorylation induced by the STZ treatment in WT mice and thereby could restore the cognitive deficits. To assess this hypothesis, WT-STZ treated mice were chronically administered lithium for a period of 5 weeks and then their cognitive performance was tested in the Morris water maze (Figure 10). Interestingly, these experiments showed significant differences between WT and WT-STZ–LiCl treated groups compared to the WT- STZ treated group. Indeed, the learning performance of the STZ only treated group was severely impaired with respect of that of animals treated with STZ and LiCl. Moreover, no differences were detected between WT compared to WT-STZ-LiCl mice suggesting that impaired spatial learning induced by STZ was rescued by the LiCl treatment (Figure 10 A). During the probe trials, to assess the spatial memory, WT-STZ-LiCl mice showed that the time in the platform quadrant and number of crosses were comparable to those seen in WT mice; and for both these parameters were significantly higher than that of WT-STZ animals (Figure 10 B-C). No statistically significant differences were noted among groups for swim speed and traveled distance; this suggests that LiCl treatment does not affect motor functions (Figure 10 D-E). These data indicate that LiCl treatment reverses the severe learning and memory deficit induced by streptozotocin very likely through the inhibition of GSK-3β activity.

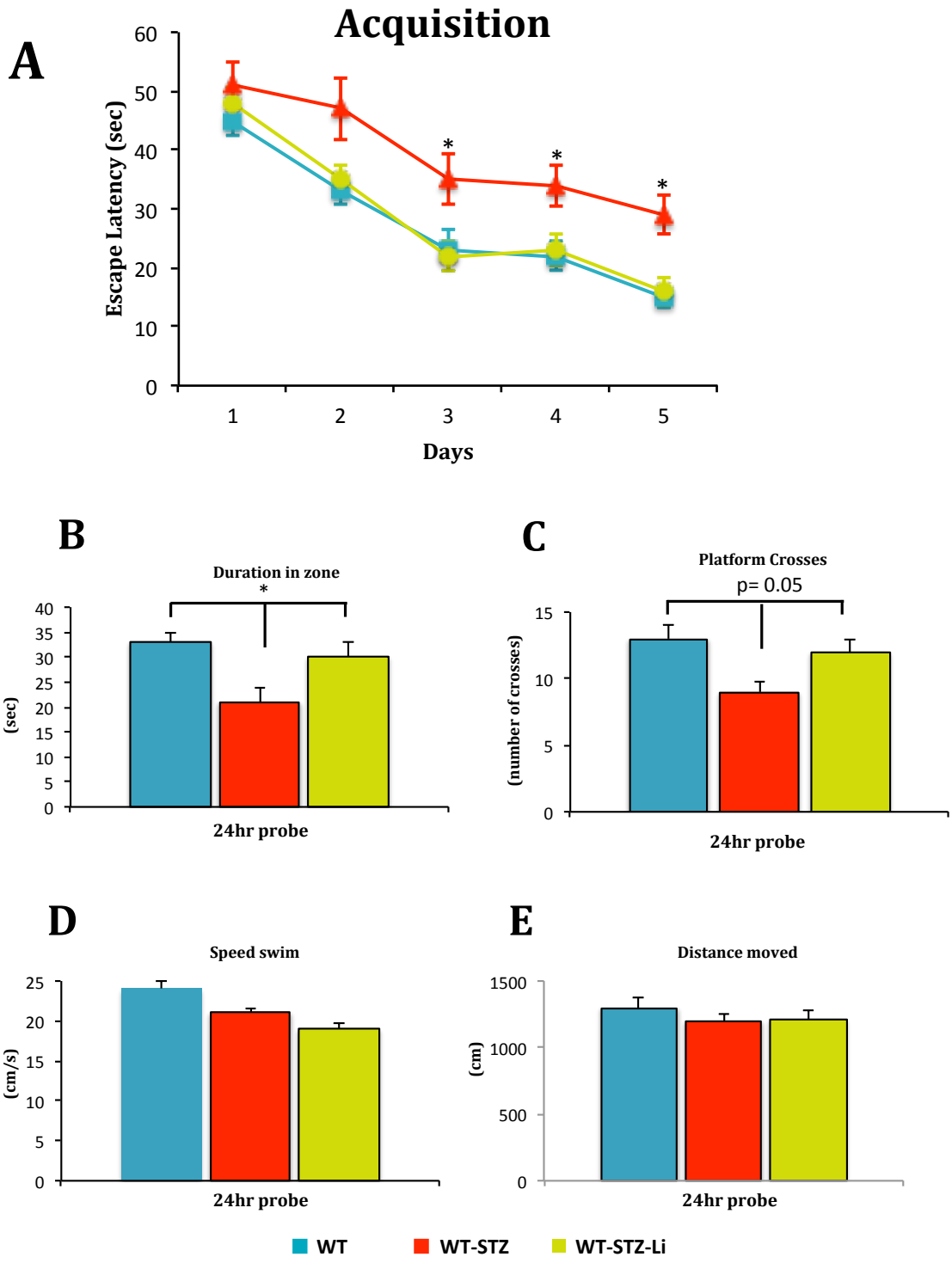

Figure 10. Lithium treatment restores the cognitive impairments of WT-STZ mice. Mice were trained on the spatial reference version of the Morris water maze (MWM; n=8-9 per group) at 4 months of age. Acquisition curves (A) are shown for the 5 days of training in the MWM. No difference in escape latency time was observed in WT-STZ-Li mice as compared to WT animals. Statistically significant differences were observed between the WT-STZ group and the WT or WT-STZ-Li treated mice. (B-C) Absence of difference between WT-STZ-Li mice and WT in the time spent in the target zone and in the number of platform's crossings. As in A) statistically significant differences were obtained between the WT-STZ group and WT or WT-STZ-Li treated mice. Data were analyzed by Two-way ANOVA followed by Bonferroni's post hoc comparisons *p<0.05 for escape latency time, time spent in target zone and number of crossing. (D-E) Two-way ANOVA analyses revealed no difference in swim speed (D) or in traveled distance (E) between groups. The values represent the mean ± S.E.M.

DISCUSSION

Growing evidence associates metabolic conditions such as diabetes mellitus to a higher chance to develop Alzheimer's disease [10-14]. This comorbidity is further supported by clinical evidence showing that AD patients, during the late onset of the disorder, develop aberrant insulin functions. Indeed, type 1 diabetes patients develop cognitive deficits, including memory and learning impairments more frequently then non-diabetic individuals of the same age group. Moreover, autopsies of type I diabetic patients, reveal that these cognitive deficits correlate with degeneration of the cerebral cortex and neuronal loss [1-2,60-61].

One of the main hystopathological features of AD is the presence of NFTs, composed by aggregation of hyperphosphorylated tau proteins. Tau proteins have a key role in the assembly and stability of microtubules; pathological conditions, such as AD, increase tau phosphorylation causing disruption of microtubules. This event interferes with intracellular vesicles transport, leading to synaptic dysfunctions and the consequent cognitive deficits [32,34-36]. In this study, we investigated the molecular connections between insulin deficit and tau phosphorylation in a mouse model of STZ-induced Type 1 diabetes. The effect of STZ in a WT background was compared to that obtained in mice lacking the tau protein expression (mtauKO mice) [52-53]. Insulin deficiency was successfully induced in both genotypes by systemic STZ injections, according to previous studies [9,47,50,51]. Interestingly, our results shows that, in WT mice, STZ-induced insulin deficiency leads to an increase of tau phosphorylation at several sites as it has been reported in previous studies [41,42,,45-47]. In AD, tau hyperphosphorylation, very likely provoked by the deregulation of kinases and/or phosphatases, has been proposed to lead to tau aggregation preventing tau binding to MTs, thereby destabilizing the MT network. This hypothesis is supported by *in vitro* studies showing that hyperphosphorylation of human tau induces microtubules

disruption and tau aggregation.

In our study, we found tau hyperphosphorylation 7 weeks after the induction of diabetes, however we could not detect deposition of tau aggregates probably due to the short time frame lapsed between the induction of diabetes and our analyses.

Alternatively, absence of NFT in this study could be dependent from an insufficient level of total tau phosphorylation in the STZ model, or to insufficient levels of phosphorylation at residues promoting insoluble aggregates. Future studies will address these points.

Impaired insulin signaling has a strong impact on the central nervous system and it is associated to impaired learning, memory and mental flexibility [2,16-19,62-63]. Indeed, insulin act as a cognitive modulator involved in synaptic plasticity by modulation of neuronal firing via action at K_{ATP} channales. Moreover, insulin affects both long-term potentiation (LTP) and depression (LTD) through modulation of AMPA and NMDA channels [23-25]. The insulin receptors are widely expressed in the brain of rodents and humans [21-22] and upon stimulation they trigger several signaling pathways including MAPKs and PI3K pathways [26,64-65].

In this study, we did not observe significant differences in the activation of MAPKs pathway. This could be explained either by compensatory homeostatic effects on this pathway or by the time frame chosen to perform these analyses. In sharp contrast, we found that the insulin deficiency caused by the STZ treatment by reducing the activation of the insulin receptors (IR) affects the activation of the PI3K pathway and of downstream kinases [41]. We found alterations of this pathway in both genotypes, WT and mtauKO, with decreased levels of AKT phosphorylation on Ser473. Phosphorylation of AKT at this site leads to the activation of this kinase. AKT has been involved in tau phosphorylation; in addition, AKT phosphorylates another important

kinase, GSK3β, thereby reducing its activity. Thus, reduction of phosphorylated AKT might translate into an increase of GSK3β activity [30,32,37-39]. Glycogen synthase kinase-3 beta (GSK3β) is a pivotal molecule in the development of Alzheimer's disease [38,39,42,43]. Indeed, GSK3β is not only involved in the production of Aβ plaques, but also in the formation of paired helical filament of (PHF)-tau, which is an integral component of the somatodendritic neurofibrillary tangle deposits that disrupt neuronal function. Thus, our results, suggest that insulin deficiency by reducing insulin signaling and AKT phosphorylation might enhance GSK3β activity leading to tau hyperphosphorylation in WT mice and consequent memory deficits. This scenario is supported by our experimental evidence obtained by the analysis of mtauKO mice, which despite the insulin deficiency do not show spatial learning and memory impairments as WT mice.

Thus, over-activation of GSK3β has a toxic effect on neurons through a mechanism involving tau hyperphosphorylation; absence of tau in a diabetic condition protects neurons from degeneration and cognitive decline [53]. In agreement with these data, we detected a significant decrease in the protein content of synaptic markers and in the phosphorylated level of CREB in WT-STZ mice. Altogether, these findings suggest that type 1 diabetes by impairing insulin signaling causes tau hyperphosphorylation through the activation of GSK3β; this leads to synaptic failure and cognitive deficits in WT mice.

To support the active involvement of GSK3β in the cognitive impairment [53][58-59] observed in this study, we submitted WT-STZ treated mice to a simultaneous Lithium treatment; lithium is reported to inhibit GSK3β activity [58-59].

Importantly, in agreement with our hypothesis we found that lithium reversed the learning and memory deficits observed in WT-STZ diabetic mice. In conclusion, I

propose that tau is a key factor in the cognitive decline observed in the reported comorbidity between diabetes and AD and modeled in this study with the WT-STZ and mtauKO-STZ diabetic mice.

Ongoing experiments are in progress to rapidly finalize this study.

We are analyzing now at the cellular and tissue levels the possibility to reverse tau hyperphosphorylation in WT-STZ treated mice by treatment with Lithium. New groups of animals are presently treated to study the protein and phosphorylation levels of the molecules whose expression is altered in WT-STZ and mtauKO-STZ versus vehicle treated mice in the absence or presence of lithium. In addition, we plan on preparing tissue extracts specifically from the hippocampus to better correlate DM with AD. Finally, we are performing microtubules binding assays to analyze the impact of type 1diabetes and of tau hyperphosphorylation on tau binding to microtubules in our model systems.

REFERENCES

1. Arvanitakis Z et al. : Diabetes mellitus and risk of Alzheimer disease and decline in cognitive function, Archives of neurology 2004, 61:661-666

2. Biessels GJ et al.: Risk of dementia in diabetes mellitus: a systematic review, Lancet neurology 2006, 5:64-74

3. Brands AM et al. : The effects of type 1 diabetes on cognitive performance: a meta-analysis, Diabetes care 2005, 28:726-735

4. Gregg EW et al. : Is diabetes associated with cognitive impairment and cognitive decline among older women? Study of Osteoporotic Fractures Research Group, Archives of internal medicine 2000, 160:174-180

5. Blaum CS et al. : Functional status and health outcomes in older americans with diabetes mellitus, Journal of the American Geriatrics Society 2003, 51:745- 753

6. Allen KV, Frier BM, Strachan MW: The relationship between type 2 diabetes and cognitive dysfunction: longitudinal studies and their methodological limitations, European journal of pharmacology 2004, 490:169-175

7. Munshi M et al. : Cognitive dysfunction is associated with poor diabetes control in older adults, Diabetes care 2006, 29:1794-1799

8. Alencar RC et al. : Assessment of cognitive status in patients with type 2 diabetes through the Mini-Mental Status Examination: a cross-sectional study, Diabetology & metabolic syndrome 2010, 2:10

9. Wild S et al. : Global prevalence of diabetes: estimates for the year 2000 and projections for 2030, Diabetes care 2004, 27:1047-1053

10. Craft S et al. : Cerebrospinal fluid and plasma insulin levels in Alzheimer's disease: relationship to severity of dementia and apolipoprotein E genotype, Neurology 1998, 50:164-168

11. Gasparini L, Netzer WJ, Greengard P, Xu H: Does insulin dysfunction play a role in Alzheimer's disease?, Trends in pharmacological sciences 2002, 23:288-293

12. Leibson CL et al. : The risk of dementia among persons with diabetes mellitus: a population-based cohort study, Annals of the New York Academy of Sciences 1997, 826:422-427

13. MacKnight C et al. : Diabetes mellitus and the risk of dementia, Alzheimer's disease and vascular cognitive impairment in the Canadian Study of Health and Aging, Dementia and geriatric cognitive disorders 2002, 14:77-83

14. Ott A et al. : Diabetes mellitus and the risk of dementia: The Rotterdam Study, Neurology 1999, 53:1937-1942

15. Haan MN: Therapy Insight: type 2 diabetes mellitus and the risk of late-onset Alzheimer's disease, Nature clinical practice Neurology 2006, 2:159-166

16. McNay EC and Cotero VE: Mini-review: impact of recurrent hypoglycemia on cognitive and brain function , Physiol Behav. 2010, 234-8

17. Zhao W et al : Brain Insulin Receptors and Spatial Memory, J Biol Chem. 1999 34893-902.

18. Zhao W et al : Insulin and the insulin receptor in experimental models of learning and memory, Eur J Pharmacol. 2004, 71-81.

19. Stranahan AM et al : Diabetes impairs hippocampal function through glucocorticoid-mediated effects on new and mature neurons. Nat Neurosci. 2008, 309-17.

20. McNay EC, Recknagel AK : Brain insulin signaling: a key component of cognitive processes and a potential basis for cognitive impairment in type 2 diabetes. Neurobiol Learn Mem. 2011, 432-42.

21. Schwartz MW, Porte D: Diabetes, obesity, and the brain. Science. 2005, 375-9.

22 Chiu SL et al. : Insulin receptor signaling regulates synapse number, dendritic plasticity, and circuit function in vivo. Neuron. 2008, 708-19

23. Cole AR, Astell A, Green C, Sutherland C: Molecular connexions between dementia and diabetes. Neurosci Biobehav Rev. 2007, 1046-63.

24. Pocai A et al. : Hypothalamic K(ATP) channels control hepatic glucose production, Nature 2005, 434:1026-1031

25. Spanswick D et al. : Insulin activates ATP-sensitive K+ channels in hypothalamic neurons of lean, but not obese rats, Nature neuroscience 2000, 3:757-758

26. Saltiel AR et al. : New perspectives into the molecular pathogenesis and treatment of type 2 diabetes, Cell. 2001,517-29.

27. Scott R : CREB and the discovery of cognitive enhancers. J Mol Neurosci. 2002, 171-7.

28. Munoz L, Ammit AJ :Targeting p38 MAPK pathway for the treatment of

Alzheimer's disease. Neuropharmacology. 2010, 561-8

29. Kelleher I : Kinase activities increase during the development of tauopathy in htau mice. J Neurochem. 2007, 2256-67.

30. Cross DA: Inhibition of glycogen synthase kinase-3 by insulin mediated by protein kinase B. Nature. 1995, 785-9.

31. Balaraman Y: Glycogen synthase kinase 3beta and Alzheimer's disease: pathophysiological and therapeutic significance. Cell Mol Life Sci. 2006,1226-35

32. Querfurth HW, LaFerla FM: Alzheimer's disease, The New England journal of medicine 2010, 362:329-344

33. Vetrivel KS, Thinakaran G: Amyloidogenic processing of beta-amyloid precursor protein in intracellular compartments. Neurology. 2006S69-73.

34. Johnson GV, Stoothoff WH: Tau phosphorylation in neuronal cell function and dysfunction, Journal of cell science 2004, 117:5721-5729

35. Lindwall G, Cole RD: Phosphorylation affects the ability of tau protein to promote microtubule assembly, The Journal of biological chemistry 1984, 259:5301-5305

36. Lindwall G, Cole RD: The purification of tau protein and the occurrence of two phosphorylation states of tau in brain, The Journal of biological chemistry 1984, 259:12241-12245

37. Jope RS, Johnson GV: The glamour and gloom of glycogen synthase kinase-3, Trends in biochemical sciences 2004, 29:95-102

38. Lovestone S et al. : Phosphorylation of tau by glycogen synthase kinase-3 beta in intact mammalian cells: the effects on the organization and stability of microtubules, Neuroscience 1996, 73:1145-1157

39. Rockenstein E et al. : Neuroprotective effects of regulators of the glycogen synthase kinase-3beta signaling pathway in a transgenic model of Alzheimer's disease are associated with reduced amyloid precursor protein phosphorylation, The Journal of neuroscience : the official journal of the Society for Neuroscience 2007, 27:1981-1991

40. Hong M, Lee VM: Insulin and insulin-like growth factor-1 regulate tau phosphorylation in cultured human neurons, The Journal of biological chemistry 1997, 272:19547-19553

41. Asano T et al. : Role of phosphatidylinositol 3-kinase activation on insulin action and its alteration in diabetic conditions, Biological & pharmaceutical bulletin 2007, 30:1610-1616

42. Jolivalt CG et al. : Defective insulin signaling pathway and increased glycogen synthase kinase-3 activity in the brain of diabetic mice: parallels with Alzheimer's disease and correction by insulin, Journal of neuroscience research 2008, 86:3265-3274

43. Sutherland C et al. : Inactivation of glycogen synthase kinase-3 beta by phosphorylation: new kinase connections in insulin and growth-factor signalling, The Biochemical journal 1993, 296:15-19

44. Taniguchi CM et al. : Critical nodes in signalling pathways: insights into insulin action, Nature reviews Molecular cell biology 2006, 7:85-96

45. Jolivalt CG et al. : Type 1 diabetes exaggerates features of Alzheimer's disease in APP transgenic mice, Experimental neurology 2010, 223:422-431

46. Li ZG et al. : Alzheimer-like changes in rat models of spontaneous diabetes, Diabetes 2007, 56:1817-1824

47. Qu Z et al. : Effects of streptozotocin-induced diabetes on tau phosphorylation in the rat brain, Brain research 2011, 1383:300-306

48. Sims-Robinson C et al.: How does diabetes accelerate Alzheimer disease pathology? Nat Rev Neurol. 2010 , 551-9

49. Gasparini L, Xu H: Potential roles of insulin and IGF-1 in Alzheimer's disease. Trends Neurosci. 2003, 404-6.

50. Ke YD et al. : Experimental diabetes mellitus exacerbates tau pathology in a transgenic mouse model of Alzheimer's disease, PloS one 2009, 4:e7917

51. Wang X et al. : Insulin deficiency exacerbates cerebral amyloidosis and behavioral deficits in an Alzheimer transgenic mouse model, Molecular neurodegeneration 2010, 5:46

52. Dawson HN et al. : Inhibition of neuronal maturation in primary hippocampal neurons from tau deficient mice, Journal of cell science 2001, 114:1179-1187

53. Gómez de Barreda E: Tau-knockout mice show reduced GSK3-induced hippocampal degeneration and learning deficits. Neurobiol Dis. 2010, 622-9

54. Medeiros R: Loss of muscarinic M1 receptor exacerbates Alzheimer's disease-like pathology and cognitive decline, The American journal of pathology 2011, 179:980-991

55. Clodfelder-Miller BJ: Tau is hyperphosphorylated at multiple sites in mouse brain in vivo after streptozotocin-induced insulin deficiency, Diabetes 2006, 55:3320-3325

56. Stork O, Welzl H: Memory formation and the regulation of gene expression, Cellular and molecular life sciences : CMLS 1999, 55:575-592

57. Tischmeyer W, Grimm R: Activation of immediate early genes and memory formation, Cellular and molecular life sciences : CMLS 1999, 55:564-574

58. Caccamo A et al : Lithium reduces tau phosphorylation but not A beta or working memory deficits in a transgenic model with both plaques and tangles. Am J Pathol. 2007, 1669-75.

59. Noble W et al : Inhibition of glycogen synthase kinase-3 by lithium correlates with reduced tauopathy and degeneration in vivo. Proc Natl Acad Sci U S A. 2005, 6990-5

60. Frolich L et al : Brain insulin and insulin receptors in aging and sporadic Alzheimer's disease, J Neural Transm 1998, 105:423-438

61. Steen E et al: Impaired insulin and insulin-like growth factor expression and signaling mechanisms in Alzheimer's disease--is this type 3 diabetes?, Journal of Alzheimer's disease : JAD 2005, 7:63-80

62. Cukierman T, Gerstein HC, Williamson JD: Cognitive decline and dementia in diabetes--systematic overview of prospective observational studies, Diabetologia 2005, 48:2460-2469

63. Manschot SM, et al. : Brain magnetic resonance imaging correlates of impaired cognition in patients with type 2 diabetes, Diabetes 2006, 55:1106-1113

64. Kahn CR et al.: The insulin receptor and its substrate: molecular determinants of early events in insulin action, Recent progress in hormone research 1993, 48:291-339

65. Saltiel AR: New perspectives into the molecular pathogenesis and treatment of type 2 diabetes, Cell 2001, 104:517-529

AKNOWLEGMENT

To my mom and my aunt Emiliana.

First and foremost I want to thank my advisors Diego Di Bernardo and Frank LaFerla. The joy and enthusiasm they have for research was contagious and motivational for me, it has been an honor to be their Ph.D. student. I also like to thank my first advisor, Maria Pia Cosma, she was very important for me. I appreciate all the time she took for me all her and contagious inspiration. She is an excellent example of a successful woman and accomplished researcher.

Thanks to my wonderful family, specially my beloved “mamma”, “papa” and my brother Vale, all have accepted without complaints my endless peacks of stress. Their love were priceless. Thanks to my grandfather and grandmother, whose memory and love are only increased after so many years since they left us.

Thanks to Emiliana, more than an aunt for me : a second mother, friend and a good teacher. She and my uncle Paolo supported me during all my studies and encouraged me to do my best: I am working on it, still.

A Special thanks to Andrea, my other half, for all the love and support that he gave me during these years.

Finally, I would also thank all my friend and colleagues. The first thought goes to Vinicia Polito and Irene Cantone, they helped me in the work with insightful advices and outside of the lab with friendship.

And at last thank to all the labmates of Cosma’s lab and LaFerla’s lab with whome I have shared with me these years of PhD.